Functional manipulation of interhemispheric connections through brain-computer interfacing

August 2022

Masaaki Hayashi

A Thesis for the Degree of Ph.D. in Science

Functional manipulation of interhemispheric connections through brain-computer interfacing

August 2022

Graduate School of Science and Technology

Keio University

Masaaki Hayashi

Contents

List of Figures

List of Tables

Abbreviations

ADM	abductor digiti minimi
ANOVA	analysis of variance
BCI	brain-computer interface
BOLD	blood-oxygen-level dependent
ciCOH	corrected imaginary part of coherence
CS	conditioning stimulus
CST	corticospinal tract
DA	deltoid anterior
EDC	extensor digitorum communis
EEG	electroencephalogram
EMG	electromyogram
ERD	event-related desynchronization
ERS	event-related synchronization
FDI	first dorsal interosseous
FFT	fast Fourier transform
fMRI	functional magnetic resonance imaging
GABA	γ-aminobutyric acid
GLM	general linear model
IHI	interhemispheric inhibition
ISI	inter-stimulus interval
M1	motor cortex
MEG	magnetoencephalogram
MEP	motor-evoked potential
MI	motor imagery
MRI	magnetic resonance imaging
MNS	median nerve stimulation
MVC	maximum voluntary contraction
PMC	premotor cortex
RCT	randomized controlled trial
rmANOVA	repeated-measures ANOVA
rTMS	repetitive transcranial magnetic stimulation

SD	standard deviation
SMA	supplementary motor area
SM1	sensorimotor cortex
SMR	sensorimotor rhythm
tDCS	transcranial direct current stimulation
TMS	transcranial magnetic stimulation
TS	test stimulus

Chapter 1: General introduction

1.1. Functional role of interhemispheric interaction

Projection neurons connect the brain over long distances and create a network between different brain regions. In particular, both hemispheres are structurally and functionally connected by interhemispheric projections through the corpus callosum (Hofer and Frahm, 2006; Jarbo et al., 2012) (**Figure 1-1**). The functions of interhemispheric projections have informed the development of theories that deal with several aspects of the human condition, including hand preference (Witelson, 1985), creativity (Bogen and Bogen, 1988), and attentional functioning (Banich, 1998). In the motor domain, interhemispheric interaction is required to maintain appropriate motor control. Suring unimanual motor tasks, neurons in the monkey primary motor cortex (M1) fire bilaterally and motor signals from both hemispheres interact with each other (Ames and Churchland, 2019); in the human motor cortex, unilateral motor behaviors and bimanual motor coordination rely on the interactions between the contralateral and ipsilateral sensorimotor areas (Picazio et al., 2014; Stefanou et al., 2018).

As a conduit for transferring information between the two hemispheres, interhemispheric inhibition (IHI) is fundamental for the interaction between bilateral M1 areas; IHI refers to the phenomenon in which the left and right M1 areas suppress each other (Carson, 2020; Ferbert et al., 1992). Since such IHI was reduced in patients with callosal infarction (Li et al., 2013), IHI has been considered to be predominantly mediated via the corpus callosum. IHI between the M1 areas may play an important role in

suppressing the activity of the contralateral side, which contributes critically to motor control (Duque et al., 2007; Morishita et al., 2012).

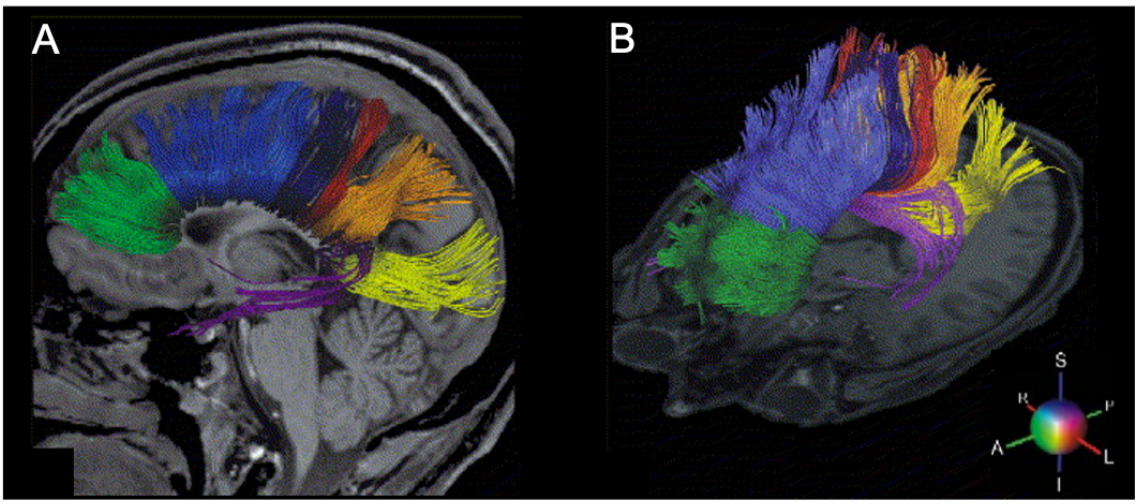

Figure 1-1. Transcallosal projections overlaid onto anatomical reference images
(A) Sagittal and **(B)** oblique views of 3D reconstruction of transcallosal fiber tracts comprising bundles projecting into the prefrontal lobe (green), premotor and supplementary motor areas (light blue), primary motor cortex (dark blue), primary sensory cortex (red), parietal lobe (orange), occipital lobe (yellow), and temporal lobe (violet). The colors correspond to the local mean diffusion direction, as indicated by the color code in the lower right side of the figure: A, anterior; I, inferior; L, left; P, posterior; R, right; S, superior (modified from Hofer and Frahm, 2006).

1.2. Interhemispheric imbalance after stroke

Motor deficits due to focal brain injury often lead to subsequent brain dysfunction, e.g., the balance of reciprocal inhibitory projections between both hemispheres is disturbed in patients with cortical lesions, such as stroke (**Figure 1-2**). In particular, chronic stroke patients show an abnormally high IHI drive from the intact (contralesional) M1 to the affected M1 in the process of generation of a voluntary movement by the paretic hand

(Carson, 2020; Duque et al., 2005; Murase et al., 2004). In addition, the magnitude of IHI targeting a moving index finger correlated with poor motor performance in a simple reaction time paradigm (Murase et al., 2004). Previous studies using functional magnetic resonance imaging (fMRI) also demonstrated that the degree of inhibitory coupling estimated by fMRI dynamic causal modeling correlated with the degree of motor impairment (**Figure 1-3**) (Grefkes et al., 2008; Grefkes and Fink, 2014). Therefore, imbalanced IHI due to excessive suppression from the contralesional to the ipsilesional hemisphere further suppresses the ipsilesional sensorimotor activity beyond that which could be due only to the anatomical damage.

In general, the presence of interhemispheric asymmetry, termed interhemispheric imbalance/competition model, influences not only temporary motor performance but also the functional recovery process after stroke. Although the contralesional M1 exerts a positive effect on the ipsilesional M1 to support motor performance during the subacute phase, contralesional M1 loses its supporting effects in patients with poor functional recovery (Grefkes et al., 2008; Rehme et al., 2011). The shift from an early, supportive role of the contralesional M1 to an inhibitory effect probably constitutes a maladaptive process that contributes to poor motor performance (Rehme et al., 2011). Furthermore, patients with severe impairment retain abnormal contralesional activation, whereas those who demonstrate substantial recovery over time show normalization of brain activity to activation, predominantly in the ipsilesional hemisphere (Harris-Love et al., 2016; Marshall et al., 2000; Ward et al., 2003a). A previous review discussed that the

interhemispheric imbalance/competition model would dominate in patients with limited damage in the affected hemisphere (Di Pino et al., 2014).

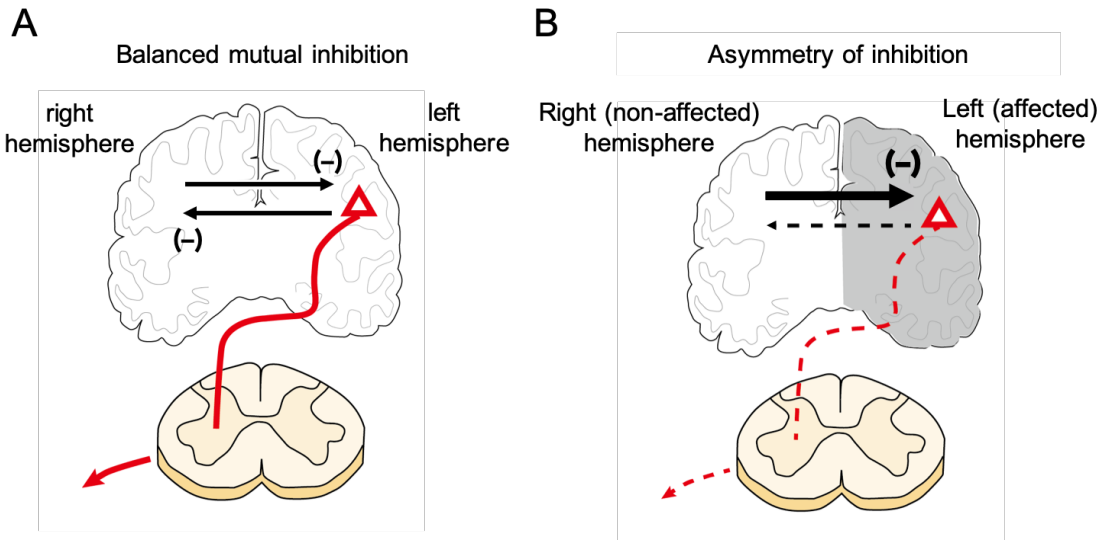

Figure 1-2. Schematic representation of interhemispheric inhibition

(A) Illustration of the assumption of balanced mutual inhibition between M1 areas in the healthy brain. **(B)** Illustration of the assumption that damage to a cerebral hemisphere due to stroke leads to a reduced IHI from the affected to the non-affected hemisphere. As a result, increased excitability of the non-affected side leads to greater IHI of the affected side.

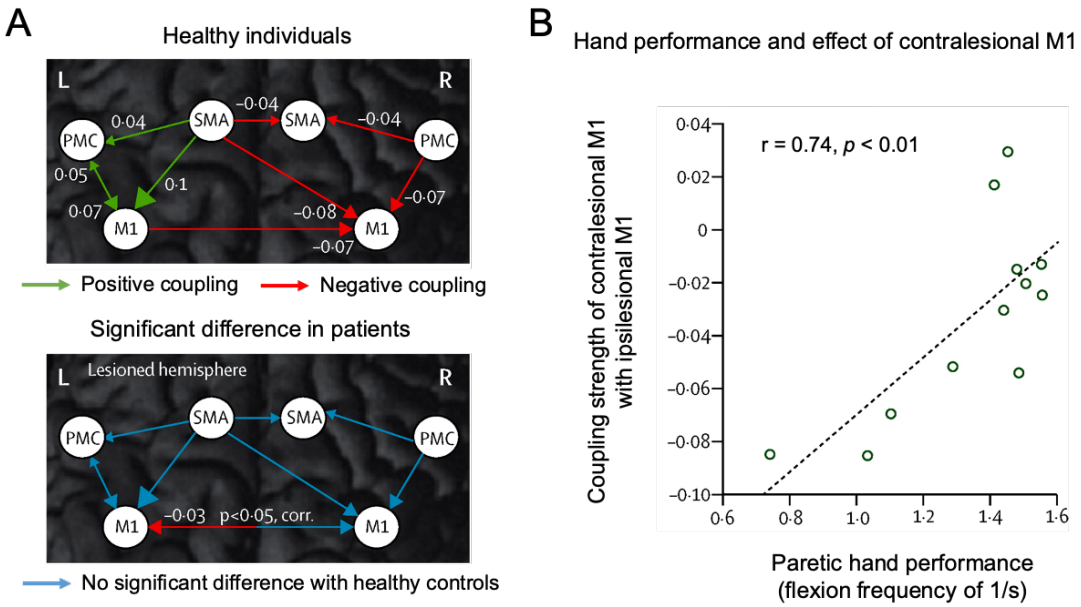

Figure 1-3. Interhemispheric imbalance and its effect on motor function in post-stoke patients

(A) Connectivity during hand movements in healthy individuals (upper) and stroke patients (lower). In healthy individuals, unilateral hand movements are associated with increased coupling of premotor areas with contralateral M1 (green arrows; numbers next to the arrows refer to coupling strength), whereas activity in the ipsilateral hemisphere is suppressed (red arrows). In stroke patients, the intact (contralesional) M1 exerts an inhibitory influence (red arrow) on the ipsilesional M1 (blue arrows indicate no difference to healthy controls). **(B)** The degree of inhibitory coupling exerted by contralesional M1 correlates with the degree of motor impairment (i.e., greater inhibitory coupling is associated with greater impairment). PMC, lateral premotor cortex; SMA, supplementary motor area; M1, primary motor cortex (modified from Grefkes and Fink, 2014).

1.3. Manipulation of interhemispheric interaction

For several decades, techniques are available for the treatment of motor impairment and restoration of upper limb motor function after stroke. Understanding the interhemispheric imbalance is highly relevant to the development of new treatment approaches. In particular, non-invasive brain stimulation techniques, such as repetitive transcranial

magnetic stimulation (rTMS), transcranial direct current stimulation (tDCS), and median nerve stimulation (MNS), can be used to enhance or suppress the sensorimotor activity of the stimulated region (**Figure 1-4**) (Boddington and Reynolds, 2017; Di Pino et al., 2014; Hummel and Cohen, 2006). Previous studies demonstrated that a temporary guide to down-conditioning in the contralesional hemisphere reduced IHI and improved the motor performance of the affected hand in stroke patients (Takeuchi et al., 2012). In addition, two meta-analyses of clinical trials concluded that both rTMS and tDCS enhance motor recovery after stroke with no major adverse effects; however, the treatment effect sizes were medium (Adeyemo et al., 2012; Hsu et al., 2012). Hence, it is likely that using non-invasive brain stimulation may guide the inhibitory interhemispheric network to the appropriate pattern through up-conditioning in the ipsilesional hemisphere and down-conditioning in the contralesional hemisphere, which contributes to reduced abnormal IHI and enhanced functional recovery (Boddington and Reynolds, 2017; Di Pino et al., 2014; Hummel and Cohen, 2006).

However, in contrast to the aforementioned promising results, the treatment efficacy of these approaches is inconsistent. Some patients improved after stimulation-induced suppression of contralesional M1, but others did not (Grefkes and Fink, 2012). Additionally, their long-term sustained effects are often limited due to their passive modulation by externally administered interventions and they do not have spatial specificity (Di Pino et al., 2014; Notturno et al., 2014; Weiskopf et al., 2004). Moreover, two systematic reviews (Elsner et al., 2013, 2020; Hao et al., 2013) concluded that high-quality evidence for the efficacy of rTMS and tDCS in improving the motor function of

stroke patients is lacking. Although the possible factors underlying these inconsistent findings are controversial, alternative neuromodulation techniques are required to enhance the effects of extensive physical/occupational therapy, thereby improving the recovery.

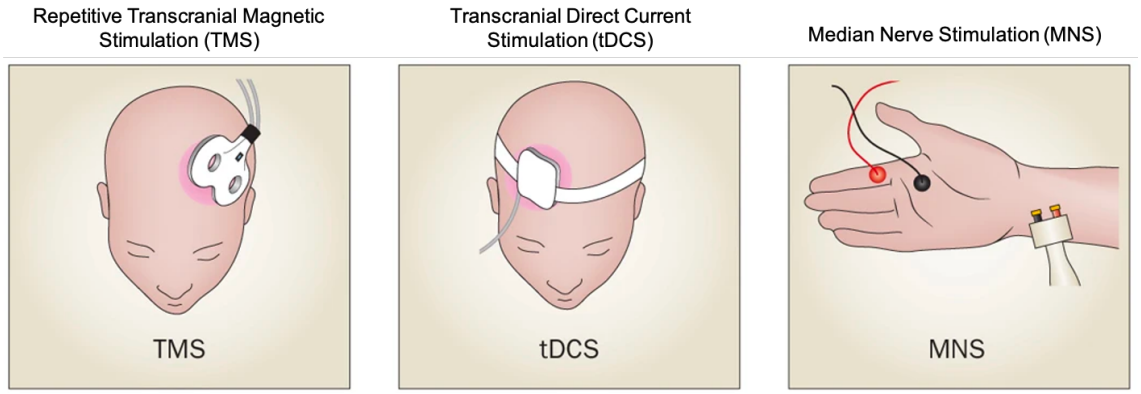

Figure 1-4. Non-invasive brain stimulation techniques to manipulate interhemispheric interaction

Neuromodulation techniques, such as repetitive TMS, tDCS, or MNS, can be used to enhance or suppress the sensorimotor activity of the stimulated region. TMS, transcranial magnetic stimulation; tDCS, transcranial direct current stimulation; MNS, median nerve stimulation (modified from Di Pino et al., 2014).

1.4. Brain-Computer Interface (BCI) for neurorehabilitation

To address the aforementioned problems, it is necessary to evaluate whether targeted interhemispheric activity can be volitionally controlled. As a recent neural manipulative tool, there is increasing interest in BCI technology, which allows direct translation of brain activity (e.g., electroencephalogram: EEG or magnetoencephalogram: MEG) into control signals for a machine, robot, or computer cursor to learn voluntary movement

(Daly and Wolpaw, 2008). Volitional control of the intrinsic neural activity via a closed-loop operant conditioning paradigm helps users recognize how to modulate their own brain activity via feedback and induces plastic changes in the central nervous system (Sitaram et al., 2017). For example, a previous study suggested that volitional control of the amplitude of motor-evoked potential (MEP) under the self-learning environment is retained for at least 6 months without further training (Ruddy et al., 2018). Additionally, stroke patients learn to volitionally control the sensorimotor activity in the ipsilesional hemisphere through visual and/or somatosensory feedback, with the goal of transitioning the residual spared area of the sensorimotor system into a more excitable/relaxed state as a precursor for enhanced neural plasticity and accelerated recovery (**Figure 1-5**) (Bai et al., 2020; Cervera et al., 2018; Mansour et al., 2022; Nojima et al., 2022).

Based on the theory of the interhemispheric imbalance model after stroke, BCI-based neurofeedback can guide sensorimotor cortical activation to the targeted hemisphere, which may enable volitional manipulation of the IHI magnitude. However, less is known about whether BCI-based neurofeedback can explicitly guide sensorimotor cortical activation to the targeted hemisphere. In conventional BCI-based neurofeedback, users learn to volitionally desynchronize and synchronize oscillatory sensorimotor rhythms (SMR-ERD/ERS) in the ipsilesional sensorimotor area (SM1) through visual and/or somatosensory feedback (Ang and Guan, 2017; Chaudhary et al., 2016; Ramos-Murguialday et al., 2013; Soekadar et al., 2015b). Sensorimotor circuits in the left and right hemispheres might influence each another, suggesting that conventional BCI-based neurofeedback of the SMR signal from one hemisphere does not always guarantee

spatially specific activation of the targeted hemisphere (Buch et al., 2008; Caria et al., 2011; Soekadar et al., 2015a). Therefore, the author hypothesized that if the sensorimotor activity is guided to the targeted contralateral or ipsilateral hemisphere with spatial specificity, a new BCI approach can be realized that has the potential to manipulate the interhemispheric balance.

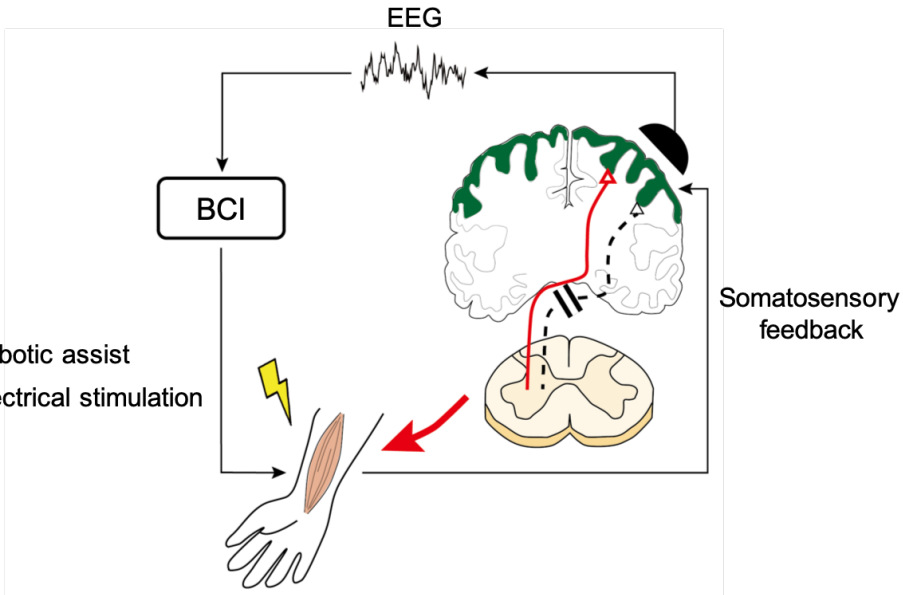

Figure 1-5. Brain-Computer Interface for neurorehabilitation

Brain-Computer Interface (BCI) system monitors the sensorimotor cortical activities in EEG during upper-limb motor imagery. The brain signals are translated into control signals for a robotic device and electrical stimulation. Users learn to volitionally control the sensorimotor activity in the ipsilesional hemisphere through visual and/or somatosensory feedback.

1.5. Purpose of the dissertation

In this dissertation, the author explored whether individuals could explicitly guide sensorimotor activity to the targeted hemisphere and whether users could learn to

volitionally manipulate the IHI magnitude through a BCI-based neurofeedback paradigm. To achieve this, the author first developed a spatially bivariate BCI-based neurofeedback, which concurrently monitors both left and right hemispheric SMR-ERDs, thereby allowing participants to regulate these two variates simultaneously and to modulate target-hemisphere-dependent SMR-ERD. Thereafter, the author evaluated whether healthy individuals can modulate the interhemispheric balance via spatially bivariate BCI-based neurofeedback. These approaches provide evidence for the dynamic interplay between distinct regions underlying IHI through BCI-based neurofeedback, and therefore may form the basis of interhemispheric sensorimotor activity.

In Chapter 2, the new BCI-based neurofeedback approach that monitors bi-hemispheric sensorimotor cortical activities and guides target-hemisphere-dependent activation was described. In Chapter 3, the manipulation of IHI state through spatially bivariate BCI-based neurofeedback, as assessed by the paired-pulse TMS paradigm, was examined (**Figure 1-6**). Finally, in Chapter 4, the author provides a perspective on the contribution of this dissertation to the basic science and technological applications in the field of neurofeedback by integrating the findings of the two aforementioned studies.

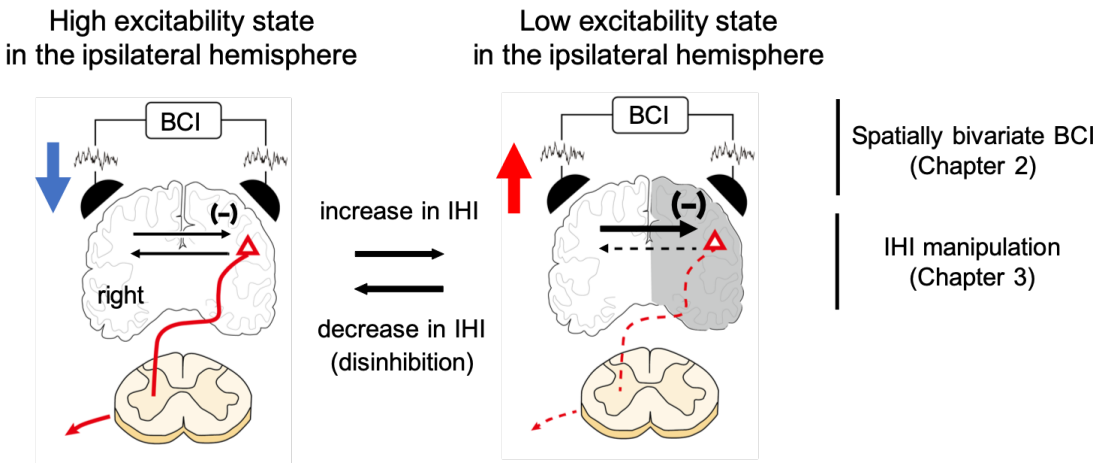

Figure 1-6. Hypothesis of this dissertation

The author hypothesized that if the sensorimotor activity is guided to the targeted contralateral or ipsilateral hemisphere with spatial specificity, a new BCI approach can be realized that has the potential to manipulate the interhemispheric balance. In Chapter 2, the spatially bivariate BCI-based neurofeedback approach that monitors bi-hemispheric sensorimotor cortical activities and guides target-hemisphere-dependent activation was described. In Chapter 3, the manipulation of IHI state through spatially bivariate BCI-based neurofeedback, as assessed by the paired-pulse TMS paradigm, was examined.

Chapter 2: Neurofeedback of scalp bi-hemispheric EEG sensorimotor rhythm guides hemispheric activation of sensorimotor cortex in the targeted hemisphere

* This chapter was based on the following author's original article:
"Hayashi M, Tsuchimoto S, Mizuguchi N, Ushiba J, Neurofeedback of scalp bi-hemispheric EEG sensorimotor rhythm guides hemispheric activation of sensorimotor cortex in the targeted hemisphere. *NeuroImage* 223, 117298 (15 pages), 2020".
The author has a right to use this dissertation.

2.1. Introduction

Oscillatory EEG activity is associated with the excitability of cortical regions. Visual feedback of EEG-oscillations via BCI may promote sensorimotor cortical activation, but its spatial specificity is not truly guaranteed due to signal interaction among interhemispheric brain regions (Buch et al., 2008; Caria et al., 2011; Soekadar et al., 2015a). Guiding spatially specific activation is important for facilitating neural rehabilitation processes (Chieffo et al., 2013; Di Pino et al., 2014; Dong et al., 2006; Hummel and Cohen, 2006). To clarify whether the sensorimotor cortical activity can be guided to the targeted hemisphere, the author conducted a BCI experiment focusing on the neuroanatomical properties of skeletal muscle innervation. Since recent studies suggested that there is a relationship between intrinsic functional/structural architecture of the brain and successful learning of brain activity (Halder et al., 2013; Young et al., 2016), two different motor imageries (MIs) were selected: "shoulder" MI in a first setting and "hand" MI in a second setting as a negative control. It is known that the deltoid

anterior (DA) muscle for flexing proximal muscles is innervated bilaterally (Carson, 2005; Colebatch et al., 1990). Conversely, the extensor digitorum communis (EDC) muscle, which is for extending distal muscles and is predominantly innervated from the contralateral hemisphere (Carson, 2005; Colebatch et al., 1990), was used as a contrast to the bilateral corticomuscular connections of the DA muscle. In addition, shoulder and hand muscles are critical in the rehabilitation strategy of the upper limb motor function since the action of lifting the hand to the target object using the proximal muscles such as the shoulder, reaching, and then grasping the object with the fingers (hand grip) is performed (Thrasher et al., 2008). Therefore, the author hypothesized that, if BCI-based neurofeedback is a potent up-regulator of hemispheric activation to the targeted side, shoulder MI-associated BCI-based neurofeedback should enable the sensorimotor excitability to be lateralized to the targeted hemisphere, either contralaterally or ipsilaterally. In contrast, hand MI-associated BCI-based neurofeedback might enable the sensorimotor excitability to be lateralized to the contralateral hemisphere, while the lateralization of the ipsilateral excitability is limited by its neuroanatomical constraint.

In this chapter, participants performed shoulder/hand MI-associated BCI-based neurofeedback to learn volitional regulation of sensorimotor cortical excitability in the contralateral or ipsilateral hemisphere in a double-blind, randomized, within-subject crossover design. The author used a new BCI-based neurofeedback approach during unilateral repetitive kinesthetic MI to volitionally regulate sensorimotor cortical excitability, as reflected by SMR-ERD/ERS, with the aim of guiding its intensity to only the targeted hemisphere. To this end, the author designed a spatially bivariate BCI-based

neurofeedback that displays both left and right hemispheric SMR-ERDs concurrently, allowing participants to learn to regulate these two variates at the same time and to modulate target-hemisphere-dependent SMR-ERD.

2.2. Materials and Methods

2.2.1. Study design

Based on a systematic, phased, developmental approach to rehabilitation research that respects the critical importance of all milestones along the developmental research trajectory, the author examined the mechanism of BCI-based neurofeedback as a pre-clinical trial and a First-in-Person Proof-of-Concept study for "healthy" participants (Thabane et al., 2010). The author adhered to the principles of good clinical practice, including human subject protection, as required for the ethical conduct of clinical research (U.S. Food & Drug Administration).

The study was conducted with a double-blind, randomized, crossover design. The current methodology was performed in accordance with approved guidelines and regulations, such as the CONSORT Statement (Moher et al., 2001) and CRED-nf checklist (Ros et al., 2020). All participants, the experimenter, and the analyst were blinded to the intervention assignment. Additionally, since this study is a pre-clinical trial and a First-in-Person Proof-of-Concept study for healthy participants, it was necessary to conduct the experiment with the minimum number of participants and the minimum experimental period including the washout period (Kim, 2013). Therefore, a within-subject crossover design with a single-day intervention was optimal compared to a

parallel-group comparison study, where a larger sample size would have been required to eliminate inter-individual variance (Kim, 2013).

To estimate the appropriate sample size for this study, a preliminary experiment was conducted before the main experiment. In the preliminary experiment, four additional healthy participants who were not participants in the main experiment performed two sessions with BCI-based neurofeedback training during shoulder MI (one session aimed at contralateral SM1 lateralization and the other aimed at ipsilateral SM1 lateralization: Shoulder-contra and Shoulder-ipsi sessions). This preliminary experiment was conducted under the same protocol as the first setting in the main experiment. Note that the main purpose of this study was to test whether users could volitionally lateralize sensorimotor activity to the contralateral or ipsilateral hemisphere using “shoulder” MI-associated BCI-based neurofeedback. Because “hand” MI was used as a negative control to see how neuroanatomical properties influence the training effects, the preliminary experiment was conducted with only "shoulder" MI to calculate the effect size on lateralized sensorimotor activities to the contralateral or ipsilateral hemisphere.

The author first performed pre-processing and time-frequency analyses to calculate the left and right SMR-ERDs and their laterality (see "Offline time-frequency analysis" for details). Then, the author conducted an *a-priori* power analysis ($\alpha = 0.05$, $1-\beta = 0.8$, two-sided tests) focusing on the contralateral/ipsilateral SMR-ERDs and their laterality using the statistical package G*Power 3 (Faul et al., 2007). Because the preliminary experiment showed a large effect size on the improvement of the contralateral/ipsilateral SMR-ERDs during both Shoulder-contra session (pre = 5.55%, post = 18.81%, Cohen’s

d = 0.89) and Shoulder-ipsi session (pre = –0.81%, post = 5.73%, Cohen's d = 0.88), the author calculated that 12 participants were needed (Cohen, 1992).

2.2.2. Participants

Twelve healthy male volunteers (aged 21-30 years) participated in the study; none had participated in any other of our studies. All participants had normal or corrected-to-normal vision and reported no history of neurological or psychological disorders. Eleven of the participants were right-handed as assessed by the Edinburgh Inventory (Oldfield, 1971). Laterality Quotient was 90.3 ± 27.4 % (mean ± standard deviation [SD]). Laterality Quotient of the one non-right-handed person was 0%. Note that this participant was not used as a representative participant. The study was conducted in accordance with the Declaration of Helsinki. The experimental procedure was approved by the Ethics Committee of the Faculty of Science and Technology, Keio University (Number: 30-78). Written informed consent was obtained from all participants prior to the experiments.

2.2.3. Intervention assignment

Twelve age-matched participants were randomly assigned to four (2×2) groups using a table generated prior to study onset; each group completed the four BCI-based neurofeedback sessions in different orders (**Figure 2-1A**). In this within-subject crossover design, participants were first assigned to a group that started with shoulder MI and a group that started with hand MI. The group that performed shoulder MI was further divided into a subgroup that started with a session aimed at contralateral SM1

lateralization (Shoulder-contra) and a subgroup that started with a session aimed at ipsilateral SM1 lateralization (Shoulder-ipsi). Similarly, the group that first performed hand MI was divided into a subgroup that started with the 'Hand-contra' session and a subgroup that started with the 'Hand-ipsi' session. Because this study was a within-subjects crossover design, all participants performed all four BCI-based neurofeedback sessions, all statistical analyses were performed by merging subgroups ($N = 12$).

To minimize any carryover effects of the preceding intervention in a crossover design, a washout period was arranged. According to previous studies focusing on short-term neuromodulation effects induced by BCI (Mayaud et al., 2013; Vukelić and Gharabaghi, 2015; Zhang et al., 2019) or tDCS (Amatachaya et al., 2015; Shekhawat and Vanneste, 2018), it was reasonable to set the washout period between the first and second sessions and between the third and fourth sessions to seven days or more because the intervention effect seems to be disappeared after that period. Furthermore, the aftereffect of BCI-based neurofeedback for healthy participants can be confirmed by five consecutive day training or more (Ono et al., 2013), but the 1-day BCI training effect returns to the baseline the next day. Because the carryover effects of different MIs have never been investigated, the washout period between the second and third sessions (i.e., Shoulder and Hand MIs) was set to 1 month or more. The learning effects were empirically examined from the results of the pre-evaluation block in each session.

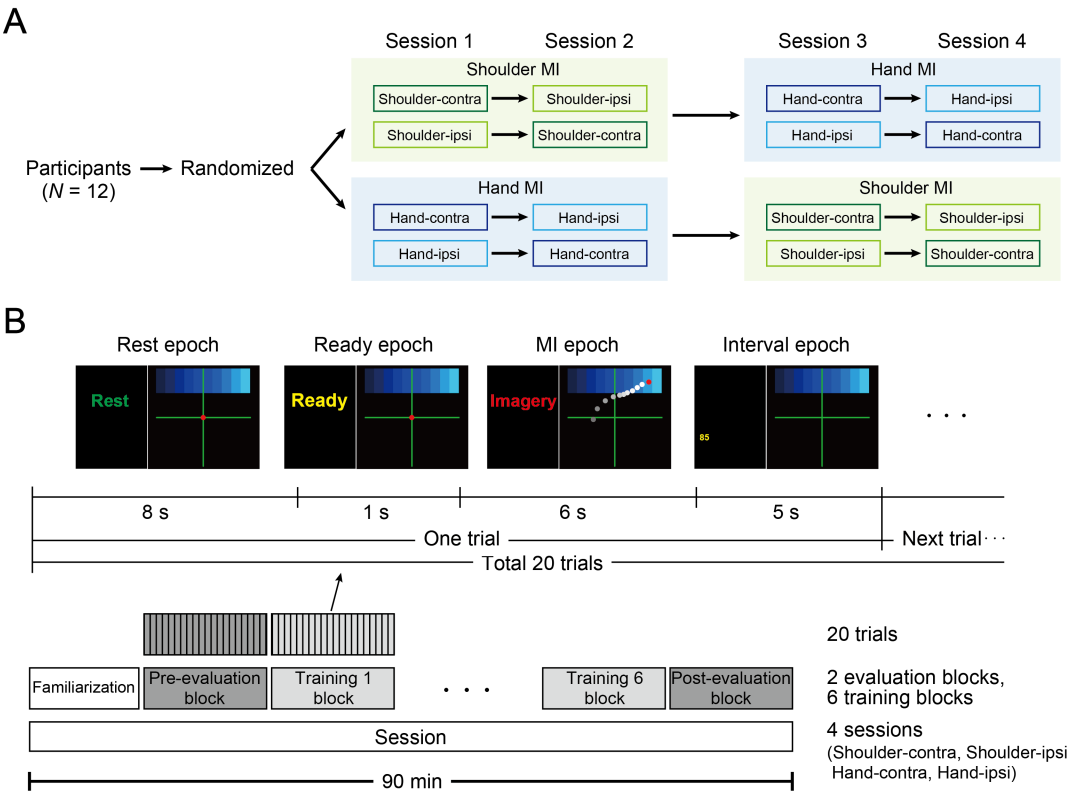

Figure 2-1. Study design and experimental paradigm

(A) Participants were divided into four (2×2) groups in a double-blind, randomized, crossover design. Each group performed four BCI-based neurofeedback training sessions over separate days as follows: Shoulder-contra and Shoulder-ipsi MI-associated neurofeedback training sessions aimed at lateralizing to the contralateral or ipsilateral SM1, respectively; and Hand-contra and Hand-ipsi MI-associated neurofeedback training sessions aimed at lateralizing to the contralateral or ipsilateral SM1, respectively. **(B)** Task instructions and visual SMR-ERD feedback in the contralateral and ipsilateral SM1 were provided in the form of computer cursors in a two-dimensional coordinate on a computer screen. The cursor position was updated every 100 ms and calculated the score based on the contralateral and ipsilateral SMR-ERDs during the MI epoch. Additionally, a cumulative sum score in each MI epoch was provided at the interval period. The axes ranged from -100% (i.e., ERS) to 100%, and the cursors were presented at the origin-positioned (x = 0, y = 0) at the initiation of a trial.

2.2.4. Outcomes

After the MI-associated neurofeedback interventions, contralateral/ipsilateral SMR-ERDs and their laterality were analyzed as the primary neurophysiological outcome measures to examine whether SMR-ERD became more intense over the targeted SM1. SMR-ERD is a reliable surrogate monitoring marker of sensorimotor cortical excitability level for several reasons: (1) sensorimotor cortex activity is known to be associated with amplitude modulation of the SMR during the resting state (Tsuchimoto et al., 2017); (2) SMR-ERD and a task-induced increase in blood oxygenation level-dependent (BOLD) signals during MI are co-localized and co-varied at SM1 (Yuan et al., 2010); (3) the intensity of SMR-ERD reflects sensorimotor cortical excitability that innervates agonist muscle (Takemi et al., 2013, 2018) and spinal motoneurons (Takemi et al., 2015); (4) SMR-ERD control is associated with the contribution of SM1 modulated by transcranial direct current stimulation (Soekadar et al., 2015b); and (5) data-driven EEG features discriminating the presence/absence of muscle contraction were localized predominantly in the parieto-temporal regions, indicating SMR-ERD (Hayashi et al., 2019). The author also examined resting-state functional connectivity as a secondary neurophysiological outcome measure, because intrahemispheric and interhemispheric brain networks in the resting-state are well-established, with their neurophysiological signatures reflecting the aftereffect of neurofeedback training (Pichiorri et al., 2011, 2015; Várkuti et al., 2013; Young et al., 2014).

2.2.5. Data acquisition

EEG data were recorded using a 128-channel Hydrogel Geodesic Sensor Net 130 system (Electrical Geodesics Incorporated, Eugene, OR, USA) with a sampling rate of 1 kHz in a quiet room. The ground and reference channels were placed at CPz and Cz, respectively. The impedance of all channels was maintained below 30 kΩ throughout the experiment for the compliance of EEG recordings (Ferree et al., 2001).

Surface electromyograms (EMGs) were recorded from the DA and EDC muscles in the left and right hand with a pair of Ag/AgCl electrodes. The 10-mm diameter electrodes were placed on the skin over the muscle belly along the muscle fibers with the anode 20 mm proximal to the cathode. The experimenter used the surface EMG signals to monitor muscular contraction due to shoulder/hand movement so they could remind the participants to relax their muscles and to ensure the absence of muscle activity during MI. These signals were sampled at 1 kHz using the Physio 16 MR input box (Electrical Geodesics Incorporated, Eugene, OR, USA). All EEG/EMG data were recorded to a file for offline analysis. Simultaneously, 5–10-ms data segments were transferred immediately after collection to a computer for real-time analysis.

Throughout the experiment, the participants were seated in a comfortable chair with a stable forearm support and performed unilateral right shoulder flexion MI or finger extension MI. Unilateral right MI was selected because the author aim to develop this study as neurofeedback exercise for post-stroke hemiplegic patients. In addition, left hand MI for right-handers may not be suitable for a single-day neurofeedback experiment because only a small increase in SMR-ERD is ordinarily observed during non-dominant

hand MI (Stancák and Pfurtscheller, 1996). Shoulder flexion MI was performed until the shoulder joint angle was 90°. The wrist and elbow joint angles were fixed to a neutral posture of 0°. Finger extension MI was performed with all four fingers excluding the thumb. The wrist joint angle was fixed to a neutral posture of 0° at the armrest. All participants were instructed to try to keep this posture and were visually monitored by the experimenter throughout the experiment. During both shoulder and hand MIs, the forelimbs were placed in a prone position, with an elbow joint angle of 90° and a shoulder joint angle of 0° to help muscle activity (O'Sullivan and Gallwey, 2002).

2.2.6. Experimental paradigm

Figure 2-1B shows an overview of the time course of the experimental paradigm. Each session comprised eight 7-min blocks, including a pre 'evaluation' block, six 'training' blocks, and a post 'evaluation' block. Between blocks, participants had short, 5-min breaks. The number of blocks performed was limited by the time required to perform the experiments (i.e., a total of 2.5 h including a preparation). To familiarize each subject with the MI, a practice block with 20 trials immediately preceded the first pre-evaluation block, during which participants were asked to perform kinesthetic MIs from the first-person perspective. Kinesthetic MI was instructed because a previous study demonstrated that the focus of EEG activity during kinesthetic MI was found close to the sensorimotor hand area, whereas visual MI did not reveal a clear spatial pattern (Neuper et al., 2005). In addition, the subjective vividness of kinesthetic MI, not visual MI was significantly

associated with the similarity between SMR-ERD magnitude during motor execution and that during MI (Toriyama et al., 2018).

Each evaluation/training block consisted of twenty trials. Each trial was initiated by an 8-s resting epoch, followed by a 1-s ready epoch, and completed by a 6-s MI epoch. During this 15-s trial period, participants were asked not to move, blink, or swallow to prevent EEG artefacts derived from non-neural activity. After each 15-s trial was completed, the screen went black for 5 s. Participants were allowed to move freely to avoid mental fatigue during this interval period, before the next trial started.

During the MI epoch, participants were asked to perform a shoulder flexion MI or a finger extension MI with equal time constants of 0.5 Hz cycle (i.e., in total, 3 MIs per trial). The participant's compliance with the given MI task was measured using the EMG of the DA and EDC muscles, the major agonist muscle group for shoulder flexion and finger extension (Smania et al., 2007). The surface EMG signal was applied at 5–450 Hz with a second-order Butterworth bandpass filter and 50-Hz notch filter. The filtered EMG signal was then full-wave rectified, and the rectified EMG signal was integrated with respect to the last 300-ms time window. To ensure the absence of muscle activity during MI, the author checked whether the integrated EMG during the MI was within the baseline magnitude (mean ± SD in the resting-state). Trials that exceeded the baseline magnitude were rejected.

To improve MI task compliance, which is whether all participants successfully performed the MI in the same manner, the author not only asked them to perform kinesthetic MIs from a first-person perspective, but the author also asked them to perform

a rehearsal in the 5-min break between each block. In addition, the author carefully confirmed during every block that SMR was observed in a frequency-specific, spatiotemporal-specific, and task-related manner. These characteristics of SMR-ERD indicate that kinesthetic MI, not visual MI, was performed correctly (Neuper et al., 2005; Pfurtscheller and Neuper, 1997).

2.2.7. Spatially bivariate BCI-based neurofeedback session

All participants completed the four different neurofeedback sessions on separate days; each session consisted of the pre- and post-evaluation blocks and the six training blocks (**Figure 2-1A**).

Evaluation block

In the pre- and post-evaluation blocks, no visual feedback was provided. The aim of the pre-evaluation block was to evaluate the baseline brain activity and to calibrate parameters in the neurofeedback settings each day. First, the target frequency was calibrated for each participant in order to feedback the most reactive frequency. The target frequency was selected from the alpha band (8–13 Hz) by calculating the mean intensity of SMR-ERD with a 3-Hz sliding bin and 2-Hz overlap. SMR-ERD in the alpha band is a reliable EEG biomarker representing increased neuronal excitability in SM1, corticospinal tract, and thalamocortical systems (Neuper et al., 2006; Soekadar et al., 2015b; Takemi et al., 2013, 2015, 2018; Yuan et al., 2010). Second, the target level of SMR-ERD during MI was normalized for each participant at the third quartile of the

contralateral or ipsilateral SMR-ERD in the pre-evaluation block. This setting was empirically approved by the authors as a moderate load for effective operant learning (Naros et al., 2016).

Training block

In the training blocks, participants received visual feedback based on the SMR-ERDs from both left and right hemispheres. The real-time SMR-ERD intensity in each hemisphere (relative to the average power of the last 6 s of the resting epoch) was obtained every 100 ms and calculated using the last 1-s data as follows: (1) acquired raw EEG signals recorded over SM1 underwent a 1–70-Hz second-order Butterworth bandpass filter and a 50-Hz notch filter; (2) filtered EEG signals were spatially filtered with a large Laplacian (60 mm to set of surrounding channels), which subtracted the average value of the surrounding six channel montage from that of the channel of interest (i.e., C3 or C4). This method enabled us to extract the task-related EEG signature and to improve the signal-to-noise ratio of SMR signals (McFarland et al., 1997). In addition, the large Laplacian method is better matched to the topographical extent of the EEG control signal than the small Laplacian and ear reference methods (McFarland et al., 1997); (3) a fast Fourier transform (FFT) applied the spatially filtered EEG signals; (4) the power spectrum was calculated by squaring the Fourier spectrum; (5) the alpha band power was obtained by averaging the power spectrum across the predefined alpha target frequencies from the pre-evaluation block; (6) the alpha band power was time-smoothed by averaging across the last five windows (i.e., 500 ms) to extract low-frequency component for high

controllability. It is reported that the slow fluctuation component is beneficial to neurofeedback training because it reduced flickering and improved the signal-to-noise ratio of the SMR signal (He et al., 2020; Kober et al., 2018); and (7) SMR-ERD was obtained by calculating relative power to the average power during the resting epoch (2~8 s). SMR-ERDs of the last ten segments were displayed and updated every 100 ms, allowing participants to view and compare current and past conditions. In addition, SMR-ERD was generally computed using the following classic formula:

$$SMR - ERD\ (f,t) = \frac{R\ (f) - A\ (f,t)}{R\ (f)} \times 100$$

where A was the power at time *t* and frequency *f*, and R was the average power during the resting epoch.

To modulate target hemisphere-dependent SMR-ERD, the author developed BCI-based neurofeedback that displayed both left and right hemispheric SMR-ERDs concurrently, allowing participants to learn to regulate these two variates at the same time. Visual feedback was provided on a computer screen in the form of cursor movements in a two-dimensional coordinate, in which each axis corresponded to the degree of the contralateral or ipsilateral SMR-ERD. The axis range was set from -100% (i.e., ERS) to 100%, and the cursors were presented at the origin-position (x = 0, y = 0) at the initiation of a trial. Values less than -100% were all rounded to "-100%". A key point of this study is that participants were always instructed to try to move the cursor toward the upper right

in the two-dimensional coordinate during MI in all four neurofeedback training sessions. In the case of shoulder MI, for example, participants performed the same MI and tried to move the cursor to the upper right regardless of whether it was a Shoulder-contra or Shoulder-ipsi session. However, the coordinate systems during the two sessions differed as follows: in the Shoulder-contra session, the x-axis and y-axis corresponded to the ipsilateral SMR-ERS and contralateral SMR-ERD, respectively. Conversely, in the Shoulder-ipsi session, the x-axis and y-axis corresponded to the contralateral SMR-ERS and ipsilateral SMR-ERD, respectively. Thus, the upper right position always indicated a reduction in alpha rhythm in the targeted hemisphere with respect to the baseline (i.e., SMR-ERD) and an increase in the non-targeted side (i.e., SMR-ERS). Using such a gimmicked environment, the author aimed at lateralizing cortical activity in the sensorimotor cortex, blinding which task was being performed.

A score was calculated when the most recent cursor on the screen reached the ten blue boxes representing the scoring range. The coordinates of each blue box corresponded to the degree of bilateral SMR-ERDs, with the x-axis set in steps of 10% SMR-ERS in the non-targeted hemisphere, and y-axis ranged from the predefined threshold to 100% SMR-ERD in the target hemisphere. At the end of the trial, the computer cursor returned to the origin position. A score for each segment (each computer cursor updated every 100 ms) was obtained during the MI epoch to provide feedback about the overall performance of each trial. The darkest blue box in the upper left in **Figure 2-1B** had a low score (5 points), whereas the lightest blue box in the upper right had a high score (15 points). The boxes in the middle were set in steps of 1 point. Finally, a cumulative sum calculated by

adding all scores was displayed for 5 s in the left side of the screen at the interval period in each trial (range: 0–765 points). To boost learning of self-regulation in sensorimotor cortical activity, participants were encouraged to get a higher cumulative sum than during the previous trial and asked to keep improving their performance. The cumulative sum in each trial was displayed including the past ones. Such screen presentation of the total score at the end of the trial is referred to as 'intermittent feedback' (Johnson et al., 2012). Previous studies demonstrated that providing intermittent feedback is a useful element for neurofeedback training (Posse et al., 2003; Shibata et al., 2011) because it probably reduces cognitive loads during MI.

2.2.8. Offline time-frequency analysis

Pre-processing and time-frequency analyses were performed to calculate the left and right SMR-ERDs and their laterality. The EEG signal underwent a 1–70-Hz, second-order Butterworth bandpass filter and a 50-Hz notch filter. The EEG signals of all channels were then spatially filtered with a common average reference, which subtracted the average value of the entire electrode montage (the common average) from that of the channel of interest to remove the entire brain-derived signal from global noise (McFarland et al., 1997). EEG channels in each trial were rejected during further analysis when they contained an amplitude above 100 μV.

The power time series were calculated every 100 ms by FFT with a 1-s sliding window and 90% overlap. The power time series in the alpha target frequencies were then obtained from a band power in each time window by averaging the magnitudes of the

Fourier coefficients in the target frequency bins. The average SMR-ERD during the MI epoch (6 s, attaining and maintaining ERD/ERS) was evaluated.

Changes in SMR-ERD due to neurofeedback training between shoulder and hand MI tasks were compared using a three-way repeated-measures ANOVA (rmANOVA), with Session (aiming for lateralizing to the contralateral vs. ipsilateral hemisphere), Hemisphere (contralateral vs. ipsilateral), and Limb (shoulder MI vs. hand MI) as the within-subject factors. Following the three-way rmANOVA, a post-hoc analysis was performed using the Bonferroni correction for multiple comparisons. A two-way rmANOVA among Group (A to D) and Period (1^{st} to 4^{th}) was applied to SMR-ERD data for each hemisphere in the pre-evaluation block to check the order and carryover effects from the previous session. The assumption of normality was verified using the Shapiro-Wilk test. The assumption of sphericity was checked using the Mauchly's test. If the test was significant, a Greenhouse-Geisser correction was applied.

To evaluate target-hemisphere-dependent modulation (i.e., difference between the contralateral and ipsilateral sensorimotor activation, a laterality index (LI) of the bihemispheric SMR-ERDs was calculated (Seghier, 2008). The LI value is generally computed using the following classic formula:

$$Laterality\ Index\ (LI) = \left(\frac{ERD_{ipsi} - ERD_{contra}}{|ERD_{ipsi}| + |ERD_{contra}|} \right)$$

where ERD_{ipsi} was the SMR-ERD calculated from the ipsilateral hemisphere to the imagined hand and ERD_{contra} was the SMR-ERD calculated from the contralateral hemisphere. LI yields a value of 1 or -1 when the activity was purely ipsilateral or contralateral, respectively. Differences between the pre- and post-evaluation blocks for each were assessed using a paired *t*-test.

To evaluate BCI performance, a total cumulative score was calculated in each session by cumulatively adding the total score for each trial. Differences in the cumulative score between the pre- and post-evaluation blocks were examined using a paired *t*-test. Differences in the cumulative score between the 6 training blocks were further assessed using a one-way rmANOVA. Statistical significance was set at $p = 0.05$. Note that because this study had a within-subjects crossover design, statistical analyses were performed by merging subgroups (N = 12).

2.2.9. Connectivity analysis

High-density electroencephalography was used to examine the reactivity of the cortical motor system by studying both local oscillatory power entrainment (i.e., SMR-ERD) and distributed interregional neural communication. Interregional communication is thought to be accompanied by synchronization of oscillations between different brain regions (Fries, 2005; Varela et al., 2001). Synchronous activity even between distant brain regions is considered to have some functional linkage, and their synchronization can be evaluated by functional connectivity measures (van Diessen et al., 2015). The human brain maintains an organized pattern of functional connectivity even at rest without an

externally given task. Resting-state functional connectivity is associated with task-induced functional connectivity (Damoiseaux et al., 2006; Greicius et al., 2003; Vincent et al., 2007). In addition, changes in resting-state functional connectivity is a well-established neurophysiological signature that reflects the aftereffect of BCI-based neurofeedback training (Pichiorri et al., 2011, 2015; Várkuti et al., 2013; Young et al., 2014). Therefore, the author focused on the resting epoch (2-8 s) for the analysis of functional connectivity.

To calculate functional connectivity and to compensate for long-range synchronization preference, the author utilized the corrected imaginary part of coherence (ciCOH) (Ewald et al., 2012; Vukelić and Gharabaghi, 2015). This method systematically ignores any functional relation occurring at vanishing phase delay that includes the influence of volume conduction of the head, which is widely accepted as occurring at zero phase lag. Thus, ciCOH is a robust connectivity measure indicating the relative coupling of phases between two brain regions. Further, ciCOH generally results in a signal-to-noise ratio increase, which may reveal interactions that are otherwise hidden in the noise when studying connectivity between sensors. To estimate the ciCOH following a complex coherency function, the resting epoch was subdivided into 1-s segments with 50% overlap (11 segments in total) and multiplied with a Hanning window. The above-mentioned pre-processing for the connectivity analysis was confirmed by previous EEG-connectivity studies (Nolte et al., 2004; Vukelić and Gharabaghi, 2015).

In the EEG-connectivity analysis, $x_i(f)$ and $x_j(f)$ were the Fourier transforms of the time series $\hat{x_i}(t)$ and $\hat{x_j}(t)$ of channel i and j, respectively. The complex cross-

spectrum was then defined for each frequency *f* and for channels *i* and *j*, respectively, as follows:

$$S_{ij}(f) \equiv \langle x_i(f) x_j{}^*(f) \rangle$$

where $*$ is the complex conjugation and $\langle \cdot \rangle$ is the expectation value. The expectation value can only be estimated as an average over a sufficiently large number of epochs. The complex coherency function was defined as the normalized cross-spectrum:

$$C_{ij}(f) = \frac{S_{ij}(f)}{\sqrt{S_{ii}(f) S_{jj}(f)}}$$

where $S_{ii}(f)$ and $S_{jj}(f)$ are the auto-spectra for channels *i* and *j*, respectively. The ciCOH function was then calculated from the complex coherency function (Ewald et al., 2012) as follows:

$$ciCOH_{ij}(f) = \frac{Im(C_{ij}(f))}{\sqrt{(1 - Re(C_{ij}(f))^2)}}$$

where *Im*(·) and *Re*(·) denote the imaginary and real parts, respectively. Although the imaginary part of coherency (i.e., $Im(C_{ij}(f))$) exhibits a spatial bias towards remote interactions, it is suppressed using the ciCOH which is corrected by the real part of the coherency (Ewald et al., 2012).

A subsequent analysis was performed, during which the author focused on the intrahemispheric and interhemispheric connections (Pichiorri et al., 2015). Our assumption was that a change toward an increase in ciCOH values was associated with the BCI-based neurofeedback training aiming to lateralize sensorimotor cortical activities to either hemisphere. Accordingly, the author examined the network intensity in each hemisphere calculated as follows:

$$Network\ intensity_{hem}(f) = \sum_{seed=1}^{7} \sum_{j=1}^{44} ciCOH_{seed.j}(f)$$

where *Network intensity*$_{hem}$ is computed within the targeted hemisphere, $\sum\sum ciCOH$ is the sum of significant ciCOH values of a given hemisphere, seed denotes the 7 seed channels (i.e., C3 or C4 and its neighboring 6 channels), and *f* indicates the frequency of interest (i.e., the predefined alpha frequencies). In addition, for the intrahemispheric interactions, *j* denotes the channels of a given hemisphere excluding the seed channels (44 channels in total). Conversely for the interhemispheric interactions, *j* denotes the seed channels of the opposite hemisphere (non-targeted side) (7 channels in total). In this case, it was not normalized in the present form because the author aimed to measure total interaction rather than total interaction per channel. To obtain significant connections, the author performed a 1-tailed *t*-test to analyze the significance threshold for ciCOH (Astolfi et al., 2007; Pichiorri et al., 2015). Significant connections were obtained from 91 of 129 EEG channels, omitting the peripheral electrode leads to reduce computational

complexity. A paired *t*-test ($p < 0.05$) was then performed in each session to determine whether significant differences in intrahemispheric and/or interhemispheric network intensity could be detected after the neurofeedback interventions (the pre- vs post-evaluation blocks).

2.2.10. Correlation analysis

A correlation analysis was conducted to examine whether large-scale resting-state functional connectivity in the alpha band was associated with regional SMR-ERD modulation. The author initially calculated the percent change in SMR-ERD in a targeted hemisphere from the pre- to the post-evaluation blocks in each session. In addition, the percent change in intrahemispheric network intensity of a targeted hemisphere and in interhemispheric network intensity were computed. A Spearman's rank correlation was applied to find significant positive correlations between the ΔSMR-ERD and ΔNetwork intensity for each neurofeedback session.

2.3. Results

Rejected trials, in which surface EMG signals during MI exceeded the baseline amplitude (mean ± SD in the resting-state), were less than 5% in all participants. In all sessions, all participants subjectively confirmed that they were able to perform kinesthetic MIs of the targeted muscle. Furthermore, it was confirmed that the data of the non-right-handed participant did not statistically show an outlier ($p = 0.79$). EEG signals with amplitudes ≤ 100 μV were recorded stably throughout all sessions. SMR amplitudes were greater

during the resting epoch than during the MI epoch, irrespective of imagined movement, indicating the desynchronization of sensorimotor neural activity induced by MI. The averaged power spectrum density from the C3 channel during the resting epoch showed peak frequencies at 8–13 Hz and 21–24 Hz across the participants (Crone et al., 1998; Nakayashiki et al., 2014; Neuper et al., 2006; Pfurtscheller, 2001). The averaged powers in the alpha and beta bands were $1.7 \times 10^{-4} \pm 0.4 \times 10^{-4}$ V^2 and $2.9 \times 10^{-5} \pm 0.6 \times 10^{-5}$ V^2 (mean ± standard deviation [SD]), respectively. Although the target frequency was calibrated for each session conducted on separate days to feedback the most reactive frequency, the variation in the targeted frequency among 4 sessions was within ± 1 Hz in all participants. In addition, there were no significant differences among the four sessions in the target level of SMR-ERD defined in the pre-evaluation block (all $p > 0.05$, one-way rmANOVA). No adverse events, adverse events leading to withdrawal, or serious adverse events occurred.

2.3.1. BCI performance

Figure 2-2 illustrates the changes in BCI performance (i.e., total cumulative score) in each session. In shoulder MI, the total cumulative score was improved in both the Shoulder-contra session (pre = 1170, post = 1651, difference = 481, Cohen's $d = 0.72$, $p = 0.007$, paired t-test) and the Shoulder-ipsi session (pre = 891, post = 1310, difference = 419, Cohen's $d = 0.84$, $p = 0.011$, paired t-test). On the other hand, in hand MI, the total cumulative score was improved in the Hand-contra session (pre = 1783, post = 1136, difference = 647, Cohen's $d = 1.20$, $p = 0.018$, paired t-test), but not in the Hand-ipsi

session (pre = 1249, post = 1253, difference = 4, Cohen's d = 0.01, p = 0.97, paired t-test). The author also found that the total cumulative score in the evaluation blocks was lower than that in the training blocks, which is in keeping with the well-known information that visual feedback enhances MI-based BCI performance (Ono et al., 2015; Pichiorri et al., 2015). Differences between the 6 training blocks for cumulative score were not statistically significant (all $p > 0.05$, one-way rmANOVA).

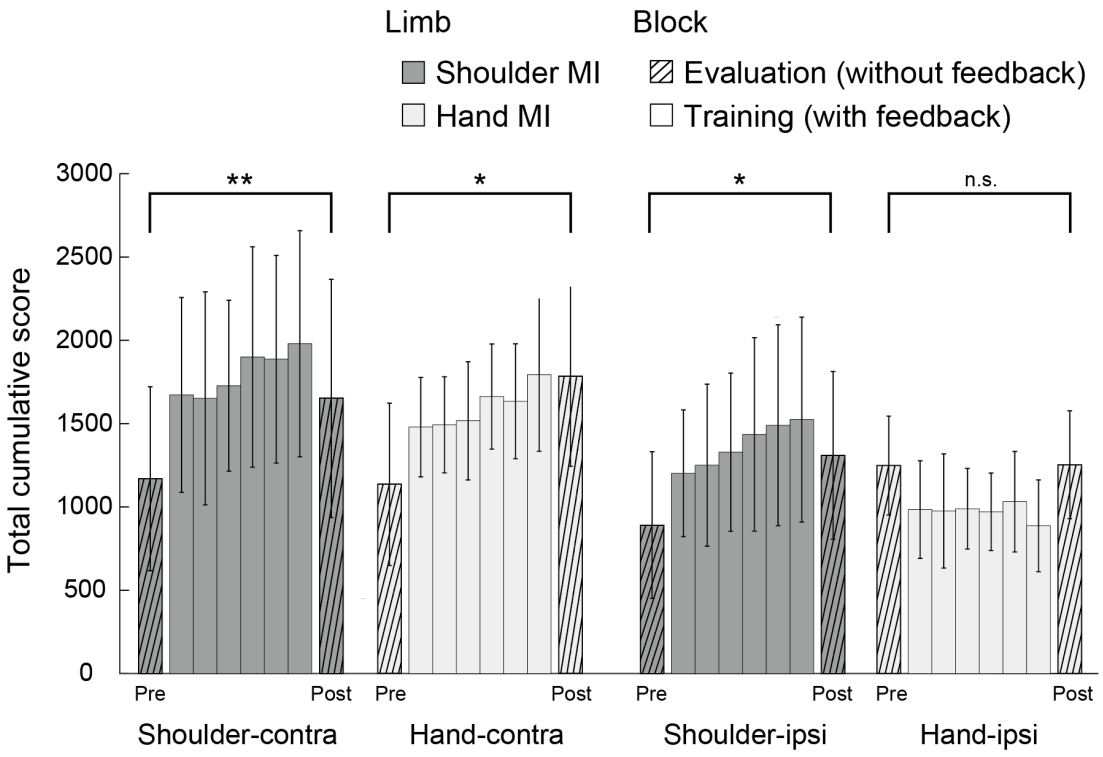

Figure 2-2. Changes in BCI performance (i.e., total cumulative score) in each session
The bars on the left side represent the results of shoulder-contra and Hand-contra sessions, while those on the right side represent the results of Shoulder-ipsi and hand-ipsi sessions. Hatched bars represent evaluation blocks, and those without hatches represent training blocks. Error bars indicate the standard deviation of the mean. The dendrograms above the bars represent the results of the post-hoc analyses. *p < 0.05 and **p < 0.01; all comparisons were Bonferroni corrected.

2.3.2. Effects of BCI-based neurofeedback on SMR-ERD during shoulder MI

Figure 2-3 shows an example of the EEG power time series in the alpha band recorded over the contralateral and ipsilateral SM1 (channels C3 and C4, respectively) in the pre- and post-evaluation blocks of a representative participant. During the Shoulder-contra session, the power in only the contralateral SM1 during the MI epoch decreased after the intervention (**Figure 2-3A**). By contrast, the author observed the opposite effect during the Shoulder-ipsi session, where the power in the contralateral SM1 during MI epoch did not decrease, while that in the ipsilateral SM1 did decrease (**Figure 2-3B**). The representative participant in the figure is a typical example showing the general tendency (the same applies to the subsequent figures).

Spatial patterns of SMR-ERD during the MI epoch in the pre- and post-evaluation blocks of a representative participant are shown in **Figure 2-4A, B**. The SMR-ERDs were localized predominantly in the bilateral parieto-temporal regions (around the C3 and C4 channels and their periphery) during the pre-evaluation block, regardless of whether it was a Shoulder-contra or Shoulder-ipsi session. During the Shoulder-contra session, the contralateral SMR-ERD increased after the neurofeedback training session, whereas the ipsilateral SMR-ERD did not (**Figure 2-4A)**. Conversely, during the Shoulder-ipsi session, the contralateral SMR-ERD did not increase, but the ipsilateral SMR-ERD did (**Figure 2-4B**). During the Shoulder-contra session, the average change in the contralateral SMR-ERD was 15.79% (pre = 9.53%, post = 25.32%, Cohen's d = 0.94). During the Shoulder-ipsi session, however, the average change in the ipsilateral SMR-ERD was 11.27% (pre = -2.21%, post = 9.06%, Cohen's d = 1.02).

The orders and carryover effects from previous sessions were not statistically significant. A two-way ANOVA yielded no main effects for Group ($F_{(3, 32)} = 0.30$, $p = 0.82$) and Phase ($F_{(3, 32)} = 0.03$, $p = 0.99$) and no interaction ($F_{(3, 32)} = 0.43$, $p = 0.91$) in the contralateral SMR-ERD during the pre-evaluation block. Additionally, in the contralateral SMR-ERD during the pre-evaluation block, a two-way ANOVA yielded no main effects for Group ($F_{(3, 32)} = 1.19$, $p = 0.33$) and Phase ($F_{(3, 32)} = 0.02$, $p = 0.99$), and no interaction ($F_{(3, 32)} = 0.66$, $p = 0.74$).

Figure 2-4C, D show Laterality Index (LI) changes during the Shoulder-contra and Shoulder-ipsi sessions, respectively. During the Shoulder-contra session, the LI in the post-evaluation block (-0.113 ± 0.072) was significantly lower than that in the pre-evaluation block (-0.030 ± 0.089) (difference = 0.083, Cohen's $d = 1.76$, $p = 0.023$, paired t-test; **Figure 2-4C**). By contrast, during the Shoulder-ipsi session, the LI in the post-evaluation block (0.017 ± 0.103) was significantly higher than that in the pre-evaluation block (-0.067 ± 0.103) (difference = 0.084, Cohen's $d = 0.86$, $p = 0.039$, paired t-test; **Figure 2-4D**). Target-hemisphere-dependent SMR-ERDs were modulated during both the Shoulder-contra and Shoulder-ipsi sessions, even though participants repeated the same MI under the neurofeedback setting with only a change in the rule of cursor movement (i.e., reversal of x-axis and y-axis).

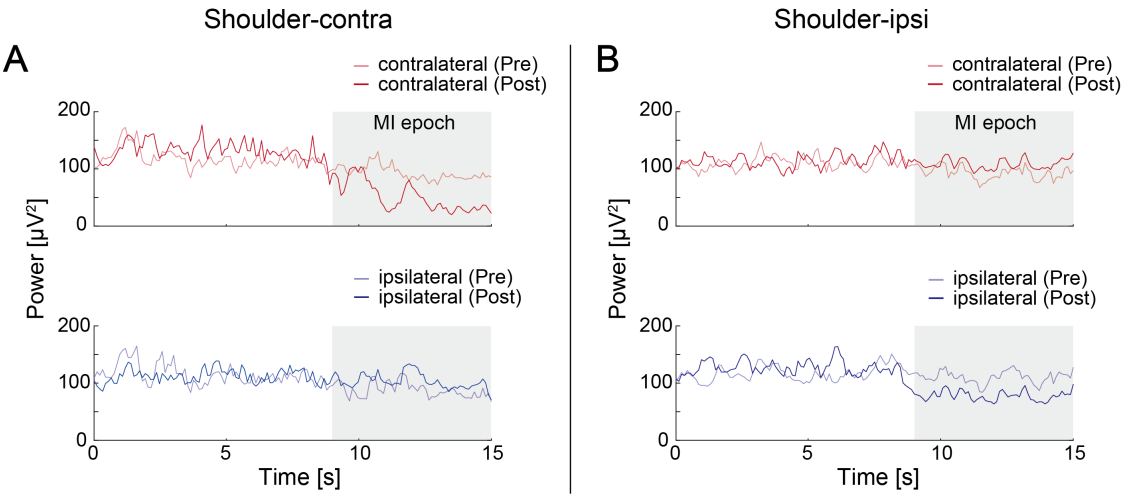

Figure 2-3. EEG power time series in the alpha band

EEG power time series in the alpha band recorded over the contralateral and ipsilateral SM1 (C3 or C4 and its neighboring 6 channels, respectively) during the pre- (light lines) and post-evaluation (dark lines) blocks of a representative participant. The gray shade indicates the motor imagery (MI) epochs. **(A)** Shoulder-contra session. **(B)** Shoulder-ipsi session.

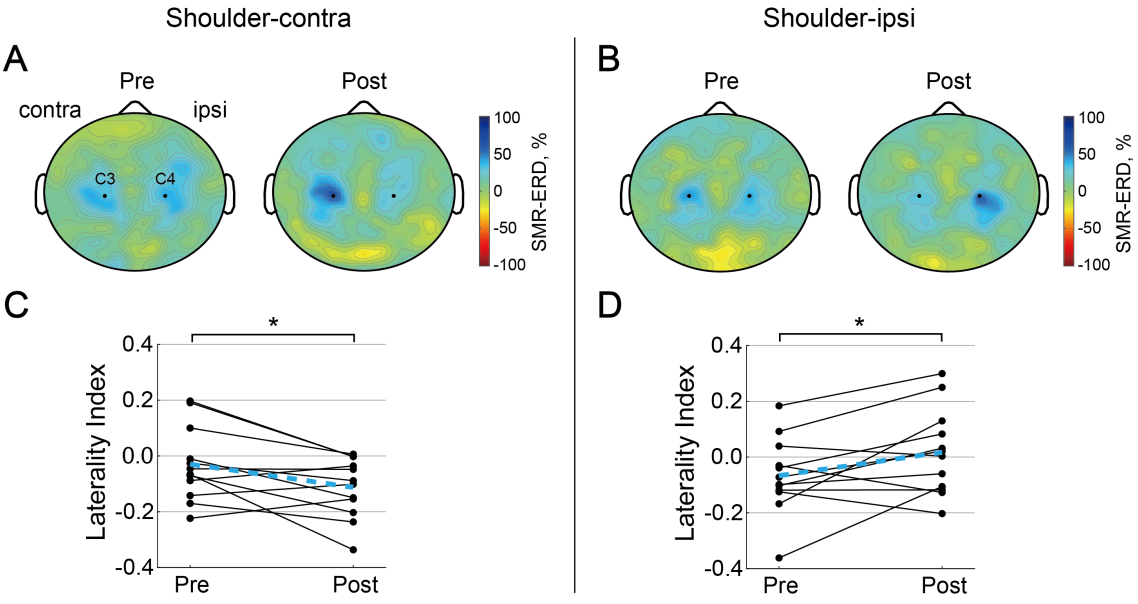

Figure 2-4. Effects of shoulder MI-associated neurofeedback on SMR-ERD

(A), (B) Spatial patterns of SMR-ERD during the MI epoch in the pre- and post-evaluation blocks of a representative participant. The large positive values (blue colors)

represent larger SMR-ERD (i.e., higher excitability of the SM1). The black dots represent the C3 and C4 channels. **(C), (D)** Laterality index (LI) in the pre- and post-evaluation blocks of all participants. LI yields a value of 1 or -1 when the activity is purely ipsilateral or contralateral, respectively. Each solid line represents one participant and dashed blue lines represent mean values. *$p < 0.05$, paired *t*-test.

2.3.3. Effects of BCI-based neurofeedback on resting-state functional connectivity during shoulder MI

The author assessed seed-based corrected imaginary part of coherence (ciCOH during the resting-state in the pre- and post-evaluation blocks to evaluate interregional synchronization (i.e., functional connectivity). **Figure 2-5A, B** show significant intrahemispheric connections in each hemisphere of a representative participant**.** The number of significant connections in the contralateral hemisphere increased from the pre- to the post- epochs during the Shoulder-contra session, whereas it increased in the ipsilateral hemisphere during the Shoulder-ipsi session (**Figure 2-5B**). Intrahemispheric network intensity changes in the targeted hemisphere during the Shoulder-contra and Shoulder-ipsi sessions are shown in **Figure 2-5C** and **D**, respectively. During the Shoulder-contra session, the network intensity on the contralateral side was significantly higher in the post-evaluation block (12.57 ± 3.35) than it was in the pre-evaluation block (10.09 ± 1.73) (difference = 2.47, Cohen's $d = 0.93$, $p = 0.032$, paired t-test; **Figure 2-5C**). At the same time, there was no difference in network intensity on the ipsilateral side (i.e., non-targeted hemisphere) between the pre- and post-evaluation blocks (10.57 ± 1.85 and 10.07 ± 1.65, respectively; difference = -0.50, Cohen's $d = 0.29$, $p = 0.473$, paired t-test).

Similarly during the Shoulder-ipsi session, the ipsilateral network intensity was significantly higher in the post-evaluation block (11.76 ± 2.46) than in the pre-evaluation block (9.50 ± 2.93) (difference = 2.26, Cohen's $d = 0.84$, $p = 0.033$, paired t-test; **Figure 2-5D**), and there was no difference in the contralateral network intensity (i.e., non-targeted hemisphere) between the pre- and post-evaluation blocks (10.09 ± 2.29 and 10.62 ± 2.43, respectively; difference = 0.53, Cohen's $d = 0.22$, $p = 0.217$, paired t-test).

Figure 2-5E, F show significant *inter*hemispheric connections of a representative participant, which increased during both the Shoulder-contra and Shoulder-ipsi sessions. Changes in interhemispheric network intensity for all participants during the Shoulder-contra and Shoulder-ipsi sessions are outlined in **Figure 2-5G** and **H**, respectively. During the Shoulder-contra session, the interhemispheric network intensity was significantly higher during the post-evaluation block (2.01 ± 0.28) than during the pre-evaluation block (1.80 ± 0.19; difference = 0.21, Cohen's $d = 0.88$, $p = 0.030$, paired t-test; **Figure 2-5G**). Similarly, during the Shoulder-ipsi session, the interhemispheric network intensity was significantly higher in the post-evaluation block (2.09 ± 0.42) than in the pre-evaluation block (1.77 ± 0.37) (difference = 0.31, Cohen's $d = 0.81$, $p = 0.006$, paired t-test; **Figure 2-5H**).

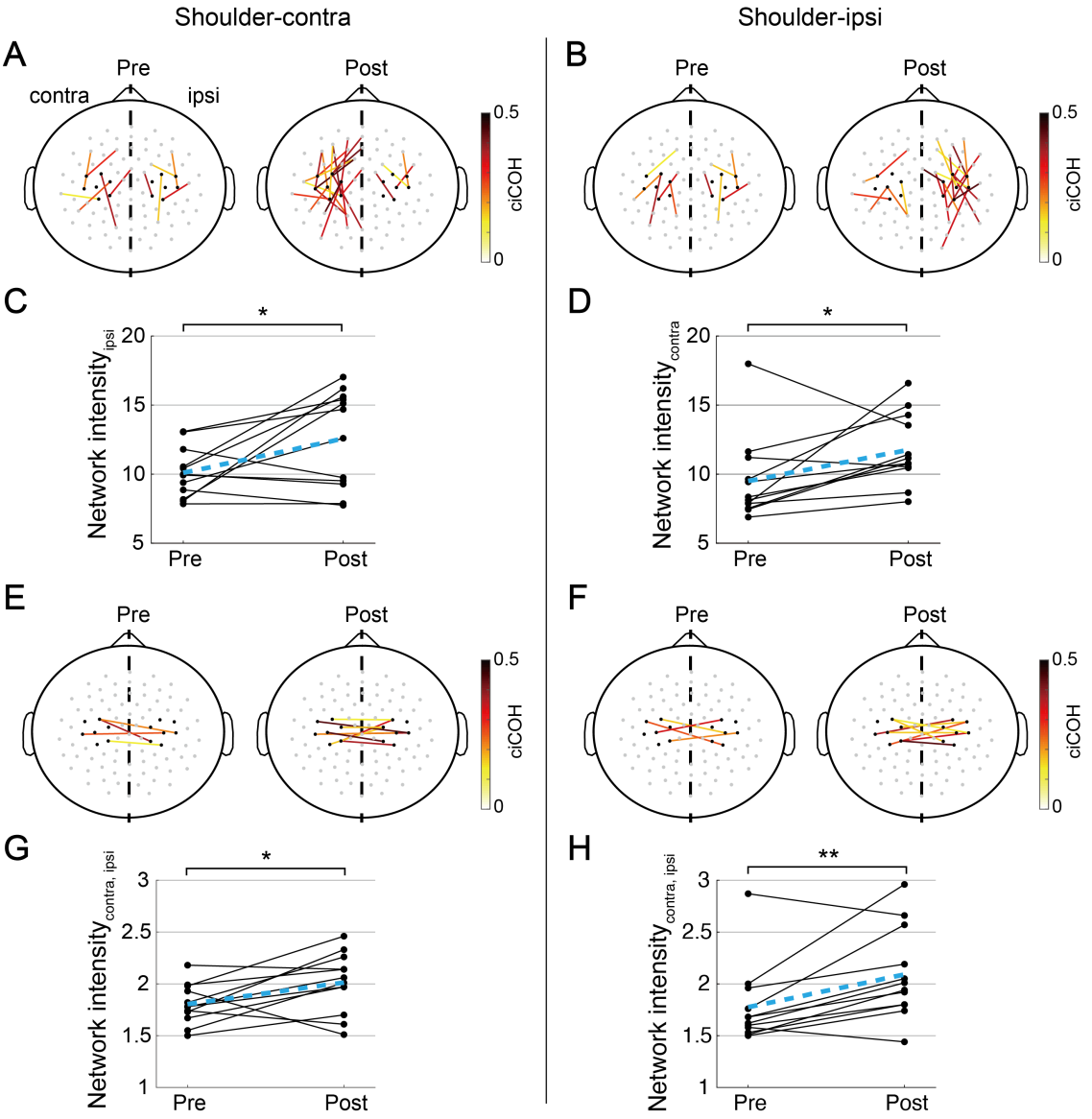

Figure 2-5. Effects of shoulder MI-associated neurofeedback on resting-state functional connectivity

(A), (B) Significant intrahemispheric connections (see "Connectivity Analysis" in Methods) in each hemisphere during the pre- and post-evaluation blocks of a representative participant. Each solid line indicates a significant connection, and the large positive values (dark red colors) represent strong connections. The black dots around the bilateral SM1 denote the seed channels, C3 or C4, and their neighboring 6 channels. The gray dots represent other EEG channels. **(C), (D)** Intrahemispheric network intensity within the contralateral and ipsilateral hemispheres (i.e., targeted hemisphere) during the Shoulder-contra **(C)** and Shoulder-ipsi **(D)** sessions. Each solid line represents one participant and dashed blue lines represent mean values. *$p < 0.05$, paired t-test. **(E), (F)**

Significant interhemispheric connections in the pre- and post-evaluation blocks of a representative participant. **(G), (H)** Interhemispheric network intensity between the contralateral and ipsilateral SM1 in Shoulder-contra **(G)** and Shoulder-ipsi **(H)** sessions. *$p < 0.05$, **$p < 0.01$, paired *t*-test.

2.3.4. Correlation between SMR-ERD and resting-state functional connectivity during shoulder MI

A correlation analysis was conducted to determine whether intrahemispheric/interhemispheric functional connectivity at rest was associated with regional SMR-ERD modulation during the MI epoch. The relationships between the changes in SMR-ERD in a targeted hemisphere (ΔSMR-ERD$_{hem}$) and changes in intrahemispheric network intensity in a targeted hemisphere (ΔNetwork intensity$_{hem}$) during the Shoulder-contra and Shoulder-ipsi sessions are shown in **Figure 2-6A** and **B**, respectively. During the Shoulder-contra session, considering the intrahemispheric connectivity, there was a correlation between ΔSMR-ERD$_{contra}$ and ΔNetwork intensity$_{contra}$ ($\rho = 0.594$, $p = 0.046$, Spearman's rank correlation), but not between ΔSMR-ERD$_{ipsi}$ and ΔNetwork intensity$_{ipsi}$ (i.e., non-targeted hemisphere; $\rho = 0.077$, $p = 0.817$, Spearman's rank correlation; **Figure 2-6A**). Similarly, during the Shoulder-ipsi session, ΔSMR-ERD$_{ipsi}$ and ΔNetwork intensity$_{ipsi}$ were correlated ($\rho = 0.583$, $p < 0.047$, Spearman's rank correlation), while ΔSMR-ERD$_{contra}$ and ΔNetwork intensity$_{contra}$ (i.e., non-targeted hemisphere) were not ($\rho = 0.035$, $p = 0.921$, Spearman's rank correlation; **Figure 2-6B**). Thus, changes in SMR-ERDs were associated with intrahemispheric network intensity only in the targeted hemisphere. **Figure 2-6C, D** outline the correlation

between ΔSMR-ERD$_{hem}$ and interhemispheric network intensity (ΔNetwork intensity$_{contra, ipsi}$) during the Shoulder-contra session (ρ = 0.608, p = 0.040, Spearman's rank correlation) and between the ΔSMR-ERD$_{ipsi}$ and ΔNetwork intensity$_{contra, ipsi}$ during the Shoulder-ipsi session (ρ = 0.713, p = 0.012, Spearman's rank correlation), respectively.

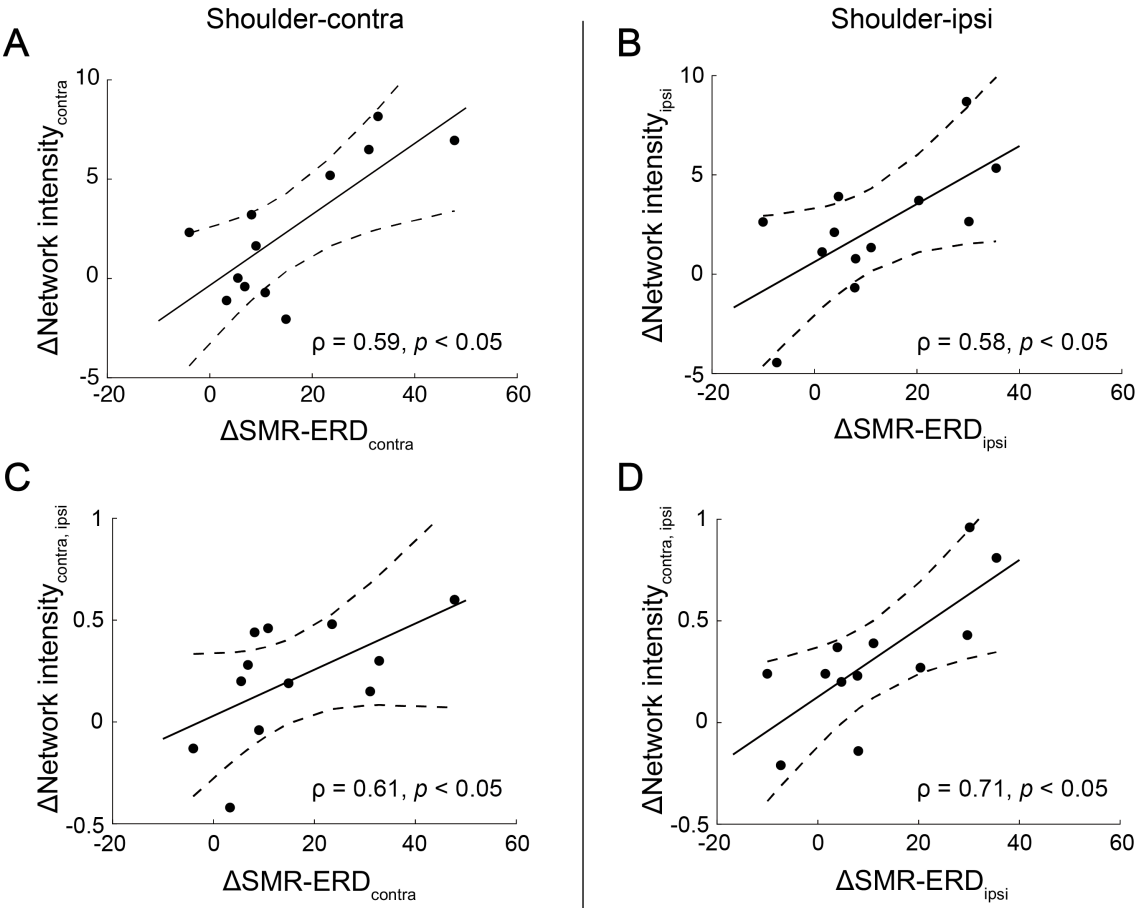

Figure 2-6. Correlation between SMR-ERD and resting-state functional connectivity

(A), (B) The associations between changes in SMR-ERD and in *intra*hemispheric network intensity (ΔNetwork intensity) in the targeted hemisphere during the Shoulder-contra **(A)** and Shoulder-ipsi **(B)** sessions. **(C), (D)** the associations between ΔSMR-ERD in the targeted hemisphere and in *inter*hemispheric network intensity (ΔNetwork intensity$_{contra, ipsi}$) during the Shoulder-contra **(C)** and Shoulder-ipsi **(D)** sessions. Each dot

represents one participant. Solid and dotted lines indicate the estimated linear regression and 95% confidence interval, respectively. Spearman's rank correlation.

2.3.5. Effects of BCI-based neurofeedback on SMR-ERD during hand MI

Figure 2-7A, B illustrate the spatial patterns of SMR-ERD during the MI epoch in the pre- and post-evaluation blocks of a representative participant. During the pre-evaluation block, SMR-ERDs were localized predominantly in the bilateral parieto-temporal regions (around the C3 and C4 channels and their periphery) regardless of whether it was a Hand-contra or Hand-ipsi session, as in the shoulder MI sessions. During the Hand-contra session, the contralateral SMR-ERD increased after the neurofeedback session, whereas the ipsilateral SMR-ERD did not (**Figure 2-7A**). In contrast, during the Hand-ipsi session there was no increase in either the contralateral or ipsilateral SMR-ERDs (**Figure 2-7B)**. The average change in the contralateral SMR-ERD during the Hand-contra session was 12.02% (pre = 12.60%, post = 24.62%, Cohen's d = 0.68). The average change in the ipsilateral SMR-ERD during the Hand-ipsi session was 2.17% (pre = -2.86%, post = -0.69%, Cohen's d = 0.16).

During the Hand-contra session the LI was significantly lower in the post-evaluation block (-0.143 ± 0.091) than in the pre-evaluation block (-0.043 ± 0.064) (difference = -0.100, Cohen's d = 1.29, p = 0.008, paired t-test; **Figure 2-7C**). However, during the Hand-ipsi sessions, there was no significant difference in LI between the post-evaluation (-0.044 ± 0.051) and pre-evaluation (-0.042 ± 0.060) blocks (difference = -0.001, Cohen's d = 0.02, p = 0.96, paired t-test; **Figure 2-7D**).

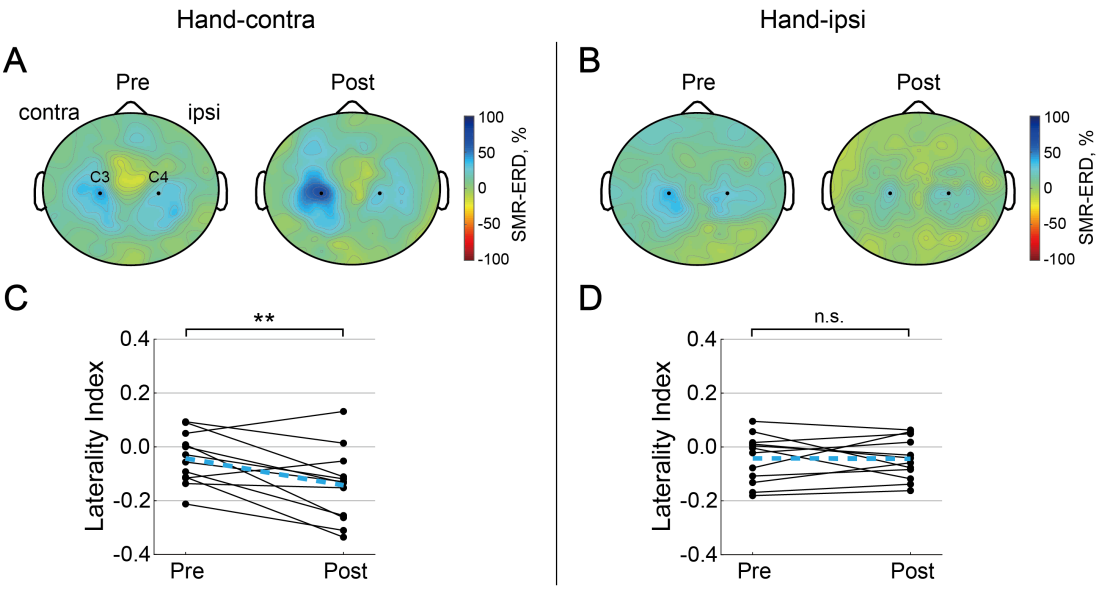

Figure 2-7. Effects of hand MI-associated neurofeedback on SMR-ERD

(A), (B) Spatial patterns of SMR-ERD during the MI epochs in the pre- and post-evaluation blocks of a representative participant. The large positive values (blue colors) represent larger SMR-ERD (i.e., higher excitability of the SM1). The black dots represent the C3 and C4 channels. **(C), (D)** Laterality index (LI) in the pre- and post-evaluation blocks of all participants. LI yields a value of 1 or -1 when the activity was purely ipsilateral or contralateral, respectively. Each solid line represents one participant and dashed blue lines represent mean values. $^{**}p < 0.01$, paired *t*-test.

2.3.6. Effects of BCI-based neurofeedback on resting-state functional connectivity during hand MI

During the Hand-contra session, the contralateral network intensity was significantly higher in the post-evaluation block (12.76 ± 2.69) than in the pre-evaluation block (10.18 ± 1.71) (difference = 12.02, Cohen's d = 1.14, p = 0.004, paired t-test); however, there was no difference in the ipsilateral network intensity (i.e., non-targeted hemisphere) between pre- and post-evaluation block (9.33 ± 1.38 and 9.23 ± 1.74, respectively;

difference = -0.10, Cohen's d = 0.07, p = 0.858, paired t-test). Alternatively, during the Hand-ipsi session, there were no differences in either the ipsilateral network intensity between the post- and pre-evaluation blocks (9.79 ± 1.73 and 10.09 ± 3.31, respectively; difference = -0.30, Cohen's d = 0.11, p = 0.707, paired t-test) or the contralateral network intensity (i.e., non-targeted hemisphere) between the pre- and post-evaluation blocks (9.77 ± 1.90 and 10.98 ± 3.09, respectively; difference = 1.21, Cohen's d = 0.47, p = 0.123, paired t-test).

During the Hand-contra session, the interhemispheric network intensity in the post-evaluation block (2.04 ± 0.29) was significantly higher than that in the pre-evaluation block (1.85 ± 0.17) (difference = 0.18, Cohen's d = 0.82, p = 0.032, paired t-test). By contrast, during the Hand-ipsi session, there was no difference in the interhemispheric network intensity between the post- and pre-evaluation blocks (1.98 ± 0.39 and 1.82 ± 0.41, respectively; difference = 0.17, Cohen's d = 0.41, p = 0.263, paired t-test).

2.3.7. Correlation between SMR-ERD and resting-state functional connectivity during hand MI

During the Hand-contra session, considering the intrahemispheric connectivity, there was a correlation between ΔSMR-ERD$_{contra}$ and ΔNetwork intensity$_{contra}$ (ρ = 0.706, p = 0.013, Spearman's rank correlation), whereas ΔSMR-ERD$_{ipsi}$ and ΔNetwork intensity$_{ipsi}$ (i.e., non-targeted hemisphere) were not correlated (ρ = 0.336, p = 0.287, Spearman's rank correlation). In contrast during the Hand-ipsi session, no significant correlations were

found between ΔSMR-ERD and ΔNetwork intensity in either hemisphere (contralateral: $\rho = 0.343$, $p = 0.276$, ipsilateral: $\rho = 0.231$, $p = 0.471$, Spearman's rank correlation).

During the Hand-contra session, there was a positive correlation between ΔSMR-ERD in the targeted hemisphere and $\Delta\text{Network intensity}_{\text{contra, ipsi}}$ ($\rho = 0.657$, $p = 0.024$, Spearman's rank correlation), but there was no significant correlation between $\Delta\text{SMR-ERD}_{\text{ipsi}}$ and $\Delta\text{Network intensity}_{\text{contra, ipsi}}$ ($\rho = -0.126$, $p < 0.670$, Spearman's rank correlation) during the Hand-ipsi session.

2.3.8. Comparison of SMR-ERDs during shoulder MI and hand MI

Comparing the spatial patterns of SMR-ERD during shoulder and hand MIs (**Figure 2-4** and **Figure 2-7**), there was no significant difference in the contralateral/ipsilateral SMR-ERDs in the pre-evaluation block between shoulder and hand MIs (contralateral SMR-ERD: $p = 0.154$, ipsilateral SMR-ERD: $p = 0.803$). Additionally, the strongest contralateral/ipsilateral SMR-ERDs were seen at the C3/C4 channels in both shoulder and hand MIs, indicating there was no spatial difference due to low spatial resolution of EEG.

To further examine the effectiveness in BCI-based neurofeedback training purported to lateralize sensorimotor cortical activities, the author compared the changes in SMR-ERD during shoulder MI and hand MI (**Figure 2-8**). A three-way ANOVA revealed a significant interaction between Session × Hemisphere × Limb ($F_{(1, 88)} = 4.98$, $p = 0.047$) and Session × Hemisphere ($F_{(1, 88)} = 26.7$, $p < 0.001$), but no interaction between Session × Limb ($F_{(1, 88)} = 1.44$, $p = 0.255$) or Hemisphere × Limb ($F_{(1, 88)} = 2.06$

$p = 0.179$). Although Limb had a significant main effect ($F_{(1, 88)} = 5.43$, $p = 0.040$), Session ($F_{(1, 88)} = 1.29$, $p = 0.28$) and Hemisphere ($F_{(1, 88)} = 2.39$, $p = 0.15$) did not have any effects. Post-hoc two-way ANOVA with Hemisphere × Limb in the sessions aiming for lateralization to the contralateral hemisphere (i.e., Shoulder-contra and Hand-contra) showed a significant main effect for Hemisphere ($F_{(1, 44)} = 12.39$, $p = 0.001$); however, there was no main effect for Limb ($F_{(1, 44)} = 0.27$, $p = 0.608$) and no interaction ($F_{(1, 44)} = 0.30$, $p = 0.589$). By contrast, post-hoc two-way ANOVA with Hemisphere × Limb in the sessions aiming for lateralization to the ipsilateral hemisphere (i.e., Shoulder-ipsi and Hand-ipsi) indicated a significant main effect for Hemisphere ($F_{(1, 44)} = 4.51$, $p = 0.039$) and interaction ($F_{(1, 44)} = 5.70$, $p = 0.021$), but no main effect for Limb ($F_{(1, 44)} = 1.99$, $p = 0.166$). Thus, there were interhemispheric differences in ΔSMR-ERD during the shoulder MI and hand MI tasks. Moreover, a post-hoc paired *t*-test demonstrated a significant difference in Hemisphere ($p = 0.001$) during shoulder MI, but no difference in Hemisphere ($p = 0.859$) during hand MI (Bonferroni corrected). Thus, the ΔSMR-ERD in the ipsilateral hemisphere was significantly more positive than that in the contralateral hemisphere during the shoulder MI task, but no significant difference was observed during the hand MI task.

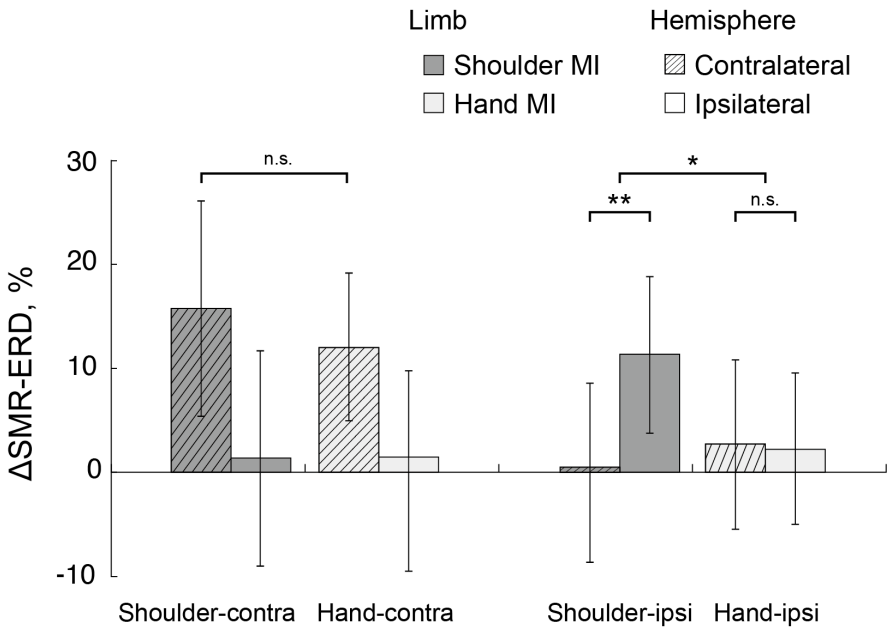

Figure 2-8. Two-way interaction in ΔSMR-ERD during shoulder MI and hand MI tasks

The four bars on the left represent the results of Shoulder-contra and Hand-contra sessions, while those on the right represent the results of Shoulder-ipsi and Hand-ipsi sessions. Bars with hatched lines represent the contralateral hemisphere, and those without shading represent the ipsilateral hemisphere. Error bars indicate the standard deviation of the mean. The dendrogram above the bars in the sessions aiming at lateralization to the ipsilateral hemisphere represent the results of the post-hoc analyses. *$p < 0.05$ and **$p < 0.01$; all comparisons were Bonferroni corrected.

2.4. Discussion

In the chapter, subjects participated in four neurofeedback training sessions on separate days in a double-blind, randomized, within-subject crossover design. During the Shoulder-contra and Shoulder-ipsi sessions, the SMR-ERD in the targeted contralateral and ipsilateral hemispheres, respectively, increased selectively after a single one-hour intervention (i.e., there was no increase in the non-targeted hemisphere). Additionally, the intrahemispheric and interhemispheric network intensities involving the targeted

hemisphere evaluated by ciCOH also increased during both the Shoulder-contra and Shoulder-ipsi sessions. Conversely, after hand MI-associated neurofeedback training, the contralateral SMR-ERD increased selectively during the Hand-contra session, but the ipsilateral SMR-ERD did not increase during the Hand-ipsi session. In neurofeedback training session, the author used time-smoothed power in order to reduce flickering and improved the signal-to-noise ratio of the SMR signal (He et al., 2020; Kober et al., 2018), which is beneficial for effective neurofeedback. However, time-smoothing causes a time delay in a trade-off manner. In addition, optimal smooth depth for SMR-ERD also remains debatable. Those are open questions, and future studies will clarify them.

During Shoulder-contra and Hand-contra sessions, the contralateral SMR-ERD to the imagined limb increased. Previous studies also demonstrated up-conditioning of the contralateral SM1 using contralateral-based neurofeedback during hand MI (Ang et al., 2011; Birbaumer and Cohen, 2007; Caria et al., 2011; Daly and Wolpaw, 2008; Prasad et al., 2010; Shindo et al., 2011). Repetitive induction of the SMR-ERD contralateral to the imagined limb through visual or sensory feedback with neuromuscular electrical stimulation or robotic movement supports are considered to induce the use-dependent, error-based, and/or Hebbian-like plasticity of the contralateral SM1 (Birbaumer and Cohen, 2007; Gharabaghi et al., 2014; Soekadar et al., 2015a; Ushiba and Soekadar, 2016). As contralateral SMR-ERD is a surrogate monitoring marker of contralateral SM1 excitability during MI (Takemi et al., 2013, 2015), BCI-based neurofeedback can promote operant learning of contralateral sensorimotor cortical activity. This is an expected phenomenon because distal muscles such as the EDC muscle are innervated

from the contralateral hemisphere, which is most influential for muscle contraction (Carson, 2005; Colebatch et al., 1990).

However, the BCI-based neurofeedback-derived SMR signal from the contralateral hemisphere does not always guarantee spatially specific activation of the contralateral SM1 because both hemispheres are connected by intrinsic transcallosal projections and exhibit functional crosstalk (Arai et al., 2011; Hofer and Frahm, 2006; Meyer et al., 1995; Waters et al., 2017). Indeed, conventional contralateral-based BCI-based neurofeedback has induced a global increase including the ipsilateral SMR-ERD, indicating conventional BCI is considered as a modulation technique without spatial specificity (Birbaumer and Cohen, 2007; Caria et al., 2011; Ono et al., 2014; Pichiorri et al., 2015; Shindo et al., 2011). A key advantage of our study was that the BCI-based neurofeedback that the author developed monitored both contralateral and ipsilateral SMR-ERDs, demonstrating explicitly guided sensorimotor cortical activation in the targeted contralateral hemisphere alone.

During the shoulder-ipsi session, the ipsilateral SMR-ERD increased significantly. Although increasing evidence suggests that the contribution of the ipsilateral hemisphere is salient in motor control (Bundy et al., 2017; Derosière et al., 2014; Dodd et al., 2017; Ward et al., 2003b, 2003a), no previous study has shown that sensorimotor cortical activity can be guided to the ipsilateral hemisphere. Chiew and his colleagues indicated that different MI-based (right and left hands) fMRI neurofeedbacks of the LI (i.e., the difference in BOLD responses between the contralateral M1 and the ipsilateral M1 to the imagined hand) is capable of lateralizing to the contralateral hemisphere (Chiew et al.,

2012) but lateralizing to the ipsilateral was not successful due to “hand” MI-associated neurofeedback. Therefore, our study is the first to clear that BCI-based neurofeedback is a potent up-regulator of hemispheric activation to the targeted hemisphere, either contralaterally or ipsilaterally in the same participants, depending on the targeted muscle.

Successful up-conditioning of the ipsilateral SM1 during shoulder MI may be associated with its neuroanatomical properties, because ipsilateral SMR-ERD reflects the excitability of the ipsilateral corticospinal tract (CST) (Hasegawa et al., 2017), which mainly innervates proximal muscles (Alawieh et al., 2017; Carson, 2005). Unlike hand motor muscles, the functional recovery of axial or shoulder muscles following stroke hemiplegia is promoted by unmasking the ipsilateral pathway to the paretic hand (Colebatch et al., 1990; Muellbacher et al., 2002; Schwerin et al., 2008). Thus, neurofeedback aimed at ipsilateral lateralization would be conceptually useful for stroke rehabilitation, particularly for functional maturation of ipsilateral CST and proximal muscle motor recovery.

During the Hand-ipsi session, the ipsilateral SMR-ERD did not increase. This implied that the extent of corticospinal projection from the ipsilateral hemisphere to the imagined body part affected the modulation of the laterality of sensorimotor cortical activity. With recent developments in neuroimaging techniques, there is an emerging interest in understanding the intrinsic functional and structural architecture of the brain that underlies successful learning of brain activity. For example, research probing the prediction of BCI aptitude from individual brain structures demonstrated that the integrity and myelination quality of deep white matter structures, such as the corpus callosum,

cingulum, and superior fronto-occipital fascicle, were positively correlated with individual BCI-performance (Halder et al., 2013). Additionally, it has been suggested that changes in the integrity of the contralesional CST may be accompanied by improved BCI-performance after stroke (Young et al., 2016). The current literature makes it clear that there is a relationship between neuroanatomical characteristics and voluntary control of brain activity. Therefore, our findings implied that intrinsic neuroanatomical properties such as the CST constrain the effectiveness in BCI-based neurofeedback training purported to lateralize sensorimotor cortical activities. Moreover, our neuroanatomically-inspired approach enabled us to investigate potent neural remodeling functions that underlie BCI-based neurofeedback. Future work that approaches the further understandings of differences in BCI-learning is warranted.

The intrahemispheric and interhemispheric network intensities involving the targeted hemisphere were modulated during the Shoulder-contra, Shoulder-ipsi, and Hand-contra sessions. Additionally, increases in network intensity were correlated with those in SMR-ERD. Several previous studies demonstrated altered resting-state functional connectivities in the targeted hemisphere and bi-hemispherically after BCI-based neurofeedback interventions (Bauer et al., 2015; Hamedi et al., 2016; Pichiorri et al., 2015). These findings indicate that changes in functional connectivity induced by BCI-based neurofeedback may be caused by the interplay with associative brain regions, because those regions are functionally and/or anatomically connected. Furthermore, Várkuti and his colleagues used fMRI to provide detailed spatial evidence that functional connectivity of the supplementary motor area, bilateral motor cortices, and associative

cortical regions increased after BCI-based neurofeedback intervention (Várkuti et al., 2013). Importantly, our findings that the interhemispheric network intensities increased after the Shoulder-contra, Shoulder-ipsi, and Hand-contra sessions are compatible with this, under the assumption that bilateral SM1 acts cooperatively in the generation of actual/imagined movements (Derosière et al., 2014; Gao et al., 2011; Hamedi et al., 2016). Therefore, the proposed neurofeedback technique might modulate not only local oscillatory power entrainment but also interregional neural communications. Future studies are expected to reveal directed signal flows for networks between these motor-related brain regions through analysis of effective connectivity.

The author focused on functional connectivity during the "resting-state" to examine intrinsic connectivity traits of the individual brain, presumably related to neural cooperation at rest (De Luca et al., 2006). Although there is ongoing discussion about the nature of resting-state functional connectivity (Cordes et al., 2001; Fransson, 2005; Greicius et al., 2003), recent studies demonstrated an association between resting-state networks and stages of brain reorganizational processes (Grefkes and Fink, 2011; Mizuguchi et al., 2019; Westlake and Nagarajan, 2011). The analysis of resting-state functional connectivity promises to become a significant neurophysiological measure for tracking progress after neurorehabilitation or neurofeedback.

Chapter 3: Spatially bivariate BCI-based neurofeedback can manipulate interhemispheric inhibition

* This chapter was based on the following author's original article:
"Hayashi M, Okuyama K, Mizuguchi N, Hirose R, Okamoto T, Kawakami M, Ushiba J, Spatially bivariate EEG-neurofeedback can manipulate interhemispheric inhibition. *eLife* 11, 76411 (29 pages), 2022".
The author has a right to use this dissertation.

3.1. Introduction

Human behavior requires interregional crosstalk to use the sensorimotor processes in the brain. Although non-invasive brain stimulation techniques, such as rTMS and tDCS, have been used to manipulate the interhemispheric sensorimotor activity (Boddsington and Reynolds, 2017; Gilio et al., 2003; Williams et al., 2010), a central controversy exists regarding whether this activity can be volitionally controlled (**Figure 3-1A**). Because both hemispheres are structurally and functionally connected, it is likely that the balance between bilateral SMR-ERDs and transcallosal excitability states are linked, as indicated by common variation in the conditioning MEP amplitude and IHI (Ferbert et al., 1992; Ghosh et al., 2013; Ni et al., 2009).

In Chapter 2, our results suggested that spatially bivariate BCI-based neurofeedback allows volitional modulation of SMR amplitude in both hemispheres and guides sensorimotor cortical activation in the contralateral or ipsilateral targeted hemisphere. Using this technique, in this chapter, the author sought to investigate the association of IHI with the balance of SMR-ERDs to understand the inhibitory

sensorimotor functions of interhemispheric interaction that may critically depend on the oscillatory brain activity in both hemispheres. Furthermore, because changes in the oscillatory brain activity influenced IHI, the author tested whether IHI can be manipulated using a dual-coil paired-pulse TMS protocol (Daskalakis et al., 2002; Ferbert et al., 1992). To assess the association of IHI with ongoing oscillatory brain activity, TMS pulses were triggered in real time at pre-determined bilateral SMR amplitudes. This system enables participants to control the bivariate sensorimotor excitability, and determines whether it is possible to manipulate the IHI magnitude.

Using the novel closed-loop bivariate (bi-hemispheric brain state-dependent) EEG-triggered dual-coil paired-pulse TMS system (bi-EEG-triggered dual-TMS), the author evaluated the effects of different states of the targeted bidirectional up- or down-regulated one-sided hemisphere on the effective inhibitory interhemispheric network expressed by IHI. The states included (1) resting state (REST), (2) right finger motor imagery without visual feedback (NoFB), and (3) high, (4) middle (MID), and (5) low (LOW) excitability states of the ipsilateral SM1 (conditioning side) to the unilateral imagined hand movement while maintaining constant the contralateral excitability during BCI-based neurofeedback (**Figure 3-1B**). Inspired by the findings that SMR-ERD was associated with corticospinal excitability amplitude (Takemi et al., 2013, 2015), the author hypothesized that the ipsilateral SMR-ERD to the imagined (right) hand is a potent up- or down-regulator of IHI from the ipsilateral (right) to the contralateral (left) hemisphere.

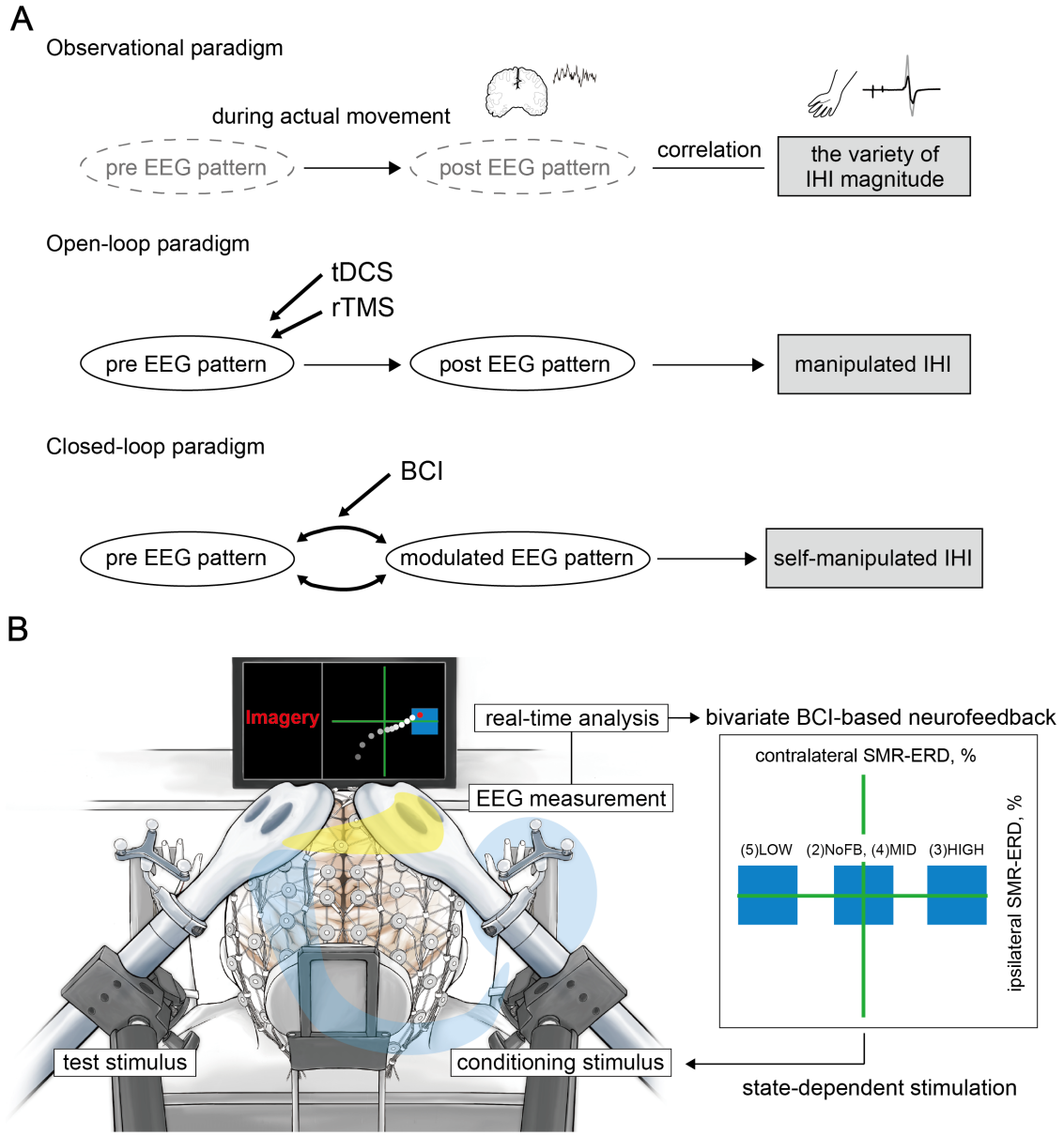

Figure 3-1. Conceptual illustration of the current study and experimental overview

(A) When a certain stimulus was input into the system, the brain was considered to vary with the state, resulting in IHI changes. The upper panel highlights the experimental limitations in the observational paradigm due to a variety of IHI magnitudes observed during the actual movement. In this case, it is unclear whether the changes in EEG patterns in both hemispheres would affect IHI. The middle panel indicates that it is unclear whether it is possible to manipulate the inhibitory interhemispheric sensorimotor activity in the open-loop neuromodulation paradigm using tDCS or rTMS. The lower panel shows that specific EEG patterns are associated with IHI magnitude, and BCI-based neurofeedback modulates the EEG activities. Therefore, if bilateral EEG patterns that

underlie IHI are identified, we may be able to volitionally regulate the IHI magnitude via BCI-based neurofeedback, suggesting the possibility of plastic interhemispheric balancing. **(B)** The current bi-EEG-triggered dual-TMS experimental system involved spatially bivariate BCI-based neurofeedback that allows volitional modulation of EEG patterns only in the targeted hemisphere, which may enable us to verify our hypothesis. Different states of the targeted bidirectional up- and down-regulated ipsilateral hemisphere to the imagined hand while maintaining constant the contralateral excitability were tested in the following states: (1) resting state, (2) motor imagery without visual feedback, and (3) high, (4) middle, and (5) low excitability states. The blue target box, based on the predetermined SMR-ERDs, was displayed corresponding to each session. A cue signal was generated to trigger the conditioning stimulus when the signal reached the target box. The yellow line on the head represents the signal flow from the conditioning hemisphere that modifies the contralateral side through the corpus callosum, and the blue line represents the test stimulus toward the right hand.

3.2. Materials and Methods

3.2.1. Study design

The current study was performed in accordance with approved guidelines and regulations, such as the CONSORT Statement (Moher et al., 2001) and CRED-nf checklist (Ros et al., 2020). The experiment consisted of five sessions: (1) resting-state (REST); (2) right finger MI without visual feedback (NoFB), (3) high (HIGH); (4) middle (MID); and (5) low (LOW) excitability states of the ipsilateral SM1 during BCI-based neurofeedback (details in "Experimental sessions"). The difference of IHI magnitude in the last three sessions (i.e., HIGH, MID, and LOW sessions) was the primary dependent variable of interest. The three neurofeedback sessions were conducted in a randomized order across participants. Prior to the three sessions, REST and NoFB sessions were performed to

estimate individual baseline during rest and MI for the offline analysis.

To estimate the appropriate sample size for this study, a preliminary experiment was conducted before the main experiment. In the preliminary experiment, four healthy participants (not included in the main experiment) performed BCI-based neurofeedback training and underwent brain state-dependent dual-coil brain stimulation, similar to the main experiment. The author calculated the IHI magnitude in each session. Then, an a priori power analysis ($\alpha = 0.05$, $1\text{-}\beta = 0.8$, two-sided tests, Bonferroni corrected) focusing on the IHI magnitude using the statistical package G*Power 3.1 (Faul et al., 2009) was conducted. Because the preliminary experiment showed a large effect size on the IHI differences between HIGH (65.0 ± 22.8, mean ± SD) and MID (90.7 ± 23.4) sessions (Cohen's $d = 1.12$), and between MID (90.7 ± 23.4) and LOW (106.3 ± 13.1) sessions (Cohen's $d = 0.82$), the author calculated that 24 participants were needed (Cohen, 1992). Since the primary outcome differed from Chapter 2 which evaluated the ERD change, the estimated number of participants was also different.

3.2.2. Participants

Twenty-four volunteers (2 females and 22 males; mean age ± SD: 23.4 ± 2.0 years; age range: 21–27 years) participated in this study. All participants had normal or corrected-to-normal vision and reported no history of neurological or psychological disorders. All participants were right-handed (Laterality Quotient: 72.2 ± 30.9%) as assessed by the Edinburgh Inventory (Oldfield, 1971). Two participants were not applied the TMS procedure due to the higher RMT (greater than 70% of the maximum stimulator output

[MSO]) of the right or left FDI muscles. This criterion ensured that the TMS stimulator would be able to perform at the required intensities for the whole duration of the experiment (Stefanou et al., 2018; Zrenner et al., 2018). The author did not exclude participants based on the EEG characteristics such as the magnitude of their endogenous SMR activity (Madsen et al., 2019; Safeldt et al., 2017), to verify our hypothesis in a Proof-of-Concept study. Twenty-two participants (2 females and 20 males; mean age ± SD: 23.3 ± 1.9 years; age range: 21–27 years; Laterality Quotient: 72.5 ± 32.2%) completed IHI experiment. Therefore, the results presented in the EEG part are from all 24 participants, while IHI results are from the 22 participants that completed the whole experiment. Four of the 120 sessions from four participants (two REST, one NoFB, and one HIGH session) were excluded due to corrupted data.

The experiments conformed to the Declaration of Helsinki and were performed in accordance with the current TMS safety guidelines of the International Federation of Clinical Neurophysiology (Rossi et al., 2009). The experimental procedure was approved by the Ethics Committee of the Faculty of Science and Technology, Keio University (no.: 31-89, 2020-38, and 2021-74). Written informed consent was obtained from participants prior to the experiments.

3.2.3. EEG/EMG data acquisition

EEG signals were acquired using a 128-channel Hydrogel Geodesic Sensor Net 130 system (Electrical Geodesics Incorporated [EGI], Eugene, OR, USA) in a quiet room. EEG data were collected at a sampling rate of 1 kHz and transmitted via an Ethernet

switch (Gigabit Web Smart Switch; Black Box, Pennsylvania, USA) to the EEG recording software (Net Station 5.2; EGI and MATLAB R2019a; The Mathworks, Inc, Massachusetts, USA). The ground and reference channels were placed at CPz and Cz, respectively. The impedance of all channels, excluding the outermost part, was maintained below 30 kΩ throughout the experiment to standardize the EEG recordings (Ferree et al., 2001). This impedance standard was consistent with other studies using the same EEG system (Carter Leno et al., 2018; Robertson et al., 2019).

Surface EMGs were recorded from the FDI and ADM of the left and right hands using two pairs of Ag/AgCl electrodes ($\phi = 10$ mm) in a belly-tendon montage. Impedance for all channels was maintained below 20 kΩ throughout the experiment. EMG signals were digitized at 10 kHz using Neuropack MEB-2306 (Nihon Kohden, Tokyo, Japan). The EMG data from each trial were stored for offline analysis on a computer from 500 ms before to 500 ms after the TMS pulse. Simultaneously, 5–10 ms of data were transferred immediately after collection to a computer for real-time analysis. In case of muscular contraction due to finger movement, the experimenter reminded participants to relax their muscles and ensure absence of muscle activity during MI. To monitor the real-time surface EMG signals, EMG signals were band-pass filtered (5–1000 Hz with 2nd order Butterworth) with a 50-Hz notch to avoid power-line noise contamination; the root mean square of the filtered EMG signal from the FDI for the previous 1000 ms of data was displayed on the second experimenter's screen in the form of a bar.

Throughout the experiment, the participants were seated in a comfortable chair

with stable forearm support and performed MI of unilateral right index finger abduction. The wrist and elbow joint angles were fixed to the armrest in a neutral posture. The participants were instructed to maintain this posture and were visually monitored by the experimenter throughout the EEG and MEP measurements. During MI, the forelimbs were placed in a prone position, with natural elbow and shoulder joint angles to prevent the muscle activity.

3.2.4. TMS protocol

For the evaluation of IHI, TMS was delivered using two interconnected single-pulse magnetic stimulators (The Magstim BiStim^2; Magstim, Whiteland, UK) producing two monophasic current waveforms in a 70-mm figure-of-eight coil. The author identified the optimal left and right coil positions over the hand representation area at which a single-pulse TMS evoked a MEP response in the FDI muscle with the lowest stimulus intensity, referred to as the motor hotspot. The TS was delivered to the motor hotspot of the left M1, with the handle of the coil pointing backward and approximately 45° to the midsagittal line. The other coil for the CS was placed over the motor hotspot of the right M1 but slightly reoriented at 45–60° relative to the midsagittal line because it was not possible to place two coils in some participants with small head size. This orientation is often chosen in IHI studies (Daskalakis et al., 2002) since it induces a posterior-anterior current flow approximately perpendicular to the anterior wall of the central sulcus, which evokes MEPs at the lowest stimulus intensities (Rossini et al., 2015). To immobilize the head and maintain fixed coil positions over the motor hotspots during the experiment,

chin support and coil fixation arms were used. The position of the TMS coil was monitored using the Brainsight TMS navigation system (Rogue Research, Cardiff, UK), so that the optimal coil orientation and location remained constant throughout the experiment.

RMT was defined as the lowest stimulator output eliciting an MEP in the contralateral side of relaxed FDI of > 50 μV peak-to-peak in 5 out of 10 consecutive trials (Groppa et al., 2012; Rossini et al., 1994). The stimulus intensities of the left and right M1 to evoke MEP of 1 mV peak-to-peak amplitude from the relaxed right and left FDIs (SI_{1mV}) were also determined for the following dual-coil paired-pulse TMS.

3.2.5. IHI evaluation

IHI from the ipsilateral (right) to the contralateral (left) M1 was probed using a dual-coil paired-pulse TMS paradigm. CS was applied to the right M1, followed a few milliseconds later by a TS delivered to the left M1 (Ferbert et al., 1992). In an animal study to get insight into the role of GABAergic interneuron in a paired-pulse paradigm, IHI was greatly reduced by antagonists of the $GABA_B$ receptor (phaclofen), whereas it was maintained in the presence of the $GABA_A$ antagonist (bicuculline methiodide) (Chowdhury and Matsunami, 2002). In humans, a previous study probing the pharmacological background of IHI showed that the $GABA_B$-agonist (baclofen) enhanced IHI, but the GABAA-agonist (midazolam) had no effect on IHI (Irlbacher et al., 2007). In addition, IHI was reduced by the sodium channel blocker carbamazepine, which raises the threshold for action potentials and reduces the spontaneous neuronal

firing rate (Sommer et al., 2012). It is discussed that possible mechanisms are a reduced firing rate of inhibitory interneurons mediating IHI. Thus, the relevant transcallosal fibers are probably excitatory (glutamatergic) and likely to synapse on inhibitory interneurons in the contralateral M1 (Carson, 2020).

Due to the time constraint, the ISI in the present study was uniformly set to 10 ms, in accordance with previous studies (Duque et al., 2005; Harris-Love et al., 2007; Murase et al., 2004; Tsutsumi et al., 2012); however, an ideal ISI would vary across individuals. Additionally, in a preliminary experiment with four participants, it was confirmed that IHI was clearly observed when ISI was set to 10 ms. The CS and TS intensities remained constant throughout the experiment for each participant.

To validate IHI measurement under bi-EEG-triggered dual-TMS setup, IHI curves at rest were obtained in 20 of 24 participants prior to the main experiment, where a CS of varying intensity (five different intensities, 100–140% of RMT, in steps of 10% RMT) preceded the TS. Ten conditioned MEPs were collected for each CS intensity, along with 10 unconditioned MEPs (i.e., TS was given alone) in randomized order. The peak-to-peak amplitudes of the conditioned MEPs were averaged for the different CS intensities and expressed as a percentage of the mean unconditioned MEP amplitude. IHI intensity curves ensured that IHI was approximately half-maximum for each participant when 120-130% RMT of CS intensity was applied, similar to previous EEG-TMS experiment (Stefanou et al., 2018; Tsutsumi et al., 2012).

3.2.6. Spatially bivariate BCI-based neurofeedback

The present study was conducted based on a spatially bivariate BCI-based neurofeedback that displays bi-hemispheric sensorimotor cortical activities, which the author recently developed in our laboratory (Hayashi et al., 2020, 2021). This method allows participants to learn to regulate these two variates at the same time and induce changes in target-hemisphere-specific SMR-ERD. Visual feedback was provided on a computer screen in the form of cursor movements in a two-dimensional coordinate, in which x- and y-axis corresponded to the degree of the ipsilateral (right) and contralateral (left) SMR-ERD to the imagined right hand, respectively. The axis range was set from the 5th (i.e., SMR-ERS) to 95th (i.e., SMR-ERD) percentile of intrinsic SMR-ERD distribution in the EEG calibration session, and the origin-position ($x = 0$, $y = 0$) represented median values of bilateral SMR-ERDs, respectively. The cursors were presented at the origin-position at the initiation of a trial, and values exceeding the boundary were rounded to the 5th or 95th percentile. A key point of the current methodology is that, for example, when participants were instructed to move the cursor toward the middle right ($x > 0$, $y = 0$) in the two-dimensional coordinate, the position showed a strong SMR-ERD in the ipsilateral hemisphere and moderate SMR-ERD in the contralateral hemisphere. Therefore, spatially bivariate BCI-based neurofeedback enables us to investigate how sensorimotor excitability in the target hemisphere (i.e., ipsilateral side to the imagined hand) contributes to IHI from the ipsilateral hemisphere to the contralateral hemisphere while maintaining constant contralateral sensorimotor excitability.

During MI, participants were asked to perform kinesthetic MI of right index finger

abduction from the first-person perspective with equal time constants of 0.5 Hz cycle. Kinesthetic MI was performed because a previous study demonstrated that the focus of EEG activity during kinesthetic MI was close to the sensorimotor hand area, whereas visual MI did not reveal a clear spatial pattern (Neuper et al., 2005). To improve MI task compliance (i.e., whether all participants successfully performed the MI in the same manner), the author not only asked them to perform kinesthetic MI from a first-person perspective, but also asked them to perform a rehearsal before each session. In addition, the author confirmed that SMR was observed in a frequency-specific, spatiotemporal-specific, and MI-related manner through offline analysis after each session. These characteristics of SMR-ERD indicate that kinesthetic MI, not visual MI, was performed appropriately (Neuper et al., 2005; Pfurtscheller and Neuper, 1997).

3.2.7. Real-time brain state-dependent dual-coil brain stimulation

The bi-EEG-triggered dual-TMS setup analyzes the raw EEG signal in real time to trigger TMS pulses depending on the instantaneous bilateral spatially filtered SMR-ERDs. The real-time SMR-ERD intensity in each hemisphere (relative to the average power of the 1-5 s of the resting epoch) was obtained every 100 ms and calculated using the last 1-s data as follows (Hayashi et al., 2020): (1) acquired raw EEG signals recorded over SM1 underwent a 1–70-Hz second-order Butterworth bandpass filter and a 50-Hz notch filter; (2) filtered EEG signals were spatially filtered with a large Laplacian (60 mm to set of surrounding channels), which subtracted the average value of the surrounding six channel montage from that of the channel of interest (i.e., C3 and C4, respectively). This method

enabled us to extract the task-related EEG signature and improve the signal-to-noise ratio of SMR signals (McFarland et al., 1997; Tsuchimoto et al., 2021). (3) a fast Fourier transform was applied to the spatially large Laplacian filtered EEG signals; (4) the power spectrum was calculated by calculating the square of the Fourier spectrum; (5) the alpha band power was obtained by averaging the power spectrum across the predefined alpha target frequencies from the EEG calibration session (described below); (6) the alpha band power was time-smoothed by averaging across the last five windows (i.e., 500 ms) to extract the low-frequency component for high controllability. The low-frequency component is beneficial to neurofeedback training because it reduced the flickering and improved the signal-to-noise ratio of the SMR signal (He et al., 2020; Kober et al., 2018); and (7) SMR-ERD was obtained by calculating the relative power to the average power during the resting epoch. SMR-ERDs of the last six segments were displayed and each plot was updated every 100 ms respectively, allowing participants to always see the SMR-ERD from 0.6-s ago to the present. Thereafter, a cue signal was generated to trigger the magnetic stimulator of CS stimulus when the signal reached the predetermined target that the SMR-ERD threshold was exceeded and transmitted Transistor-Transistor Logic pulse to the magnetic stimulator of TS stimulus 10 ms later by Neuropack MEB-2306 system. EMG and EEG data were processed using the customized analysis scripts on MATLAB R2019a.

3.2.8. Experimental sessions

First, maximal voluntary contraction (MVC) was measured (**Figure 3-2A**). Full-length

isometric abduction of the right and left index and little fingers were performed once after several exercises; each execution lasted 5 s with a 30-s rest between contractions to allow for recovery from mental fatigue. Each MVC was obtained by calculating the root mean square of stable 3 s of filtered EMG data. Then, hot spots and stimulus intensities were determined.

Next, to determine the parameters of the bi-EEG-triggered dual-TMS setup, an EEG calibration session consisting of 20 trials, providing real-time SMR-ERD only on the contralateral side, was performed for each participant prior to the IHI experiment. Each trial was initiated by a 5-s resting epoch, followed by a 1-s ready epoch, and completed by a 6-s MI epoch. During this 12-s trial period, participants were asked not to move, blink, or swallow to prevent EEG artefacts derived from non-neural activity. After each 12-s trial, the screen went black for 3 s (**Figure 3-2A**). Participants were allowed to move freely to avoid mental fatigue during this interval period, before the next trial started. Thereafter, the target frequencies in the contralateral and ipsilateral SM1 were determined for each participant in order to feedback the most reactive frequency. Since SMR-ERD in the alpha band is a reliable EEG biomarker of increased neuronal excitability in SM1, corticospinal tract, and thalamocortical systems (Neuper et al., 2006; Soekadar et al., 2015b; Takemi et al., 2013, 2015, 2018; Yuan et al., 2010), the target frequencies were selected from the alpha band (8–13 Hz) by calculating the mean intensity of SMR-ERD with a 3-Hz sliding bin and 2-Hz overlap. Second, the target ranges of SMR-ERD during bi-EEG-triggered dual-TMS setting were normalized for each participant based on SMR-ERD distribution in the contralateral and ipsilateral

hemispheres.

After the calibration session, the main IHI experiment with dual-coil paired-pulse TMS was performed in five consecutive sessions (10-min each) with fixed CS and TS intensities. Each session consisted of 12-s of 40 trials with 3-s interval periods as same as the EEG calibration session. Five experimental sessions comprised different conditions as follows: (1) resting-state where participants were instructed to relax and look at the origin of the 2-D coordinates on the computer screen in front of them (REST); (2) right finger MI without visual feedback (NoFB); participants tried to achieve (3) high (HIGH); (4) middle (MID), and (5) low (LOW) excitability states of the ipsilateral SM1 during BCI-base neurofeedback. In the last three HIGH, MID, and LOW sessions, participants received visual feedback based on the SMR-ERDs from both contralateral and ipsilateral hemispheres.

In each session, approximately equal numbers of paired pulses and unconditioned test pulses were applied. EEG-triggered TMS timing was determined based on the intrinsic sensorimotor cortical activity of each participant in the calibration session and ranged from 0.5 to 5.5 s during the MI epoch. The predetermined target ranges of SMR-ERD was expressed by a blue rectangle on the computer screen in each session are as follows (**Figure 3-2B**): (1) 37.5–62.5th percentile of SMR-ERD distribution during rest in both hemispheres (REST session); (2) 37.5–62.5th percentile of SMR-ERD distribution during MI in the contralateral hemisphere and 5–95th percentile of SMR-ERD distribution during MI in the ipsilateral hemisphere (NoFB session); (3) 37.5–62.5th percentile of SMR-ERD distribution during MI in the contralateral hemisphere and 75–

95th percentile of SMR-ERD distribution during MI in the ipsilateral hemisphere (HIGH session); (4) 37.5–62.5th percentile of SMR-ERD distribution during MI in the contralateral hemisphere and 37.5–62.5th percentile of SMR-ERD distribution during MI in the ipsilateral hemisphere (MID session); and (5) 37.5–62.5th percentile of SMR-ERD distribution during MI in the contralateral hemisphere and 5–25th percentile of SMR-ERD distribution during MI in the ipsilateral hemisphere (LOW session).

The author also applied non-triggered TMS if SMR-ERD was not achieved with the target ranges (referred to as the failed trial). In the non-triggered TMS trials, paired pulses or unconditioned test pulses were delivered in random timing ranging from 5.5 to 6 s irrespective of instantaneous SMR-ERD during the MI epoch to see the influence of spontaneous SMR fluctuations on IHI. The REST and NoFB sessions served as controls to determine the intrinsic IHI magnitude. To evaluate the difficulty of each neurofeedback session, the mean values of the success triggered trials (± 1 SD) in all participants were compared. The waiting time for a triggered event from MI onset was also measured for each session.

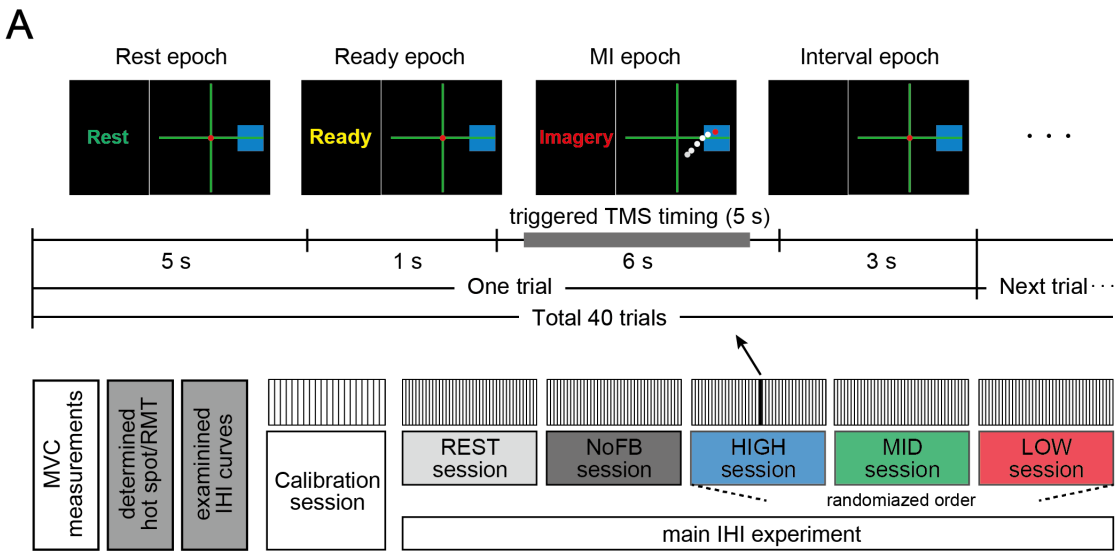

B

Session	*Contralateral SMR-ERD (percentile)*	*Ipsilateral SMR-ERD (percentile)*
REST	37.5-62.5th (rest)	37.5-62.5th (rest)
NoFB	37.5-62.5th (motor imagery)	5-95th (motor imagery)
HIGH	37.5-62.5th (motor imagery)	75-95th (motor imagery)
MID	37.5-62.5th (motor imagery)	37.5-62.5th (motor imagery)
LOW	37.5-62.5th (motor imagery)	5-25th (motor imagery)

Figure 3-2. Experimental paradigm

(A) Task instructions and visual SMR-ERD feedback in the contralateral and ipsilateral SM1 were provided in the form of computer cursors in a two-dimensional coordinate on a computer screen (upper panel). EEG-triggered TMS timing was determined based on the intrinsic sensorimotor cortical activity of each participant in the calibration session and ranged from 0.5 to 5.5 s during the MI epoch. The author also applied non-triggered TMS if SMR-ERD was not achieved with the target ranges (referred to as the failed trial). In the non-triggered TMS trials, paired pulses or unconditioned test pulses were delivered in random timing ranging from 5.5 to 6 s irrespective of instantaneous SMR-ERD during the MI epoch to see the influence of spontaneous SMR fluctuations on IHI. Lower panel indicates the experimental overview. The last three HIGH, MID, and LOW sessions were arranged in a random order, and in these sessions, participants received visual feedback based on bilateral SMR-ERDs. **(B)** The predetermined target ranges of SMR-ERD were expressed by a blue rectangle on the computer screen in each session. The author aimed for participants to volitionally increase or decrease (bidirectional) the ipsilateral sensorimotor excitability while maintaining constant contralateral sensorimotor

excitability. The REST and NoFB sessions were served in order to estimate the individual baseline during rest and MI for the offline analysis.

3.2.9. MEP analysis

For the quality control of MEP analysis, trials were rejected if: (1) coil position was shifted from the optimal orientation and location (> 3 mm and/or > 3°) despite maintaining it during the experiment using the Brainsight TMS navigation system; (2) involuntary muscle contraction in the 250 ms period before the TMS pulse was observed (> 5% MVC) because of pre-innervation increase in MEP amplitude (Devanne et al., 1997; Hallett, 2007); (3) large trial-by-trial MEP variance (mean ± 3SD) were found in order to screen out extreme values (Ruddy et al., 2018). In total, 8.8% of all trials were excluded from further analysis. Each peak-to-peak MEP amplitude was automatically determined in the remaining trials within 20–45 ms after the TMS pulse. IHI was defined as the percentage of mean conditioned MEP amplitude over mean unconditioned MEP amplitude (IHI = conditioned MEP/unconditioned MEP × 100%); therefore, smaller IHI values represent stronger inhibition.

3.2.10. Offline EEG analysis

To evaluate the sensorimotor excitability that may influence IHI, pre-processing and time-frequency analyses were performed, and the left and right SMR-ERDs were calculated. SMR-ERD in EEG is a reliable surrogate monitoring marker of sensorimotor excitability level for several reasons: (1) SMR-ERD and task-induced increase in blood

oxygenation level-dependent signals during MI are co-localized and co-varied at SM1 (Yuan et al., 2010); (2) SMR-ERD control is associated with the contribution of SM1 modulated by transcranial direct current stimulation (Soekadar et al., 2015b); and (3) data-driven EEG features discriminating the presence or absence of muscle contraction were predominantly localized in the parieto-temporal regions, indicating SMR-ERD (Hayashi et al., 2019; Iwama et al., 2020). The time segment of interest was from the initiation of the trial to before TMS-triggered time marker of the CS in order to avoid contamination by the TMS artifact (pre-stimulation period). The EEG signal underwent a 1–70-Hz, second-order Butterworth bandpass filter and a 50-Hz notch filter. The EEG signals of all channels were spatially filtered using a common average reference, which subtracted the average value of the entire electrode montage (the common average) from that of the channel of interest to remove global noise (McFarland et al., 1997; Tsuchimoto et al., 2021). EEG channels in each trial were rejected during further analysis if they contained an amplitude above 100 μV.

3.2.11. Connectivity analysis

To assess interhemispheric functional connectivity at the EEG level, distributed interregional neural communication was calculated. The author focused on both the resting epoch (1-5 s) and MI epoch (7 s [task onset] to before stimulation) for analysis. To calculate functional connectivity and compensate for long-range synchronization preference, the author used the ciCOH (Ewald et al., 2012; Hayashi et al., 2020; Vukelić and Gharabaghi, 2015). The details of the following processing for the connectivity

analysis can be obtained from our previous work (Hayashi et al., 2020). The ciCOH was obtained by subdividing the resting epoch into 1-s segments with 90% overlap (31 segments in total) and multiplied with a Hanning window. Then, interhemispheric Network-intensity was computed as follows:

$$Network\ intensity(f) = \sum_{cont=1}^{7} \sum_{ipsi=1}^{7} ciCOH_{cont,ipsi}(f) \quad (3-1)$$

where *Network-intensity* is computed between left and right hemisphere, $\sum\sum ciCOH$ is the sum of significant ciCOH values for interhemispheric interaction, *cont* denotes the 7 channels of interest (i.e., C3 and its neighboring 6 channels), *ipsi* denotes the 7 channels of interest in the opposite hemisphere (i.e., C4 and its neighboring 6 channels), and *f* indicates the frequency of interest (i.e., the predefined alpha frequencies). As a negative control, other frequency bands (theta [4-7 Hz], low-beta [14-20 Hz], high-beta [21-30 Hz], and gamma [31-50 Hz]) were also examined.

3.2.12. Correlation analysis

To investigate the association between sensorimotor brain activity at the EEG level and IHI magnitude from multimodal perspectives, within-participant and across-participant correlation analyses were performed. In the within-participant correlations between contralateral or ipsilateral SMR-ERDs and IHI magnitude in each participant, the author used Pearson's correlation since MEP/EEG data showed normal distribution. In the across-participant corrections between contralateral or ipsilateral SMR-ERDs and IHI magnitude, the author performed a repeated measures correlation. A previous study

argued that it may produce biased, specious results due to violation of independence and/or differing patterns (across-participants vs. within-participants) (Bakdash and Marusich, 2017).

To examine the neural characteristics depending on the manipulation capability of IHI, the author examined the association between the manipulated effects on IHI calculated from the percent change between HIGH and LOW sessions (ΔIHI_{H-L}), and IHI magnitude in REST session (IHI_{rest}). Next, the correlations between IHI_{rest} and intrinsic EEG profile in NoFB session (i.e., contralateral SMR-ERD and ipsilateral SMR-ERD) were investigated, respectively. Moreover, the author verified whether large-scale resting-state functional connectivity was associated with an effective inhibitory interhemispheric network assessed by IHI. An across-participant Pearson's correlation was applied to identify significant relationships between the IHI_{rest} and interhemispheric $Network\text{-}intensity_{rest}$. To attenuate the aberrant effect of values in some especially low $Network\text{-}intensity_{rest}$ or high (CS+TS)/TS at rest (outliers) in the theta, low-beta, high-beta, and gamma bands, a jackknife resampling was performed using SPSS software (version 27; IBM Corp., Armonk, NY, USA). In this study, both of two correlation coefficients and the bias were reported.

3.2.13. Statistical analysis

Statistical analyses were performed using SPSS software, MATLAB R2019a, and R 4.1.1 software. The assumption of normality was verified using the Shapiro-Wilk test. All data were normally distributed ($W > 0.91$, $p > 0.05$) and therefore analyzed with parametric

tests. The assumption of sphericity was checked using the Mauchly's test. If the test was significant, a Greenhouse-Geisser correction was applied.

Modulation effects of bilateral sensorimotor excitabilities due to BCI-based neurofeedback training were evaluated from the 1-s period immediately before stimulation onset. A one-way rmANOVA for sessions (five levels: REST, NoFB, HIGH, MID, and LOW) was performed using the contralateral and ipsilateral SMR-ERDs. Following the one-way rmANOVA, post-hoc two-tailed paired t-tests were performed using the Bonferroni correction for multiple comparisons. For the interhemispheric connectivity during MI, a one-way rmANOVA and post-hoc analysis were applied to Network-intensity$_{MI}$ as the same procedure as the SMR-ERD analysis. In addition, to verify the difficulties for neurofeedback sessions, one-way rmANOVA for sessions (HIGH, MID, and LOW) and post-hoc analysis were applied to the number of the triggered (success) trials and mean waiting time for a triggered event from MI onset.

For the IHI curves at rest, a one-way rmANOVA for intensities (six levels: 0% [TS only], 100%, 110%, 120%, 130%, and 140% RMT) and post-hoc two-tailed paired t-tests were performed in MEP amplitude. Similarly, a one-way rmANOVA for sessions (five levels: REST, NoFB, HIGH, MID, and LOW) was performed to compare the IHI magnitude. Next, for all significant main effects, post-hoc two-tailed paired t-tests were performed using the Bonferroni correction for multiple comparisons for all sessions.

The author compared the IHI magnitude across sessions, by calculating the percent changes in IHI magnitude to baseline (i.e., NoFB session) and investigating the difference between sessions (REST, HIGH, MID, and LOW). To investigate the influence

of spontaneous SMR fluctuations on IHI, a two-way rmANOVA for sessions (HIGH, MID, and LOW) and trials (triggered TMS trial and non-triggered TMS trial) as the within-participant factors. To investigate whether changes in IHI and corticospinal excitability in response to the CS over the right hemisphere are independent phenomena, a generalized linear model with the percent changes of left MEP amplitude as a covariate of no interest was conducted for the triggered and non-triggered TMS trials. Following the two-way rmANOVA, a post-hoc analysis was performed using the Bonferroni correction for multiple comparisons. The significance level for all statistical tests was set to $p = 0.05$. The author further performed mixed-effects analysis (Hussain et al., 2019; Madsen et al., 2019) incorporating the contralateral SMR-ERD and ipsilateral SMR-ERD as factors in the statistical regression model to explore the relationships between inhibitory interhemispheric activity and EEG characteristics. The linear mixed-effect model included the contralateral and ipsilateral SMR-ERD as fixed effects, treating the participant factor as a random effect to account for individual variability in IHI magnitude.

For the within-subject correlation analysis, the overall significance of all individual correlations between IHI magnitude and bilateral SMR-ERDs was examined using a chi-squared test.

3.3. Results

Values corresponding to each statistical figure are presented in each table for readability (**Table 3-1** to **Table 3-8**).

3.3.1. Data compliance

In all MI-based sessions (NoFB, HIGH, MID, and LOW), participants subjectively confirmed that they were able to perform kinesthetic MIs of unilateral right finger index finger abduction. EEG signals with amplitudes ≤ 100 μV were consistently recorded throughout the sessions. Contralateral and ipsilateral SMR amplitudes to the imagined hand were greater during the resting epoch than during the MI epoch, indicating desynchronization of the sensorimotor neural activity induced by MI. The averaged power spectrum density from the C3 channel during the resting epoch showed peak frequencies at 8–13 Hz and 21–24 Hz across the participants (Crone et al., 1998; Neuper et al., 2006; Pfurtscheller, 2001). The averaged powers in the alpha and beta bands were $1.67 \times 10^{-4} \pm 0.34 \times 10^{-4}$ V^2 and $2.85 \times 10^{-5} \pm 0.54 \times 10^{-5}$ V^2 (mean ± standard deviation [SD]), respectively. All procedures were well tolerated and no adverse events were noted.

To quantify the difficulties in each neurofeedback session, two indices were examined: (1) the number of triggered trials represents the BCI performance (i.e., success trials) since TMS was only triggered when the EEG signal exceeded the predetermined SMR-ERD threshold; (2) mean waiting time for a triggered event from task onset, which yields a range of 0–5 s (triggered TMS timing). The mean values of all triggered trials (± 1 SD) of the neurofeedback sessions were 14.2 ± 4.7 trials and post-hoc paired t-tests following a one-way rmANOVA revealed no significant difference between the three sessions (all $p > 0.05$; HIGH: 12.0 ± 5.0 trials, MID: 16.1 ± 3.8 trials, LOW: 15.9 ± 5.4 trials). The mean waiting time for a triggered event from task onset (± 1 SD) was 1.96 ± 0.81 s, and post-hoc paired t-tests following a rmANOVA showed no significant

difference between the three sessions (all $p > 0.05$; HIGH: 2.16 ± 0.76 s, MID: 2.05 ± 0.73 s, LOW: 1.71 ± 0.94 s).

3.3.2. Modulation effects of bilateral SM1 at EEG level

The author tested whether participants could learn volitional up- or down-regulation of the ipsilateral sensorimotor excitability to the imagined right hand while maintaining constant contralateral sensorimotor excitability at the EEG level using a spatially bivariate BCI-based neurofeedback. For the contralateral SMR-ERD, a one-way rmANOVA for the sessions (five levels: REST, NoFB, HIGH, MID, and LOW) revealed a significant difference ($F_{(4,102)} = 4.81$, $p = 0.014$, $\eta^2 = 0.16$). Post-hoc two-tailed paired t-tests demonstrated no significant differences in the contralateral SMR-ERD between the neurofeedback sessions (HIGH-MID: Cohen's $d = 0.13$, $p = 1.00$; HIGH-LOW: Cohen's $d = 0.22$, $p = 1.00$; MID-LOW: Cohen's $d = 0.11$, $p = 1.00$), whereas significant differences were found between REST and other sessions (all $p < 0.05$; **Figure 3-3A**). In contrast, after showing significant differences in the ipsilateral SMR-ERD between sessions ($F_{(4,102)} = 156.0$, $p < 0.001$, $\eta^2 = 0.86$), post-hoc two-tailed paired t-tests showed that ipsilateral SMR-ERD increased during HIGH session (HIGH-MID: Cohen's $d = 3.12$, $p < 0.001$; HIGH-LOW: Cohen's $d = 6.13$, $p < 0.001$) and decreased during LOW session (MID-LOW: Cohen's $d = 4.44$, $p < 0.001$), revealing a significant bidirectional modulation compared to baseline sensorimotor endogenous activity (**Figure 3-3B**). The spatial patterns of SMR-ERD in each session are depicted in **Figure 3-3C**. The author found that the SMR-ERDs were predominantly localized in bilateral parieto-temporal

regions (C3 and C4 channels and their periphery), and strong ipsilateral SMR-ERD was observed in HIGH session with constant contralateral SMR-ERD.

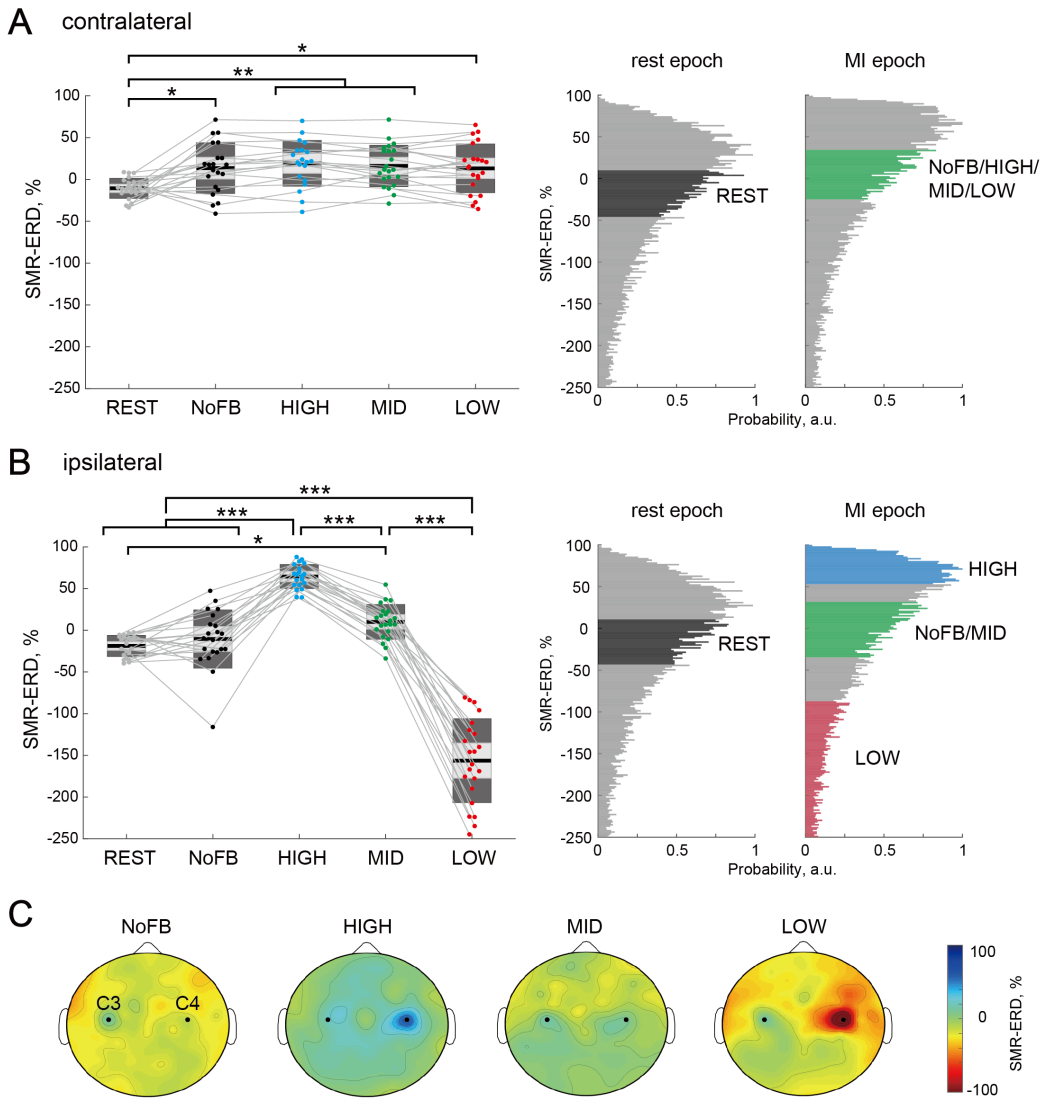

Figure 3-3. Target-hemisphere-specific modulation at the EEG level induced by spatially bivariate BCI-based neurofeedback

(A), (B) Modulation effect of the contralateral (left) and ipsilateral (right) SMR-ERDs to the imagined right hand, respectively. Individual participants are represented by colored plots and thin grey lines. The light grey box represents 1.96 SEM (95% confidence interval) and dark grey box represents 1 SD. The black line indicates the group mean of the studied sample and colored plots indicate a single session. Positive values indicate

desynchronization as compared to rest. Complete desynchronization to zero power in the frequency of interest translates to a 100% increase in SMR-ERD, whereas synchronization in the same band could theoretically be unlimited and allows for decreases in SMR-ERD > 100%. The two right-sided panels represent the SMR-ERD distributions during rest and MI epoch in the calibration session. Based on the SMR-ERD distributions in the contralateral and ipsilateral hemispheres, the target ranges of SMR-ERD during bi-EEG-triggered dual-TMS system (each color) were set for each participant. **(C)** Spatial patterns of SMR-ERD during the MI epoch in each session (group mean). Large positive values (blue color) represent larger SMR-ERD. The black dots represent the C3 and C4 channels.

3.3.3. IHI curves at rest

To validate IHI measurement under bi-EEG-triggered dual-TMS setup, IHI curves were obtained at rest (**Figure 3-4A**) in 20 out of 24 participants, with CS of varying intensity (five different intensities, 100–140% of resting motor threshold [RMT], in steps of 10% RMT). A one-way rmANOVA for intensities (six levels: 0% [single test stimulus: TS only], 100%, 110%, 120%, 130%, and 140% RMT) revealed significant difference in intensity ($F_{(5,109)} = 8.31$, $p < 0.001$, $\eta^2 = 0.28$). Post-hoc two-tailed paired t-tests showed significant difference between TS only and 100%–140% of RMT (TS only versus 100% RMT: $p = 0.039$, TS only versus 110%-140% RMT: all $p < 0.001$). There were no significant differences across conditioning stimulus [CS] intensities, while the size of MEP amplitude tended to be smaller for larger CS intensities. IHI was approximately half of the maximum when the CS intensity was approximately 130% of RMT, which was compatible with a previous EEG-TMS experiment (Stefanou et al., 2018; Tsutsumi et al., 2012). In addition, the stimulus intensities of the left and right M1 to evoke MEP of 1

mV peak-to-peak amplitude from the relaxed right and left first dorsal interosseous (FDI) muscles (SI_{1mV}) were determined and used for the following dual-coil paired-pulse TMS setup. The average SI_{1mV} of TS and CS were 124 ± 11% RMT and 132 ± 13% RMT, respectively. The author also confirmed that the SI_{1mV} of CS showed approximately 50% of the mean conditioned MEP over the mean unconditioned test MEP (**Figure 3-4B**).

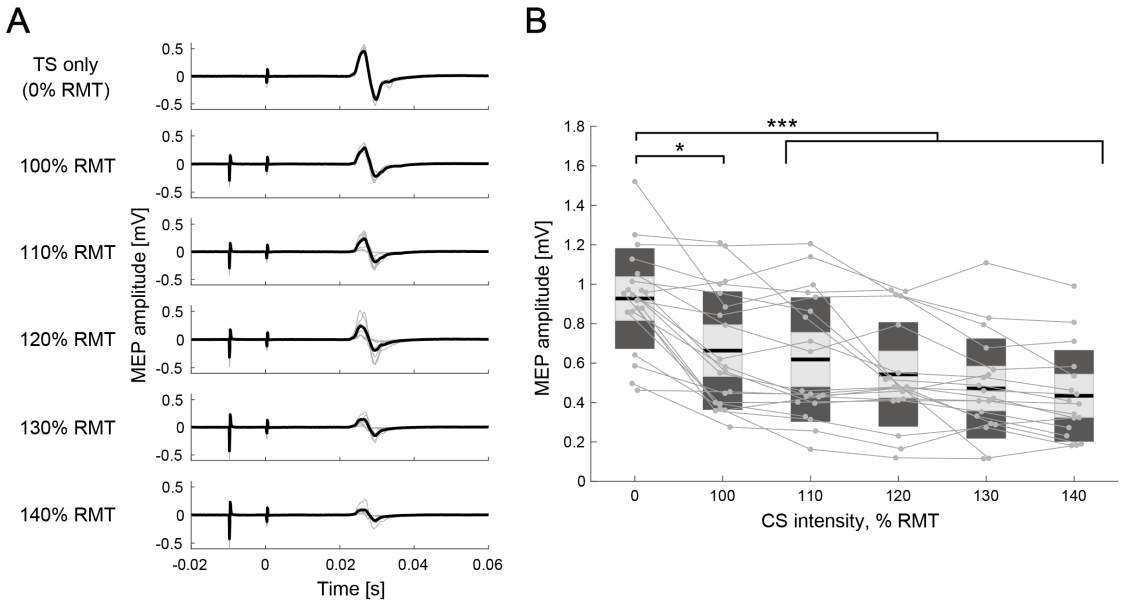

Figure 3-4. IHI curves at rest

(A) MEP amplitudes in the different intensity of conditioning stimulus of a representative participant. The thin gray lines represent each trial and black lines indicate the trial mean. **(B)** The IHI curves of the individual participants at rest are represented by thin gray plots and lines. The figure presents the individual data as an alternative to a box plot. The light grey box represents 1.96 SEM (95% confidence interval) and dark grey box indicates 1 SD. The black line indicates the group mean. The y-axis indicates raw MEP amplitude against CS intensity (x-axis, in %RMT). Dendrograms above the bars represent the results of the post-hoc analyses. * $p < 0.05$ and *** $p < 0.001$; all comparisons were Bonferroni corrected.

3.3.4. IHI manipulation via spatially bivariate BCI-based neurofeedback

Typical examples of MEP amplitude elicited by single TS (TS-only) and paired-pulse stimulation (CS+TS) of a representative participant are shown in **Figure 3-5A**. The manipulation range of IHI (i.e., the difference between HIGH and LOW sessions) was 32.6 ± 30.7% (Cohen's d = 1.50) in all participants excluding 2 participants with data corruption (i.e., 22 participants). A one-way rmANOVA of the sessions (five levels: REST, NoFB, HIGH, MID, and LOW) revealed significant differences in IHI magnitude ($F_{(4,101)} = 6.85$, $p < 0.001$, $\eta^2 = 0.22$). Across the three BCI-based neurofeedback sessions (i.e., HIGH, MID, and LOW sessions) for the comparison of IHI magnitude, post-hoc two-tailed paired t-tests showed significant difference between HIGH and MID sessions (Cohen's d = 0.94, p = 0.025), and between HIGH and LOW sessions (Cohen's d = 1.36, $p < 0.001$), but not between MID and LOW sessions (Cohen's d = 0.42, p = 0.424; **Figure 3-5B**). In addition, the author found disinhibition in NoFB session compared to REST session, although there was no statistical difference (Cohen's d = 0.42, p = 0.279); this trend is consistent with the previous studies, which reported that in healthy participants, IHI targeting the moving index finger leads to disinhibition before the movement onset to produce voluntary movement (Duque et al., 2005; Murase et al., 2004) and during isometric contraction (Nelson et al., 2009). Importantly, rmANOVA for the MEP amplitudes induced by TS-only revealed no significant differences between all sessions ($F_{(4,101)} = 2.44$, $p = 0.104$, $\eta^2 = 0.09$), suggesting that participants could learn to volitionally regulate the ipsilateral sensorimotor excitability while maintaining constant contralateral sensorimotor excitability (**Figure 3-5C**). A linear mixed-effect model that

considered the contralateral SMR-ERD and ipsilateral SMR-ERD as fixed effect in the statistical regression model, and participants as random effect revealed a significant effect of the ipsilateral SMR-ERD ($p < 0.001$) on IHI magnitude, but no main effect of the contralateral SMR-ERD or contralateral SMR-ERD × ipsilateral SMR-ERD interaction ($p = 0.828$ and $p = 0.058$, respectively).

To examine the IHI magnitude during neurofeedback, the author further compared the IHI magnitude across sessions by calculating the percent changes in IHI magnitude to baseline (i.e., NoFB session), and investigating the difference between REST, HIGH, MID, and LOW sessions. A one-way rmANOVA for sessions (four levels: REST, HIGH, MID, and LOW) revealed significant differences ($F_{(3,81)} = 8.32$, $p < 0.001$, $\eta^2 = 0.24$). Post-hoc two-tailed paired t-tests showed significant differences between HIGH and MID sessions (Cohen's $d = 1.06$, $p = 0.017$), and between HIGH and LOW sessions (Cohen's $d = 1.42$, $p < 0.001$), but not between MID and LOW sessions (Cohen's $d = 0.45$, $p = 0.734$; **Figure 3-6**). The normalized results were compatible with the results without normalization presented in **Figure 3-5**.

To further examine the influence of spontaneous SMR fluctuations on IHI, non-triggered TMS trial (referred to as the failed trial) was delivered in random timing ranging from 5.5 to 6 s during the MI epoch. For example, data from HIGH session in **Figure 3-7** were collected from MID and LOW sessions, with the target ranges of SMR-ERD in HIGH session (**Figure 3-7**). A two-way rmANOVA for sessions (three levels: HIGH, MID, and LOW) and trials (two levels: triggered TMS trials and non-triggered TMS trials) revealed a significant main effect for sessions ($F_{(2, 117)} = 5.08$, $p = 0.008$, $\eta^2 = 0.08$),

but no main effect for trials ($F_{(1, 117)} = 0.32$, $p = 0.575$, $\eta^2 < 0.01$) and for interaction ($F_{(2, 117)} = 1.82$, $p = 0.167$, $\eta^2 = 0.03$). Thus, no significant difference in IHI between the volitional control of SMR-ERDs in the closed-loop environment differs from spontaneous SMR fluctuations was observed. Post-hoc two-tailed paired t-tests showed significant differences between HIGH and MID sessions (Cohen's $d = 0.94$, $p = 0.017$), and between HIGH and LOW sessions (Cohen's $d = 1.36$, $p < 0.001$) in the triggered TMS trials. In contrast, in the non-triggered TMS trials, post-hoc two-tailed paired t-tests showed no significant differences between HIGH and MID sessions (Cohen's $d = 0.20$, $p = 1.00$), and between HIGH and LOW sessions (Cohen's $d = 0.28$, $p = 1.00$).

Although the author revealed that modulating the excitability of the right hemisphere changes IHI magnitude from the right to the left hemisphere, the specificity of the IHI manipulation was not proved yet. The author presented additional results related to changes in corticospinal excitability as assessed by MEPs in the left FDI in response to the CS over the right hemisphere (**Figure 3-8**). To investigate whether changes in IHI from the right to the left hemisphere and changes in corticospinal excitability in the right hemisphere are independent phenomena, a generalized linear model with the percent changes of left MEP amplitude as a covariate of no interest was applied. This approach tests whether the effect of IHI manipulation survives even if the covariate is added. During the triggered TMS trials, a generalized linear model for sessions (three levels: HIGH, MID, and LOW) revealed a significant main effect for sessions ($F_{(3, 60)} = 12.75$, $p < 0.001$, $\eta^2 = 0.44$). Post-hoc two-tailed paired t-tests in the increase in IHI showed significant differences between HIGH and MID sessions (Cohen's

$d = 1.06$, $p < 0.001$), and between HIGH and LOW sessions (Cohen's $d = 1.42$, $p < 0.001$). During the non-triggered TMS trials, a generalized linear model for sessions (three levels: HIGH, MID, and LOW) revealed no main effect for sessions ($F_{(3, 60)} = 1.13$, $p = 0.319$, $\eta^2 = 0.10$). Therefore, the author successfully demonstrated that IHI changes greater than the variance explained by the CS effect and manipulation is not simply an epiphenomenon.

In the control muscle (abductor digiti minimi, ADM), such observed modulation was not driven. A one-way rmANOVA for sessions (five levels: REST, NoFB, HIGH, MID, and LOW) revealed significant differences ($F_{(4,101)} = 2.51$, $p < 0.048$, $\eta^2 = 0.12$). Across the three BCI-based neurofeedback sessions (i.e., HIGH, MID, and LOW sessions) for the comparison of IHI magnitude, post-hoc two-tailed paired t-tests showed no significant difference between sessions (HIGH-MID: Cohen's $d = 0.10$, $p = 1.00$; HIGH-LOW: Cohen's $d = 0.05$, $p = 1.00$; MID-LOW: Cohen's $d = 0.15$, $p = 1.00$), whereas significant difference was observed between REST and NoFB sessions (Cohen's $d = 0.45$, $p = 0.024$; **Figure 3-9A**). Statistical analysis for TS-only revealed no significant differences in MEP amplitude between the sessions ($F_{(4,101)} = 0.62$, $p = 0.649$, $\eta^2 = 0.03$; REST: 0.54 ± 0.51 mV, NoFB: 0.50 ± 0.39 mV, HIGH: 0.73 ± 0.61 mV, MID: 0.59 ± 0.50 mV, LOW: 0.65 ± 0.51 mV; **Figure 3-9B**), indicating that IHI manipulation occurred only in the targeted muscle.

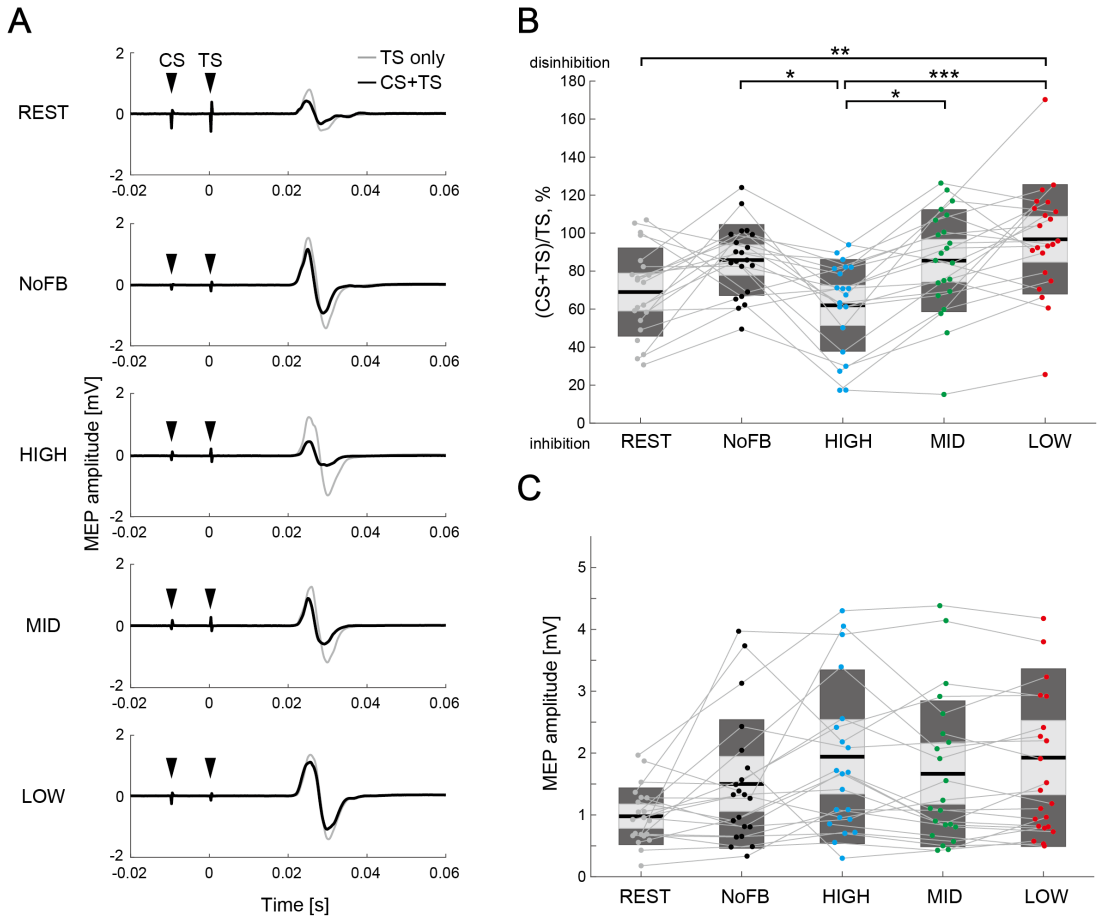

Figure 3-5. Comparison of IHI magnitude

(A) Typical examples of mean MEP amplitudes elicited by single TS (TS-only; light grey color) and paired-pulse stimulation (CS+TS; black color) in a representative participant. The black arrows represent the stimulus timings of CS and TS. **(B)** The IHI magnitudes of the individual participants are represented by colored plots and thin grey lines. The light grey box represents 1.96 SEM (95% confidence interval) and dark grey box represents 1 SD. The black line indicates the group mean of the studied sample and colored plots represent a single session. Lower values represent greater inhibitory effect from the ipsilateral hemisphere to the imagined right hand. Dendrograms above the bars represent the results of the post-hoc analyses. * $p < 0.05$, ** $p < 0.01$, and *** $p < 0.001$; all comparisons were Bonferroni corrected. **(C)** The figure shows MEP amplitude elicited by a single TS (TS-only). No significant difference in MEP amplitude was observed between sessions (all $p > 0.05$).

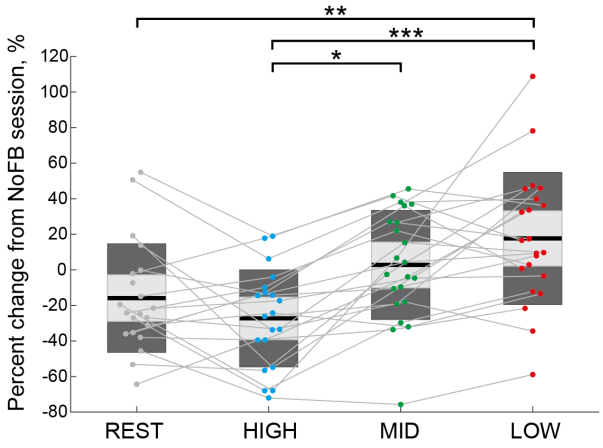

Figure 3-6. Comparison of the percent change in IHI magnitude based on values in NoFB session

The percent changes in IHI magnitude based on values in NoFB session of individual participants are represented by colored plots and thin grey lines. The light grey box represents 1.96 SEM (95% confidence interval) and dark grey box represents 1 SD. The black line indicates the group mean of the studied sample and colored plots represent a single session. Dendrograms above the bars represent the results of the post-hoc analyses. * $p < 0.05$, ** $p < 0.01$, and *** $p < 0.001$; all comparisons were Bonferroni corrected.

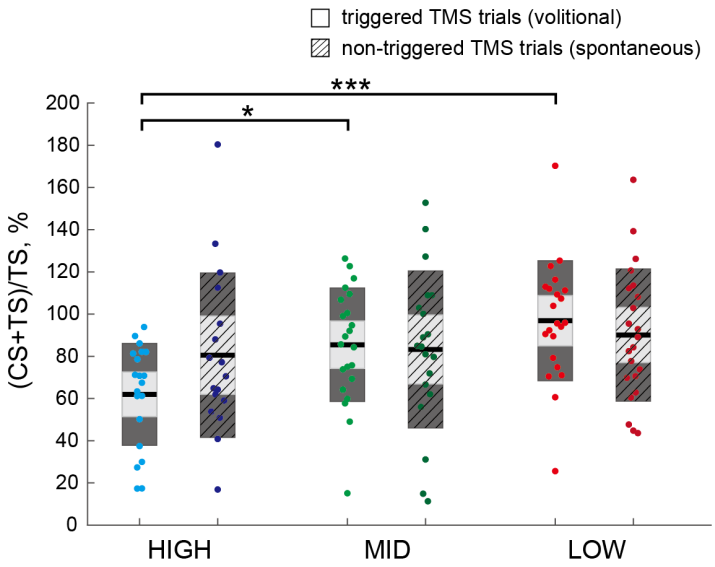

Figure 3-7. Comparison of IHI magnitudes in triggered and non-triggered TMS trials

The IHI magnitudes in triggered and non-triggered TMS trials of the individual participants are represented by colored plots. Bars with hatched lines represent the non-triggered TMS trials, and those without shading represent the triggered TMS trials. The light grey box represents 1.96 SEM (95% confidence interval) and dark grey box represents 1 SD. The black line indicates the group mean of the studied sample and colored plots represent a single session. Dendrograms above the bar represent the results of the post-hoc analyses. * $p < 0.05$ and *** $p < 0.001$; all comparisons were Bonferroni corrected.

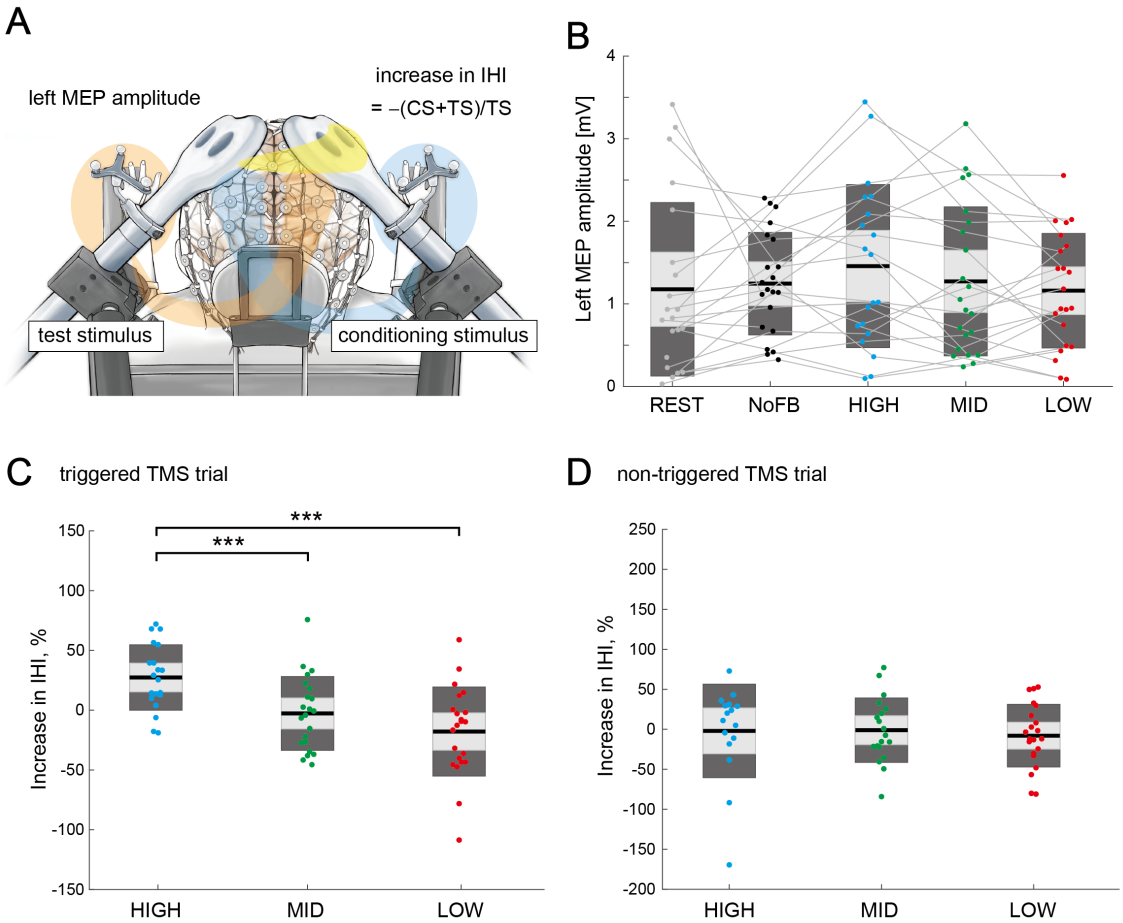

Figure 3-8. Relationship between the increase in IHI and left MEP amplitude elicited by CS

(A) Experimental overview of the MEP measurements. The yellow line on the head represents the signal flow from the conditioning hemisphere that modifies the contralateral side through the corpus callosum. The blue line represents the test stimulus

toward the right hand, and the orange line indicates the conditioning stimulus toward the left hand. **(B)** The figure shows the MEP amplitude in the left FDI elicited by CS. The light grey box represents 1.96 SEM (95% confidence interval) and dark grey box represents 1 SD. The black line indicates the group mean of the studied sample and colored plots represent a single session. **(C)** A statistical comparison with the percent changes of left MEP amplitude as a covariate of no interest during the triggered trials is shown. To compare the IHI magnitude, the percent changes based on the values in NoFB session were calculated. A significant difference in IHI magnitude between the sessions was observed ($p < 0.001$), suggesting that IHI changes greater than the variance explained by the CS effect. Dendrograms above the bars represent the results of post hoc analyses. *** $p < 0.001$; all comparisons were Bonferroni corrected. **(D)** A statistical comparison with the percent changes of left MEP amplitude as a covariate in the non-triggered trials. During the non-trigged trials, no significant difference was observed in IHI magnitude ($p = 0.319$).

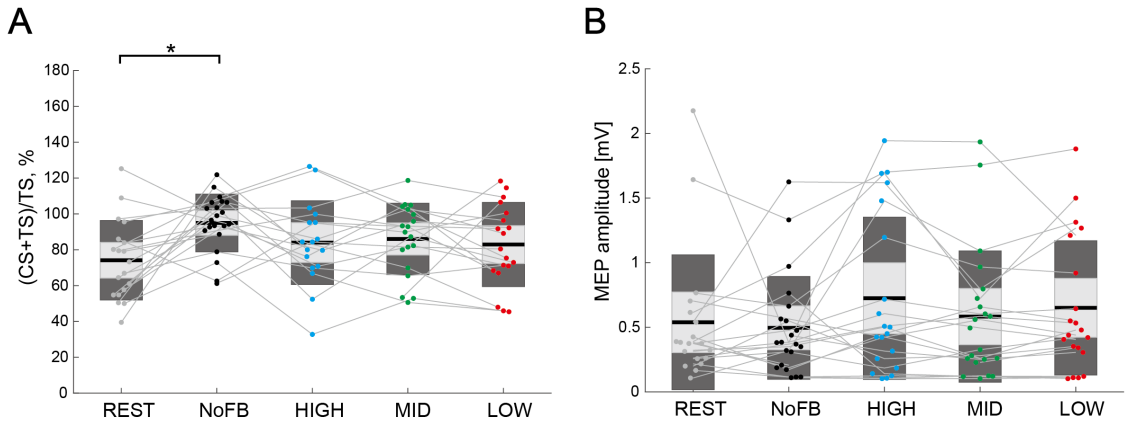

Figure 3-9. Comparison of IHI magnitude for control muscle

(A) The IHI magnitudes of the individual participants are represented with colored plots and thin grey lines. The light grey box represents 1.96 SEM (95% confidence interval) and the dark grey box indicates 1 SD. The black line indicates the group mean and colored plots indicates each session. Lower values indicate greater inhibitory effect from the ipsilateral hemisphere to the imagined hand. Dendrograms above the bars represent the results of the post-hoc analyses. * $p < 0.05$; all comparisons were Bonferroni corrected. **(B)** The figure shows MEP amplitude elicited by a single TS (TS-only). No significant

difference in MEP amplitude in the ADM muscle was observed across the sessions (all $p > 0.05$).

3.3.5. Associations between IHI magnitude and bilateral EEG patterns

To examine the association between IHI magnitude and bilateral EEG patterns, the author performed within-participant and across-participant correlation analyses, respectively. In the within-participant correlation analysis between IHI magnitude and bilateral SMR-ERDs in each participant, 7 of the 22 participants showed a significant correlation between IHI magnitude and ipsilateral SMR-ERD ($r = –0.307 \pm 0.252$ [mean ± SD]), but not between IHI magnitude and contralateral SMR-ERD in three neurofeedback sessions ($r = –0.059 \pm 0.298$ [mean ± SD]). A chi-squared test was performed to determine the overall significance of the 22 individual correlations between IHI magnitude and contralateral or ipsilateral SMR-ERDs. A comparison of the proportions of significant results obtained from the ipsilateral (7 out of 22 participants) and contralateral (1 out of 22 participants) SMR-ERDs with the proportion expected due to chance (i.e., alpha level = 0.05) showed statistically significant differences (chi squared value = 5.50, $p = 0.019$ [Fisher's exact test: $p = 0.046$]). The distributions of correlation coefficients across all participants were shown in **Figure 3-10A**.

In the across-participant correlation between IHI magnitude and contralateral or ipsilateral SMR-ERDs, the author performed a repeated measures correlation analysis (Bakdash and Marusich, 2017). The author found a significant correlation in the ipsilateral SMR-ERD ($r_{rm} = –0.436$, $p = 0.004$; **Figure 3-10B**), but not in the contralateral

SMR-ERD (r_{rm} = 0.008, p = 0.960; **Figure 3-10C**).

To analyse the associations between IHI magnitude and bilateral neural network from another perspective, interhemispheric functional connectivity during MI was examined. Interhemispheric functional connectivity was quantified as a Network-intensity measure (Hayashi et al., 2020), which is calculated from the corrected imaginary part of coherence (ciCOH) (Ewald et al., 2012; Vukelić and Gharabaghi, 2015). For the Network-intensity$_{MI}$, a one-way rmANOVA for the sessions (five levels: REST, NoFB, HIGH, MID, and LOW) revealed significant differences ($F_{(4,102)}$ = 3.04, p = 0.020, η^2 = 0.10). Post-hoc two-tailed paired t-tests in all five sessions demonstrated significant differences between HIGH and MID sessions (Cohen's d = 0.83, p = 0.033; **Figure 3-10D**). The author found no significant difference between HIGH and LOW sessions (Cohen's d = 0.40, p = 1.00; **Figure 3-10D**), suggesting that interhemispheric functional connectivity did not reflect the excitatory or inhibitory activity.

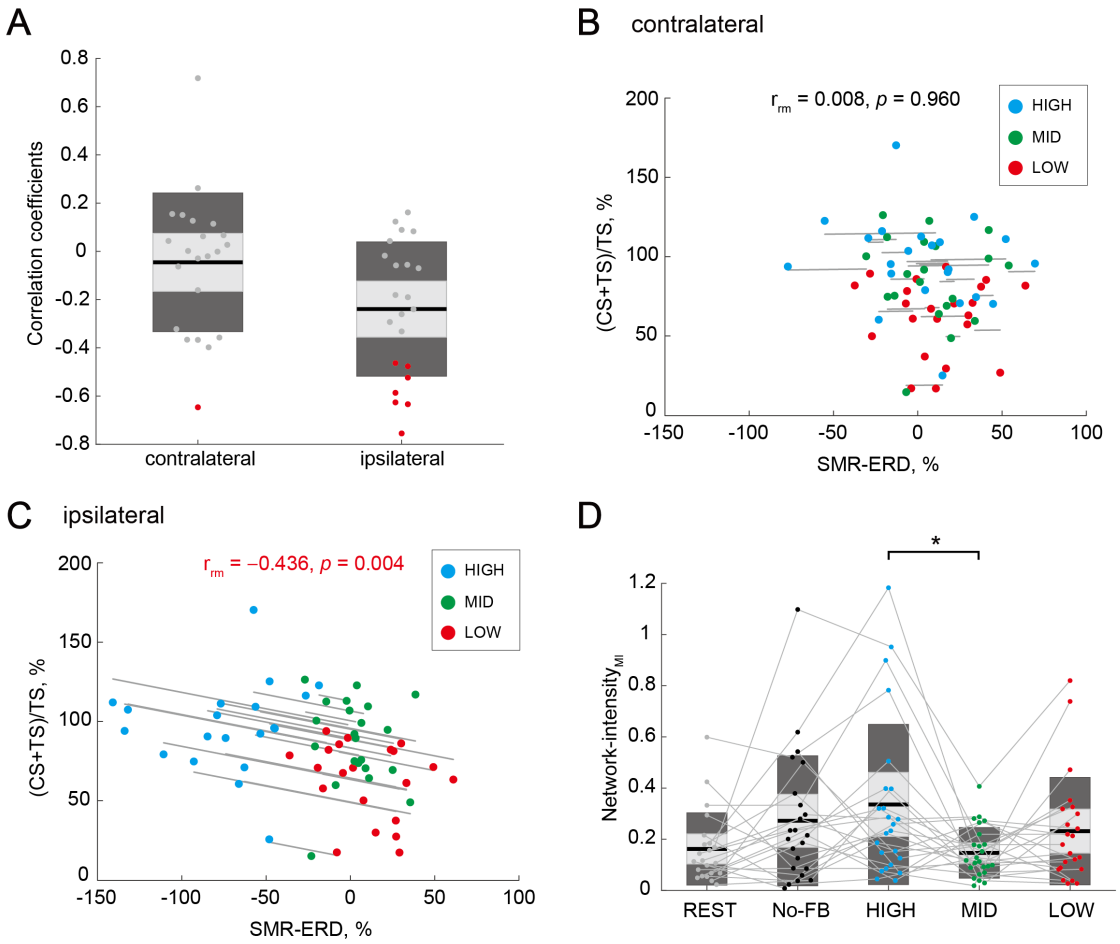

Figure 3-10. Associations of IHI magnitude and bilateral EEG patterns

(A) Distributions of within-participant correlation coefficients in all participants. Red dots represent individuals with a significant correlation between IHI magnitude and contralateral or ipsilateral SMR-ERDs, respectively. **(B), (C)** Repeated measures correlations between IHI magnitude and contralateral or ipsilateral SMR-ERDs, respectively. Dots represent mean value of a single session of each individual. Only the ipsilateral SMR-ERD and IHI magnitude were significantly correlated; high sensorimotor excitability state in the ipsilateral hemisphere would induce stronger inhibition from the ipsilateral hemisphere to the imagined hand. **(D)** Comparison of Network-intensity across sessions. Dendrograms above the bars represent the results of the post-hoc analyses. * $p < 0.05$; all comparisons were Bonferroni corrected. There was a significant difference in interhemispheric functional connectivity between HIGH and MID sessions, but not between HIGH and LOW sessions.

3.3.6. Individual characteristics associated with the manipulation capability of IHI

Finally, the author investigated the neural characteristics associated with the manipulation capability of IHI calculated from the percent change between HIGH and LOW sessions using correlation-based analysis (**Figure 3-11A**). In the relationships between the manipulation capability of IHI and IHI magnitude in REST session (IHI_{rest}), the author found a significant correlation ($r = –0.447$, $p = 0.044$), indicating that participants with greater IHI at rest were able to strongly manipulate the IHI (**Figure 3-11B**). For the relationships between resting-state effective inhibitory interhemispheric network assessed by IHI_{rest} and interhemispheric functional connectivity at the EEG level ($Network\text{-}intensity_{rest}$), participants with greater IHI_{rest} showed larger $Network\text{-}intensity_{rest}$ ($r = 0.547$, $p = 0.013$; **Figure 3-11C**). Furthermore, the author verified whether IHI_{rest} may be associated with intrinsic EEG profiles in NoFB session including bilateral SMR-ERDs. The author found a significant correlation between IHI_{rest} and ipsilateral SMR-ERD during MI ($r = –0.619$, $p = 0.004$), but not between IHI_{rest} and contralateral SMR-ERD during MI ($r = –0.283$, $p = 0.228$).

In addition to the alpha band, the beta band is also a well-established EEG signature of motor execution and imagery (Crone et al., 1998; Pfurtscheller, 2001). To verify whether resting-state functional connectivity in other frequency bands (i.e., outside of feedback frequency) was associated with IHI, an across-participant Pearson's correlation was calculated. In the across-participant correlations between IHI_{rest} and $Network\text{-}intensity_{rest}$ in the theta (4-7 Hz), low beta (14-20 Hz), high beta (21-30 Hz), and gamma (31-50 Hz) bands, the author found significant correlation in the high beta (r = –

0.618, $p = 0.004$), but not in theta (r = –0303, $p = 0.194$), low beta (r = –0.229, $p = 0.331$), and gamma (r = –0.390, $p = 0.089$) bands (**Figure 3-12A**). To attenuate the aberrant effect of values in some especially low Network-intensity$_{rest}$ or high (CS+TS)/TS at rest (outliers) in the theta, low-beta, high-beta, and gamma bands, the jackknife correlation and the bias were calculated (theta: r = –0.207, bias = 2.02; low-beta: r = –0.121, bias = 3.65; high-beta: r = –0.528, bias = –4.09; gamma: r = –0.310, bias = 0.06). In addition, the correlation between IHI$_{rest}$ and the contralateral or ipsilateral EEG patterns in frequency bands outside of a target alpha band were in **Figure 3-12B and C**, respectively.

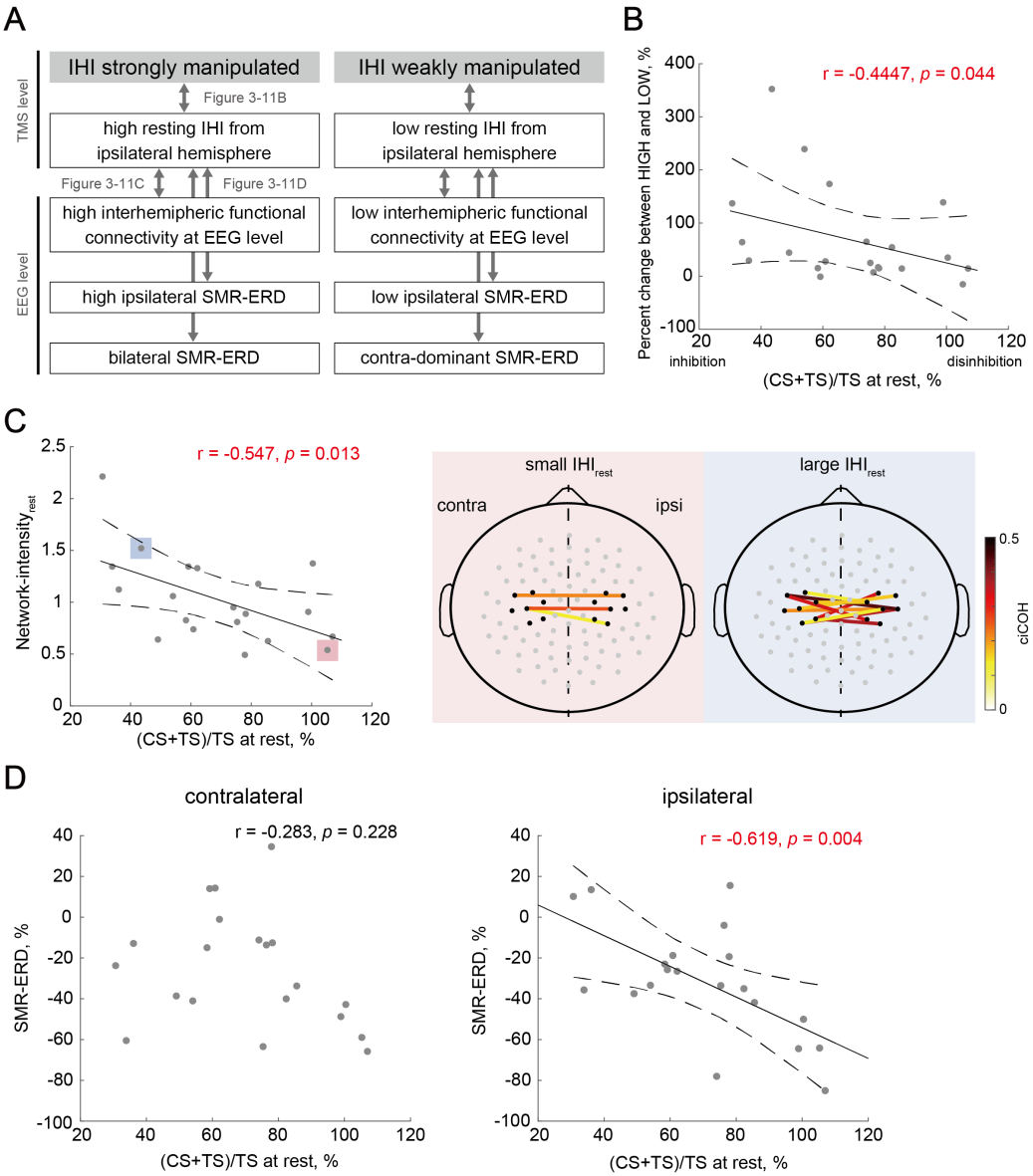

Figure 3-11. Individual characteristics associated with the manipulation capability of IHI

(A) Overview of the relationships between biomarkers from EEG and TMS levels to probe the individual signatures for strong versus weak manipulation of IHI. Arrows corresponds to a single panel. **(B)** Across-participant correlations between the manipulation capability of IHI and intrinsic IHI magnitude at rest. Dots represent a single participant. Solid and dotted lines represent the estimated linear regression and 95% confidence interval, respectively. Participants with greater IHI at rest were able to strongly manipulate IHI. **(C)** The left-sided panel shows across-participant correlations between IHI at rest and resting-state Network-intensity between bilateral SM1. The two

right-sided panels indicate the significant interhemispheric connections ("Connectivity Analysis" in Methods) of the two representative participants with small and large IHI_{rest}, respectively. The solid lines indicate a significant connection, and large positive values (dark red color) represent strong connection. The black dots around bilateral SM1 denote the seed channels, C3 or C4, and six neighboring channels. The gray dots represent other EEG channels. **(D)** Across-participant correlations between IHI at rest and EEG profiles showed significant correlation between IHI_{rest} and ipsilateral SMR-ERD, but not between IHI_{rest} and contralateral SMR-ERD.

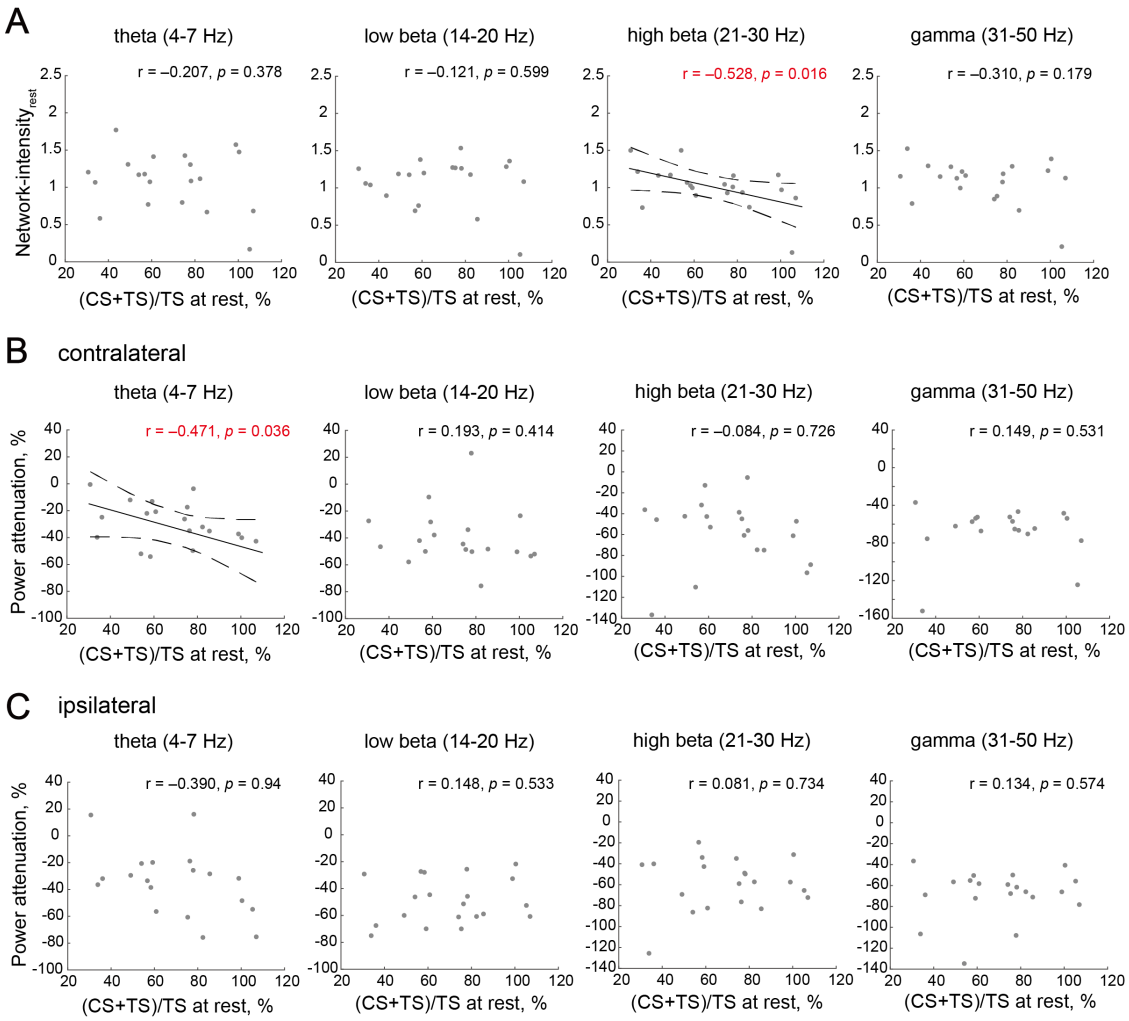

Figure 3-12. Associations of IHI magnitude and bilateral EEG patterns in frequency bands outside of a target alpha band

(A) Distributions of within-participant correlation coefficients in frequency bands outside

of a target alpha band in all participants. Red dots represent individuals with a significant correlation between IHI magnitude and contralateral or ipsilateral excitabilities (power attenuation), respectively. **(B), (C)** Repeated measures correlations between IHI magnitude and contralateral or ipsilateral excitabilities, respectively. Dots represent mean value of a single session of each individual. **(D)** Comparison of Network-intensity during MI across sessions. Dendrograms above the bars represent the results of the post-hoc analyses. * $p < 0.05$; all comparisons were Bonferroni corrected.

3.4. Discussion

In this chapter, the author aimed to determine whether it is possible to manipulate the IHI magnitude and uncover related neural activity behind IHI modulation, while controlling bilateral SMR-ERDs via spatially bivariate BCI-based neurofeedback. This was the first study to show IHI-state manipulation with a large dynamic range induced by volitional variation in ipsilateral sensorimotor excitability expressed by SMR-ERD. In addition, resting-state interhemispheric network at the TMS (IHI_{rest}) and EEG (interhemispheric $Network\text{-}intensity_{rest}$) levels were associated with the manipulation capability of IHI magnitude.

Using spatially bivariate BCI-based neurofeedback enables participants to volitionally increase or decrease (bidirectional) the ipsilateral sensorimotor excitability, while maintaining constant contralateral sensorimotor excitability. Ipsilateral SMR-ERD to the imagined hand (but not contralateral), reflecting IHI magnitude (**Figure 3-3B**) and their significant correlation (**Figure 3-10C**), were explained by previous studies (Haegens et al., 2011; Khademi et al., 2018; Kraus et al., 2016; Madsen et al., 2019; Naros et al., 2020; Ros et al., 2010; Sauseng et al., 2009; Takemi et al., 2013; Thies et al., 2018;

Zarkowski et al., 2006). The *in vivo* cortical recordings in monkeys revealed that pericentral alpha power was inversely related with the normalized firing rate in the sensorimotor regions (Haegens et al., 2011). In humans, several studies using single-pulse TMS of the motor hand area combined with EEG tested how ongoing pericentral oscillatory activity impacts corticomotor excitability reflected by the MEP amplitude. These EEG-TMS studies found a negative relationship between pre-stimulus alpha power and MEP amplitude through both offline (Sauseng et al., 2009; Takemi et al., 2013; Zarkowski et al., 2006) and online (Madsen et al., 2019) approaches, whereas the opposite of that was also found (Thies et al., 2018). Furthermore, another EEG-TMS study using neurofeedback demonstrated that the endogenous suppression of alpha rhythms at rest can produce robust increase in MEP amplitude and decrease in short-interval intracortical inhibition (Ros et al., 2010). Similarly, in the beta band, some evidences were revealed that a negative relationship between beta power and MEP amplitudes (Khademi et al., 2018; Kraus et al., 2016; Naros et al., 2020). As for IHI through the transcallosal fiber, it is predominantly regulated through direct postsynaptic mechanisms in the apical dendritic shafts of pyramidal neurons and a specific cortical microcircuitry mediated by dendritic $GABA_B$ receptors in inhibitory interneurons (Palmer et al., 2012). Additionally, consistent with this phenomenon, down-regulation of ipsilateral SMR-ERD, for example, may influence the excitation of the ipsilateral transcallosal pyramidal neuron followed by disinhibition of the contralateral inhibitory interneurons during unilateral upper limb MI. Therefore, pronounced changes in cortical mechanism despite the absence of sensory input and constant MEP amplitude in the imagined right hand elicited by single TS

suggest that the modulation of IHI magnitude from the ipsilateral (right) to the contralateral (left) hemisphere was at least partly of cortical, rather than spinal, origin. These neural mechanisms can be explored further by using triple pulse procedures (Ni et al., 2011) in which (dis)inhibition can be directly measured as the modulation of short-interval intracortical inhibition.

The potential contribution of resting-state IHI magnitude and interhemispheric functional connectivity in the alpha and high beta bands to the current results of manipulation capability in IHI (**Figure 3-11B, C**, and **Figure 3-12A**) can be speculated by considering the previous studies. Interregional communication is accompanied by synchronized oscillations in different brain regions (Fries, 2005; Varela et al., 2001), and this synchronization can be evaluated by functional connectivity. Because both hemispheres are structurally connected by transcallosal projection and exhibit functional cross talks (Hofer and Frahm, 2006; Meyer et al., 1995), the manipulation capability of IHI is likely associated with a structural connectivity as well as local oscillatory power entrainment. As for frequency band outside of neurofeedback target, it is well known that the intensity of SMR-ERD in the beta band reflects the sensorimotor cortical excitability and cortico-muscular activation (Hussain et al., 2019; Schulz et al., 2014). This multimodal EEG-TMS approach proves that the bilateral alpha and beta activities observed in the current study served to modulate the functional interhemispheric interaction over motor cortices.

For the other modalities, for example, real-time fMRI-based neurofeedback to a single region of interest (Sitaram et al., 2017; Weiskopf et al., 2004) or interregional

functional connectivity (Liew et al., 2016; Pereira et al., 2019) can be used for volitional modulation of neuronal connectivity and could serve as a possible therapeutic tool for motor or cognitive training in diseases related to impaired interregional connectivity. However, even fMRI-based neurofeedback with high spatial resolution, based on blood oxygenation level-dependent signal, cannot easily distinguish between the excitatory and the inhibitory activities from each region (Moon et al., 2021). Additionally, neurofeedback using interhemispheric functional connectivity has the possibility to counteract the modulation of IHIs from the right to left hemisphere and from the left to right hemisphere. Our results showed no significant difference in Network-intensity during MI between HIGH and LOW sessions (**Figure 3-10D**), indicating that interhemispheric functional connectivity at the EEG level was not changed, whereas IHI was modulated. This may indicate that IHI and Network-intensity simply reflect the activity of different neural populations; interhemispheric projections act via surround/lateral inhibition in the sensory and motor cortices (Carson, 2020) , while the synchrony at the EEG level reflects changes in the activity of local interactions between pyramidal neurons and interneurons in the thalamocortical loops (Pfurtscheller and Lopes da Silva, 1999). Furthermore, it is possible that Network-intensity reflects the degree of bidirectional synchrony between the two motor cortices, while IHI reflects one-way (right-to-left) inhibitory effects. Therefore, it is unclear whether fMRI-based neurofeedback using interhemispheric functional connectivity is linked to ipsilateral excitability, and whether it modulates IHI magnitude.

Interhemispheric activity is also passively modulated by externally administered interventions, e.g., tDCS or rTMS over the motor cortices (Gilio et al., 2003; Peña-Gómez et al., 2012; Williams et al., 2010). Although such tools have neuromodulation efficacy, their long-term sustained effects are often limited and they do not have spatial specificity due to their remote effects (Di Pino et al., 2014; Notturno et al., 2014; Weiskopf et al., 2004). Conversely, under the conscious self-learning environment, volitional control of MEP amplitudes is retained for at least 6 months without further training (Ruddy et al., 2018), which supports the long-term efficacy of IHI manipulation. In addition, we successfully demonstrated that IHI-specific changes greater than the variance explained by the CS effect. Based on these findings, further experiments are needed to better understand the pathway specificity. To further confirm whether the participants learned pathway-specific IHI manipulation, the CS effect should be kept constant across the conditions by adjusting the CS intensity to evoke left MEP of 1 mV peak-to-peak amplitude. Furthermore, the effect size of IHI manipulation in the current study (Cohen's d = 1.50) was comparable to that of representative tDCS studies (Cohen's d = 1.55) (Williams et al., 2010) and superior to that of rTMS studies (Gilio et al., 2003) (Cohen's d = 0.80; note that it is a value from the graph). Two meta-analyses of clinical trials using rTMS and tDCS also indicated that the effect sizes were medium (0.4–0.6) (Adeyemo et al., 2012; Hsu et al., 2012). Based on a previous study of neurofeedback training combined with externally administered interventions (Ang et al., 2015), their combination may facilitate neural plasticity.

Table 3-1. Target-hemisphere-specific modulation at the EEG level induced by spatially bivariate BCI-based neurofeedback (Figure 3-3A and B)

	REST	NoFB	HIGH	MID	LOW	F-value	*p*- value	η^2-value
contralateral SMR-ERD, %	–10.6 ± 11.6	13.5 ± 29.5*	19.3 ± 26.5**	16.1 ± 24.1**	13.3 ± 28.4*	4.81	0.014	0.16 (large)
ipsilateral SMR-ERD, %	–18.8 ± 12.2	–10.5 ± 34.0	64.5 ± 14.0***,†††	10.1 ± 20.3*,‡‡‡	–156.3 ± 49.0***,†††,‡‡‡,§§§	156.0	< 0.001	0.86 (large)

Values are mean value ± SD. Post-hoc two-tailed paired t-test showed significant difference with REST value *, NoFB value †, HIGH value ‡, and MID value §. F values and P values were calculated by repeated-measures ANOVA. The number of each dendrogram is as follows: for example, * $p < 0.05$, ** $p < 0.01$, and *** $p < 0.001$; all comparisons were Bonferroni corrected.

Table 3-2. IHI curves (Figure 3-4B)

	0% RMT	100% RMT	110% RMT	120% RMT	130% RMT	140% RMT	F-value	*p*- value	η^2-value
MEP amplitude [mV]	0.93 ± 0.25	0.66 ± 0.29*	0.62 ± 0.31***	0.54 ± 0.26***	0.47 ± 0.24***	0.43 ± 0.22***	8.31	< 0.001	0.28 (large)

Values are mean value ± SD. Post-hoc two-tailed paired t-test showed significant difference with 0% RMT value * (* $p < 0.05$, ** $p < 0.01$, and *** $p < 0.001$; all comparisons were Bonferroni corrected). F values and P values were calculated by repeated-measures ANOVA.

Table 3-3. Comparison of IHI magnitude (Figure 3-5B and C)

	REST	NoFB	HIGH	MID	LOW	F-value	*p*- value	η^2-value
(CS+TS)/TS, %	69.0 ± 22.6	85.9 ± 18.3	62.0 ± 23.5†	85.5 ± 26.2‡	96.9 ± 27.7**,‡‡‡	6.85	< 0.001	0.22 (large)
MEP amplitude [mV]	0.98 ± 0.45	1.50 ± 1.02	1.94 ± 1.37	1.67 ± 1.15	1.93 ± 1.41	2.44	0.104	0.09 (medium)

Values are mean value ± SD. Post-hoc two-tailed paired t-test showed significant difference with REST value *, NoFB value †, HIGH value ‡. F values and P values were calculated by repeated-measures ANOVA. The number of each dendrogram is as follows: for example, * $p < 0.05$, ** $p < 0.01$, and *** $p < 0.001$; all comparisons were Bonferroni corrected.

Table 3-4. Comparison of the percent change in IHI magnitude based on values in NoFB session (Figure 3-6)

	REST	HIGH	MID	LOW	F-value	*p*- value	η^2-value
% change from NoFB session, %	–15.8 ± 29.8	–27.3 ± 26.6	2.7 ± 30.2†	17.9 ± 36.4**,†††	8.32	< 0.001	0.24 (large)

Values are mean value ± SD. Post-hoc two-tailed paired t-test showed significant difference with REST value *and HIGH value †. F values and P values were calculated by repeated-measures ANOVA. The number of each dendrogram is as follows: for example, * $p < 0.05$, ** $p < 0.01$, and *** $p < 0.001$; all comparisons were Bonferroni corrected.

Table 3-5. Comparison of IHI magnitude in triggered and non-triggered TMS trials (Figure 3-7)

	HIGH		MID		LOW		F-value	*p*- value	η^2-value
	triggered	non-triggered	triggered	non-triggered	triggered	non-triggered			
(CS+TS)/TS, %	62.0 ± 23.5	80.5 ± 37.8	85.5 ± 26.2*	83.2 ± 36.3	96.9 ± 27.7***	90.1 ± 30.6	sessions: 5.08	0.008	0.08 (medium)
							trials: 0.32	0.575	< 0.01
							sessions×trials: 1.82	0.167	0.03 (small)

Values are mean value ± SD. Post-hoc two-tailed paired t-test showed significant difference with HIGH value *. F values and P values were calculated by repeated-measures ANOVA. The number of each dendrogram is as follows: * $p < 0.05$, ** $p < 0.01$, and *** $p < 0.001$; all comparisons were Bonferroni corrected.

Table 3-6. Relationship between the increase in IHI and left MEP amplitude elicited by CS (Figure 3-8B, C, and D)

	REST	NoFB	HIGH	MID	LOW	F-value	*p*- value	η^2-value
Left MEP amplitude [mV]	1.18 ± 1.02	1.25 ± 0.61	1.46 ± 0.96	1.27 ± 0.88	1.16 ± 0.68	0.39	0.813	0.02 (small)

	HIGH	MID	LOW	F-value	p-value	η2-value
% change from NoFB session, %						
triggered	27.3 ± 26.6	–2.7 ± 30.2***	–17.9 ± 36.4***	12.75	< 0.001	0.44 (large)
non-triggered	–1.98 ± 56.6	–1.10 ± 39.1	–7.9 ± 38.2	1.13	0.319	0.10 (medium)

Values are mean value ± SD. Post-hoc two-tailed paired t-test in the increase in IHI showed significant difference with HIGH value *. F values and P values were calculated by repeated-measures ANOVA. The number of each dendrogram is as follows: * $p < 0.05$, ** $p < 0.01$, and *** $p < 0.001$; all comparisons were Bonferroni corrected.

Table 3-7. Comparison of IHI magnitude for control muscle (Figures 3-9A and B)

	REST	NoFB	HIGH	MID	LOW	F-value	*p*- value	η^2-value
(CS+TS)/TS, %	74.1 ± 21.5	94.9 ± 15.7*	84.0 ± 22.6	86.0 ± 19.4	82.9 ± 22.8	2.51	0.048	0.12 (medium)
MEP amplitude [mV]	0.54 ± 0.51	0.50 ± 0.39	0.73 ± 0.61	0.59 ± 0.50	0.65 ± 0.51	0.62	0.649	0.03 (small)

Values are mean value ± SD. Post-hoc two-tailed paired t-test showed significant difference with REST value *. F values and P values were calculated by repeated-measures ANOVA. The number of each dendrogram is as follows: * $p < 0.05$, ** $p < 0.01$, and *** $p < 0.001$; all comparisons were Bonferroni corrected.

Table 3-8. Associations of IHI magnitude and bilateral EEG patterns (Figures 3-10D)

	REST	NoFB	HIGH	MID	LOW	F-value	*p*- value	η^2-value
Network-intensity$_{MI}$	0.16 ± 0.14	0.27 ± 0.28	0.34 ± 0.31	0.15 ± 0.10*	0.23 ± 0.25	3.04	0.020	0.10 (medium)

Values are mean value ± SD. Post-hoc two-tailed paired t-test showed significant difference with HIGH value *. F values and P values were calculated by repeated-measures ANOVA. The number of each dendrogram is as follows: * $p < 0.05$, ** $p < 0.01$, and *** $p < 0.001$; all comparisons were Bonferroni corrected.

Chapter 4: General conclusion

4.1. Summary of this dissertation

The purpose of this dissertation was to evaluate whether healthy individuals could explicitly guide sensorimotor cortical activity to the targeted hemisphere and whether users could learn to volitionally manipulate the IHI magnitude through the BCI-based neurofeedback paradigm. In Chapter 2, the author determined whether the sensorimotor cortical activity can be guided to the targeted hemisphere by a neuroanatomical-inspired approach. Spatially bivariate BCI-based neurofeedback enabled us to up-regulate the hemispheric activation of the ipsilateral or contralateral targeted hemisphere in the same participants, a phenomenon that has not previously been reported. The results suggest that this BCI-based neurofeedback has great potential for facilitating the resumption and shaping of the neural remodeling process. In Chapter 3, the author presented an innovative approach to manipulate the IHI state, by directly and bidirectionally modulating SMR-ERDs in a spatially bivariate BCI-based neurofeedback paradigm. The IHI magnitude was manipulated through participants learning to up- and down-regulate the ipsilateral excitability to the imagined hand while maintaining constant the contralateral excitability (**Figure 4-1**).

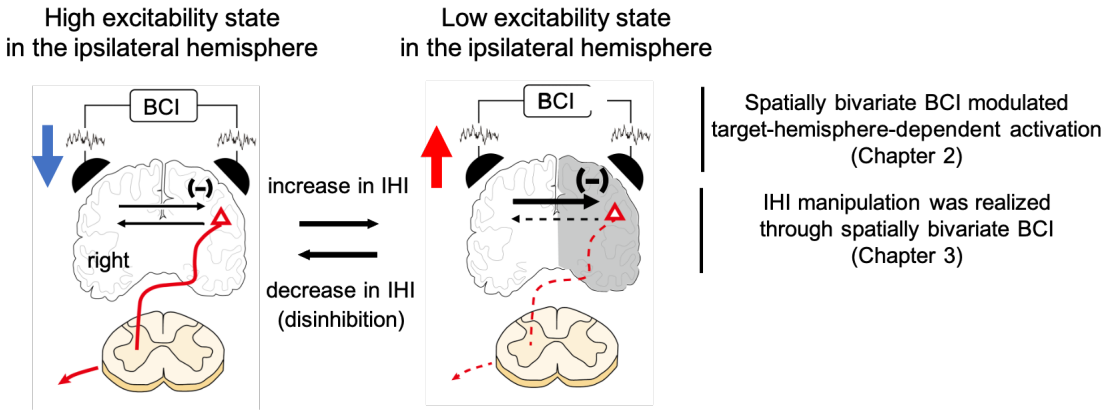

Figure 4-1. Conclusion of this dissertation

In Chapter 2, the author indicated that spatially bivariate BCI-based neurofeedback enabled us to up-regulate the hemispheric activation of the ipsilateral or contralateral targeted hemisphere. In Chapter 3, the author presented an approach to manipulate the IHI state, by directly and bidirectionally modulating sensorimotor excitabilities in a spatially bivariate BCI-based neurofeedback paradigm.

Previous neurofeedback studies have demonstrated that it is possible to gain voluntary control over the central nervous system activity without externally administered interventions, if appropriate neurofeedback is embedded in a reinforcement learning task, such as food rewards for animals (Engelhard et al., 2013; Fetz, 2013) and visual and/or somatosensory feedback for humans (Sitaram et al., 2017; Thompson et al., 2009). However, conventional BCI-based neurofeedback of the SMR signal from one hemisphere did not guarantee spatially specific activation of the sensorimotor region in the targeted hemisphere (Buch et al., 2008; Caria et al., 2011; Soekadar et al., 2015a), because the sensorimotor activities in the left and right hemispheres potentially influence one another, making IHI manipulation difficult. To address this issue, the author

demonstrated a spatially bivariate BCI-based neurofeedback technique and revealed the manipulation of IHI magnitude.

4.2. Future perspective and remaining limitations

These approaches provide an opportunity to understand the inhibitory sensorimotor functions and pave the way for new technologies that allow the user/patient to regulate various aspects of their brain function to reach the desired states. The findings are expected to be applied in various fields, e.g., in the context of neurorehabilitation. Although the rehabilitation strategy of rebalancing the interhemispheric networks to improve motor recovery after stroke is controversial (Bundy et al., 2017; Carson, 2020; Xu et al., 2019), the current technique can be tailored either by up-conditioning the damaged hemisphere, down-conditioning the intact hemisphere, a combination of both, or vice versa, depending on the patient's specific states. Furthermore, a previous review (Carson, 2020) supported the conceptual framework and suggested that a fundamental role of IHI is to support the narrowing of excitatory focus by co-opting the capacities of the two cerebral hemispheres. This framework is consistent with the known associations between the structural integrity of callosal projections and the magnitude of the motor deficits after stroke (Auriat et al., 2015; Granziera et al., 2012; Koh et al., 2018). Thus, the spatially bivariate BCI-based neurofeedback approach might be highly relevant for application in the context of stroke recovery as well as basic sciences. Future studies probing the residual ability to manipulate IHI in stroke patients are expected.

This dissertation had several limitations that need to be considered when interpreting the results. Although we successfully demonstrated the bidirectional changes in the ipsilateral SMR-ERD, the bidirectional changes in IHI from the right to the left hemisphere were not statistically significant since there was no significant difference between the MID and LOW sessions. The current results should prompt future studies to ascertain whether IHI down-regulation (i.e., disinhibition) during MI and IHI up-regulation at rest in the non-dominant hemisphere (intact hemisphere) are possible in a similar setup. With regards to the limitations of the volitional control of SMR-ERD during unilateral MI, all participants were right-handed (laterality quotient: 90.3 ± 27.4% in Chapter 2 and 72.2 ± 30.9% in Chapter 3), as assessed by the Edinburgh Inventory (Oldfield, 1971), to eliminate bias due to differences in handedness. If a left-handed participant performs the same experiment, the modulation effect via BCI-based neurofeedback may be different. Moreover, in case that the contralateral SMR-ERD was up- or down-regulated instead of maintained at a moderate level, it is unclear whether the ipsilateral SMR-ERD was modulated bidirectionally and whether the IHI changed therewith. The study involved a total of 11 sessions, including REST and NoFB, and the combinations of SMR-ERDs in both hemispheres (3 conditions vs. 3 conditions) should be evaluated in the future. In addition, it is not clear whether the bivariate neurofeedback approach is superior to the conventional BCI-based neurofeedback that exploits SMR-ERD from a single hemisphere. Since both hemispheres are connected by intrinsic transcallosal projections and exhibit functional crosstalk (Arai et al., 2011; Hofer and Frahm, 2006; Meyer et al., 1995; Waters et al., 2017), it is expected that the sensorimotor

excitability in the opposite hemisphere would also be up-regulated through univariate (i.e., ipsilateral hemisphere to the imagined hand) BCI-based neurofeedback. Consistent with the findings that unilateral up- or down-regulation of the sensorimotor excitability contributes to the manipulation of the IHI magnitude, such sensorimotor activation without spatial specificity may inhibit the other hemisphere, leading to weaker range of IHI manipulation. Thus, we presumed that it is difficult to produce the same effect as this study via univariate BCI-based neurofeedback. Future studies are required to directly compare the effect size of IHI manipulation between bivariate and univariate BCI-based neurofeedback in a within-participant cross-over design that guarantees the experiment time by omitting some experimental conditions.

4.3. Conclusion

The development of new effective therapeutic strategies relies on an understanding of the mechanisms underlying functional recovery. In conclusion, this dissertation focused on IHI, a phenomenon that particularly characterizes hemiplegia after stroke, and indicated the advances made toward understanding how sensorimotor cortical activities during BCI-based neurofeedback are related to IHI manipulation. Moreover, the author showed how these insights might be translated to clinical benefits for patients with motor impairments caused by central nervous system injuries or illnesses. Exploring the boundary of plasticity induced by BCI-based neurofeedback is the stepping stone on the road to understanding humanity and its application in neurology and physical medicine.

The author concludes this dissertation with the hope that this research will contribute to further development of neuroscience and neurorehabilitation.

Acknowledgements

This dissertation has been written under the direction and guidance of Professor Junichi Ushiba in Department of Biosciences and Informatics, Faculty of Science and Technology, Keio University, Japan.

I would like to thank all the people who have helped me during my Ph.D. study and the writing of this dissertation. I particularly appreciate:

My supervisor:
I would like to express my deepest gratitude to my advisor, Professor **Junichi Ushiba**. His careful guidance and sophisticated philosophy in science encouraged me in all the time of research and daily life during my Ph.D. course. He is the person who has had the most influence on my life. I would like to express my deepest appreciation to him.

My committee members:
I am grateful to all the professors on my dissertation committee, Professor **Kotaro Oka**, Professor **Yasubumi Sakakibara** in Department of Biosciences and Informatics, and Professor **Yasue Mitsukura** in Department of System Design Engineering for agreeing to sit on my committee. Their valuable comments improved my Ph.D. study.

My advisor:
I would also like to thank Assistant Professor **Nobuaki Mizuguchi** at Ritsumeikan University, Dr. **Shohei Tsuchimoto** at National Institute for Physiological Sciences, and Dr. **Shoko Kasuga** at Queen's University. Their guidance and persistent help have brought me variable insights into my research since I was an undergraduate student.

My collaborators in Keio University School of Medicine, Japan:
I would like to express my gratitude to Associate Professor **Michiyuki Kawakami**, Dr. **Kohei Okuyama**, and Mr. **Kohsuke Okada** in the Department of Rehabilitation Medicine, Keio University School of Medicine for collaborating study and for valuable discussions.

All the current and past members of Ushiba laboratory, particularly the following:

I would also like to appreciate Project Senior Assistant Professor **Mitsuaki Takemi**, Dr. **Ryosuke Matsuya**, Dr. **Akito Kosugi**, Mr. **Kenichi Takasaki**, Dr. **Yuta Sato**, Dr. **Shuka Shibusawa**, and Mr. **Gaku Shiraishi** for giving me helpful advice to improve my research, and Mr. **Shohei Kimura**, Mr. **Ryota Mori**, Mr. **Daijiro Hara**, Mr. **Keito Morishita**, Mr. **Kota Yamamoto**, Mr. **Taisuke Okamoto**, Mr. **Seitaro Iwama**, Mr. **Ryotaro Hirose** for their daily help and for being fun.

I am also grateful for the much supports from Ms. **Sayoko Ishii**, Ms. **Kumi Nanjo**, Ms. **Yoko Mori**, Ms. **Akiko Shinohara**, Ms. **Syoko Tonomoto**, Ms. **Aya Kamiya**, and Ms. **Yumiko Kakubari** for their support on a daily basis. Thanks to them, I enjoyed my research comfortably every day.

Lastly and most importantly, special thanks also go to my parents, sister, and friends for supporting me throughout my life.

To them I dedicate this dissertation.

Funding

This work was supported by a Grant-in-Aid for Scientific Research on Innovative Areas (#15H05880) from the Ministry of Education, Culture, Sports, Science and Technology (MEXT), a Grant-in-Aid for Scientific Research(C) (#16K01469) from MEXT, a Grant-in-Aid for Transformative Research Areas (A) (#20H05923) from MEXT, Strategic International Brain Science Research Promotion Program (Brain/MINDS Beyond) (#JP19dm0307022 and #JP20dm0307022) from the Japan Agency for Medical Research and Development (AMED), and The Keio University Doctorate Student Grant-in-Aid Program from Ushioda Memorial Fund.

References

Adeyemo BO, Simis M, Macea DD, Fregni F. Systematic review of parameters of stimulation, clinical trial design characteristics, and motor outcomes in non-invasive brain stimulation in stroke. *Front Psychiatry* 3, 00088 (27 pages), 2012.

Alawieh A, Tomlinson S, Adkins D, Kautz S, Feng W. Preclinical and clinical evidence on ipsilateral corticospinal projections: Implication for motor recovery. *Transl Stroke Res* 8(6), 529–540, 2017.

Amatachaya A, Jensen MP, Patjanasoontorn N, Auvichayapat N, Suphakunpinyo C, Janjarasjitt S, Ngernyam N, Aree-uea B, Auvichayapat P. The Short-Term Effects of Transcranial Direct Current Stimulation on Electroencephalography in Children with Autism: A Randomized Crossover Controlled Trial. *Behav Neurol* 2015, 928631 (11 pages), 2015.

Ames KC, Churchland MM. Motor cortex signals for each arm are mixed across hemispheres and neurons yet partitioned within the population response. *eLife* 8, 46159 (36 pages), 2019.

Ang KK, Guan C. EEG-Based Strategies to Detect Motor Imagery for Control and Rehabilitation. *IEEE Trans Neural Syst Rehabil Eng* 25(4), 392–401, 2017.

Ang KK, Guan C, Chua KSG, Ang BT, Kuah CWK, Wang C, Phua KS, Chin ZY, Zhang H. A large clinical study on the ability of stroke patients to use an EEG-based motor imagery brain-computer interface. *Clin EEG Neurosci* 42(4), 253–258, 2011.

Ang KK, Guan C, Phua KS, Wang C, Zhao L, Teo WP, Chen C, Ng YS, Chew E. Facilitating effects of transcranial direct current stimulation on motor imagery brain-computer interface with robotic feedback for stroke rehabilitation. *Arch Phys Med Rehabil* 96(3, Supplement), S79–S87, 2015.

Arai N, Müller-Dahlhaus F, Murakami T, Bliem B, Lu M-K, Ugawa Y, Ziemann U. State-dependent and timing-dependent bidirectional associative plasticity in the human SMA-M1 network. *J Neurosci* 31(43), 15376–15383, 2011.

Astolfi L, Cincotti F, Mattia D, Marciani MG, Baccala LA, Fallani F de V, Salinari S, Ursino M, Zavaglia M, Ding L, Edgar JC, Miller GA, He B, Babiloni F. Comparison of different cortical connectivity estimators for high-resolution EEG recordings. *Hum Brain Mapp* 28(2), 143–157, 2007.

Auriat AM, Borich MR, Snow NJ, Wadden KP, Boyd LA. Comparing a diffusion tensor and non-tensor approach to white matter fiber tractography in chronic stroke. *NeuroImage Clin* 7(1), 771–781, 2015.

Bai Z, Fong KNK, Zhang JJ, Chan J, Ting KH. Immediate and long-term effects of BCI-based rehabilitation of the upper extremity after stroke: A systematic review and meta-analysis. *J Neuroengineering Rehabil* 17(57), 20, 2020.

Bakdash JZ, Marusich LR. Repeated measures correlation. *Front Psychol* 8, 00456 (13 pages), 2017.

Banich MT. The missing link: The role of interhemispheric interaction in attentional processing. *Brain Cogn* 36(2), 128–157, 1998.

Bauer R, Fels M, Vukelić M, Ziemann U, Gharabaghi A. Bridging the gap between motor imagery and motor execution with a brain–robot interface. *NeuroImage* 108(1), 319–327, 2015.

Birbaumer N, Cohen LG. Brain-computer interfaces: Communication and restoration of movement in paralysis. *J Physiol* 579(3), 621–636, 2007.

Boddington LJ, Reynolds JNJ. Targeting interhemispheric inhibition with neuromodulation to enhance stroke rehabilitation. *Brain Stimulat* 10(2), 214–222, 2017.

Bogen JE, Bogen GM. Creativity and the corpus callosum. *Psychiatr Clin North Am* 11(3), 293–301, 1988.

Buch E, Weber C, Cohen LG, Braun C, Dimyan MA, Ard T, Mellinger J, Caria A, Soekadar S, Fourkas A, Birbaumer N. Think to move: A neuromagnetic brain-computer interface (BCI) system for chronic stroke. *Stroke* 39(3), 910–917, 2008.

Bundy DT, Souders L, Baranyai K, Leonard L, Schalk, Coker R, Moran DW, Huskey T, Leuthardt EC. Contralesional brain–computer interface control of a powered exoskeleton for motor recovery in chronic stroke survivors. *Stroke* 48(7), 1908–1915, 2017.

Caria A, Weber C, Brötz D, Ramos A, Ticini LF, Gharabaghi A, Braun C, Birbaumer N. Chronic stroke recovery after combined BCI training and physiotherapy: A case report. *Psychophysiology* 48(4), 578–582, 2011.

Carson RG. Neural pathways mediating bilateral interactions between the upper limbs. *Brain Res Rev* 49(3), 641–662, 2005.

Carson RG. Inter-hemispheric inhibition sculpts the output of neural circuits by co-opting the two cerebral hemispheres. *J Physiol* 598(21), 4781–4802, 2020.

Carter Leno V, Tomlinson SB, Chang S-AA, Naples AJ, McPartland JC. Resting-state alpha power is selectively associated with autistic traits reflecting behavioral rigidity. *Sci Rep* 8, 11982 (7 pages), 2018.

Cervera MA, Soekadar SR, Ushiba J, Millán JDR, Liu M, Birbaumer N, Garipelli G. Brain-computer interfaces for post-stroke motor rehabilitation: A meta-analysis. *Ann Clin Transl Neurol* 5(5), 651–663, 2018.

Chaudhary U, Birbaumer N, Ramos-Murguialday A. Brain–computer interfaces for communication and rehabilitation. *Nat Rev Neurol* 12(9), 513–525, 2016.

Chieffo R, Inuggi A, Straffi L, Coppi E, Gonzalez-Rosa J, Spagnolo F, Poggi A, Comi G, Comola M, Leocani L. Mapping early changes of cortical motor output after subcortical stroke: A transcranial magnetic stimulation study. *Brain Stimulat* 6(3), 322–329, 2013.

Chiew M, LaConte SM, Graham SJ. Investigation of fMRI neurofeedback of differential primary motor cortex activity using kinesthetic motor imagery. *NeuroImage* 61(1), 21–31, 2012.

Chowdhury SA, Matsunami KI. GABA-B-related activity in processing of transcallosal response in cat motor cortex. *J Neurosci Res* 68(4), 489–495, 2002.

Cohen J. A power primer. *Psychol Bull* 112(1), 155–159, 1992.

Colebatch JG, Rothwell JC, Day BL, Thompson PD, Marsden CD. Cortical outflow to proximal arm muscles in man. *Brain* 113(6), 1843–1856, 1990.

Cordes D, Haughton VM, Arfanakis K, Carew JD, Turski PA, Moritz CH, Quigley MA, Meyerand ME. Frequencies contributing to functional connectivity in the cerebral cortex in "resting-state" data. *Am J Neuroradiol* 22(7), 1326–1333, 2001.

Crone NE, Miglioretti DL, Gordon B, Sieracki JM, Wilson MT, Uematsu S, Lesser RP. Functional mapping of human sensorimotor cortex with electrocorticographic spectral analysis. I. Alpha and beta event-related desynchronization. *Brain* 121(12), 2271–2299, 1998.

Daly JJ, Wolpaw JR. Brain-computer interfaces in neurological rehabilitation. *Lancet Neurol* 7(11), 1032–1043, 2008.

Damoiseaux JS, Rombouts SARB, Barkhof F, Scheltens P, Stam CJ, Smith SM, Beckmann CF. Consistent resting-state networks across healthy subjects. *Proc Natl Acad Sci* 103(37), 13848–13853, 2006.

Daskalakis ZJ, Christensen BK, Fitzgerald PB, Roshan L, Chen R. The mechanisms of interhemispheric inhibition in the human motor cortex. *J Physiol* 543(1), 317–326, 2002.

De Luca M, Beckmann CF, De Stefano N, Matthews PM, Smith SM. fMRI resting state networks define distinct modes of long-distance interactions in the human brain. *NeuroImage* 29(4), 1359–1367, 2006.

Derosière G, Alexandre F, Bourdillon N, Mandrick K, Ward TE, Perrey S. Similar scaling of contralateral and ipsilateral cortical responses during graded unimanual force generation. *NeuroImage* 85(1), 471–477, 2014.

Devanne H, Lavoie BA, Capaday C. Input-output properties and gain changes in the human corticospinal pathway. *Exp Brain Res* 114(2), 329–338, 1997.

Di Pino G, Pellegrino G, Assenza G, Capone F, Ferreri F, Formica D, Ranieri F, Tombini M, Ziemann U, Rothwell JC, Di Lazzaro V. Modulation of brain plasticity in stroke: A novel model for neurorehabilitation. *Nat Rev Neurol* 10(10), 597–608, 2014.

van Diessen E, Numan T, van Dellen E, van der Kooi AW, Boersma M, Hofman D, van Lutterveld R, van Dijk BW, van Straaten ECW, Hillebrand A, Stam CJ. Opportunities and methodological challenges in EEG and MEG resting state functional brain network research. *Clin Neurophysiol* 126(8), 1468–1481, 2015.

Dodd KC, Nair VA, Prabhakaran V. Role of the contralesional vs. ipsilesional hemisphere in stroke recovery. *Front Hum Neurosci* 11, 00469 (9 pages), 2017.

Dong Y, Dobkin BH, Cen SY, Wu AD, Winstein CJ. Motor cortex activation during treatment may predict therapeutic gains in paretic hand function after stroke. *Stroke* 37(6), 1552–1555, 2006.

Duque J, Hummel F, Celnik P, Murase N, Mazzocchio R, Cohen LG. Transcallosal inhibition in chronic subcortical stroke. *NeuroImage* 28(4), 940–946, 2005.

Duque J, Murase N, Celnik P, Hummel F, Harris-Love M, Mazzocchio R, Olivier E, Cohen LG. Intermanual differences in movement-related interhemispheric inhibition. *J Cogn Neurosci* 19(2), 204–213, 2007.

Elsner B, Kugler J, Pohl M, Mehrholz J. Transcranial direct current stimulation (tDCS) for improving function and activities of daily living in patients after stroke. *Cochrane Database Syst Rev* 11(1), 1–293, 2013.

Elsner B, Kugler J, Pohl M, Mehrholz J. Transcranial direct current stimulation (tDCS) for improving activities of daily living, and physical and cognitive functioning, in people after stroke. *Cochrane Database Syst Rev* 11(1), 1–87, 2020.

Engelhard B, Ozeri N, Israel Z, Bergman H, Vaadia E. Inducing gamma oscillations and precise spike synchrony by operant conditioning via brain-machine interface. *Neuron* 77(2), 361–375, 2013.

Ewald A, Marzetti L, Zappasodi F, Meinecke FC, Nolte G. Estimating true brain connectivity from EEG/MEG data invariant to linear and static transformations in sensor space. *NeuroImage* 60(1), 476–488, 2012.

Faul F, Erdfelder E, Buchner A, Lang A-G. Statistical power analyses using G*Power 3.1: Tests for correlation and regression analyses. *Behav Res Methods* 41(4), 1149–1160, 2009.

Faul F, Erdfelder E, Lang A-G, Buchner A. G*Power 3: A flexible statistical power analysis program for the social, behavioral, and biomedical sciences. *Behav Res Methods* 39(2), 175–191, 2007.

Ferbert A, Priori A, Rothwell JC, Day BL, Colebatch JG, Marsden CD. Interhemispheric inhibition of the human motor cortex. *J Physiol* 453(1), 525–546, 1992.

Ferree TC, Luu P, Russell GS, Tucker DM. Scalp electrode impedance, infection risk, and EEG data quality. *Clin Neurophysiol* 112(3), 536–544, 2001.

Fetz EE. Volitional control of cortical oscillations and synchrony. *Neuron* 77(2), 216–218, 2013.

Fransson P. Spontaneous low-frequency BOLD signal fluctuations: An fMRI investigation of the resting-state default mode of brain function hypothesis. *Hum Brain Mapp* 26(1), 15–29, 2005.

Fries P. A mechanism for cognitive dynamics: Neuronal communication through neuronal coherence. *Trends Cogn Sci* 9(10), 474–480, 2005.

Gao Q, Duan X, Chen H. Evaluation of effective connectivity of motor areas during motor imagery and execution using conditional Granger causality. *NeuroImage* 54(2), 1280–1288, 2011.

Gharabaghi A, Kraus D, Leão MT, Spüler M, Walter A, Bogdan M, Rosenstiel W, Naros G, Ziemann U. Coupling brain-machine interfaces with cortical stimulation for brain-state dependent stimulation: Enhancing motor cortex excitability for neurorehabilitation. *Front Hum Neurosci* 8, 00122 (7 pages), 2014.

Ghosh S, Mehta AR, Huang G, Gunraj C, Hoque T, Saha U, Ni Z, Chen R. Short- and long-latency interhemispheric inhibitions are additive in human motor cortex. *J Neurophysiol* 109(12), 2955–2962, 2013.

Gilio F, Rizzo V, Siebner HR, Rothwell JC. Effects on the right motor hand-area excitability produced by low-frequency rTMS over human contralateral homologous cortex. *J Physiol* 551(2), 563–573, 2003.

Granziera C, Daducci A, Meskaldji DE, Roche A, Maeder P, Michel P, Hadjikhani N, Sorensen AG, Frackowiak RS, Thiran J-P, Meuli R, Krueger G. A new early and automated MRI-based predictor of motor improvement after stroke. *Neurology* 79(1), 39–46, 2012.

Grefkes C, Fink GR. Reorganization of cerebral networks after stroke: New insights from neuroimaging with connectivity approaches. *Brain* 134(5), 1264–1276, 2011.

Grefkes C, Fink GR. Disruption of motor network connectivity post-stroke and its noninvasive neuromodulation. *Curr Opin Neurol* 25(6), 670–675, 2012.

Grefkes C, Fink GR. Connectivity-based approaches in stroke and recovery of function. *Lancet Neurol* 13(2), 206–216, 2014.

Grefkes C, Nowak DA, Eickhoff SB, Dafotakis M, Küst J, Karbe H, Fink GR. Cortical connectivity after subcortical stroke assessed with functional magnetic resonance imaging. *Ann Neurol* 63(2), 236–246, 2008.

Greicius MD, Krasnow B, Reiss AL, Menon V. Functional connectivity in the resting brain: A network analysis of the default mode hypothesis. *Proc Natl Acad Sci* 100(1), 253–258, 2003.

Groppa S, Oliviero A, Eisen A, Quartarone A, Cohen LG, Mall V, Kaelin-Lang A, Mima T, Rossi S, Thickbroom GW, Rossini PM, Ziemann U, Valls-Solé J, Siebner HR. A practical guide to diagnostic transcranial magnetic stimulation: Report of an IFCN committee. *Clin Neurophysiol* 123(5), 858–882, 2012.

Haegens S, Nácher V, Luna R, Romo R, Jensen O. α-Oscillations in the monkey sensorimotor network influence discrimination performance by rhythmical inhibition of neuronal spiking. *Proc Natl Acad Sci* 108(48), 19377–19382, 2011.

Halder S, Varkuti B, Bogdan M, Kübler A, Rosenstiel W, Sitaram R, Birbaumer N. Prediction of brain-computer interface aptitude from individual brain structure. *Front Hum Neurosci* 7, 00105 (9 pages), 2013.

Hallett M. Transcranial magnetic stimulation: A primer. *Neuron* 55(2), 187–199, 2007.

Hamedi M, Salleh S-H, Noor AM. Electroencephalographic motor imagery brain connectivity analysis for BCI: A review. *Neural Comput* 28(6), 999–1041, 2016.

Hao Z, Wang D, Zeng Y, Liu M. Repetitive transcranial magnetic stimulation for improving function after stroke. *Cochrane Database Syst Rev* 5(1), 1–47, 2013.

Harris-Love ML, Chan E, Dromerick AW, Cohen LG. Neural substrates of motor recovery in severely impaired stroke patients with hand paralysis. *Neurorehabil Neural Repair* 30(4), 328–338, 2016.

Harris-Love ML, Perez MA, Chen R, Cohen LG. Interhemispheric inhibition in distal and proximal arm representations in the primary motor cortex. *J Neurophysiol* 97(3), 2511–2515, 2007.

Hasegawa K, Kasuga S, Takasaki K, Mizuno K, Liu M, Ushiba J. Ipsilateral EEG mu rhythm reflects the excitability of uncrossed pathways projecting to shoulder muscles. *J NeuroEngineering Rehabil* 14(85), 11, 2017.

Hayashi M, Mizuguchi N, Tsuchimoto S, Ushiba J. Neurofeedback of scalp bi-hemispheric EEG sensorimotor rhythm guides hemispheric activation of sensorimotor cortex in the targeted hemisphere. *NeuroImage* 223, 117298 (15 pages), 2020.

Hayashi M, Mizuguchi N, Tsuchimoto S, Ushiba J. Neurofeedback of scalp bi-hemispheric EEG sensorimotor rhythm guides hemispheric activation of sensorimotor cortex in the targeted hemisphere. *Brain-Comput Interface Res State---Art Summ* 9(1), 25–38, 2021.

Hayashi M, Tsuchimoto S, Mizuguchi N, Miyatake M, Kasuga S, Ushiba J. Two-stage regression of high-density scalp electroencephalograms visualizes force regulation signaling during muscle contraction. *J Neural Eng* 16, 056020 (14 pages), 2019.

He S, Everest-Phillips C, Clouter A, Brown P, Tan H. Neurofeedback-linked suppression of cortical β bursts speeds up movement initiation in healthy motor control: A double-blind sham-controlled study. *J Neurosci* 40(20), 4021–4032, 2020.

Hofer S, Frahm J. Topography of the human corpus callosum revisited: Comprehensive fiber tractography using diffusion tensor magnetic resonance imaging. *NeuroImage* 32(3), 989–994, 2006.

Hsu W-Y, Cheng C-H, Liao K-K, Lee I-H, Lin Y-Y. Effects of repetitive transcranial magnetic stimulation on motor functions in patients with stroke: A meta-analysis. *Stroke* 43(7), 1849–1857, 2012.

Hummel FC, Cohen LG. Non-invasive brain stimulation: A new strategy to improve neurorehabilitation after stroke? *Lancet Neurol* 5(8), 708–712, 2006.

Hussain SJ, Claudino L, Bönstrup M, Norato G, Cruciani G, Thompson R, Zrenner C, Ziemann U, Buch E, Cohen LG. Sensorimotor oscillatory phase–power interaction gates resting human corticospinal output. *Cereb Cortex* 29(9), 3766–3777, 2019.

Irlbacher K, Brocke J, Mechow J v., Brandt SA. Effects of GABAA and GABAB agonists on interhemispheric inhibition in man. *Clin Neurophysiol* 118(2), 308–316, 2007.

Iwama S, Tsuchimoto S, Hayashi M, Mizuguchi N, Ushiba J. Scalp electroencephalograms over ipsilateral sensorimotor cortex reflect contraction patterns of unilateral finger muscles. *NeuroImage* 222, 117249 (11 pages), 2020.

Jarbo K, Verstynen T, Schneider W. In vivo quantification of global connectivity in the human corpus callosum. *NeuroImage* 59(3), 1988–1996, 2012.

Johnson KA, Hartwell K, LeMatty T, Borckardt J, Morgan PS, Govindarajan K, Brady K, George MS. Intermittent 'real-time' fMRI feedback is superior to continuous presentation for a motor imagery task: A pilot study. *J Neuroimaging* 22(1), 58–66, 2012.

Khademi F, Royter V, Gharabaghi A. Distinct beta-band oscillatory circuits underlie corticospinal gain modulation. *Cereb Cortex* 28(4), 1502–1515, 2018.

Kim JH. Book review: fundamentals of clinical trials. 4th ed. *Int Neurourol J* 17(2), 96, 2013.

Kober SE, Witte M, Grinschgl S, Neuper C, Wood G. Placebo hampers ability to self-regulate brain activity: A double-blind sham-controlled neurofeedback study. *NeuroImage* 181(1), 797–806, 2018.

Koh C-L, Tang P-F, Chen H-I, Hsu Y-C, Hsieh C-L, Tseng W-YI. Impaired callosal motor fiber integrity and upper extremity motor impairment are associated with stroke lesion location. *Neurorehabil Neural Repair* 32(6–7), 602–612, 2018.

Kraus D, Naros G, Bauer R, Leão MT, Ziemann U, Gharabaghi A. Brain-robot interface driven plasticity: Distributed modulation of corticospinal excitability. *NeuroImage* 125(1), 522–532, 2016.

Li J-Y, Lai P-H, Chen R. Transcallosal inhibition in patients with callosal infarction. *J Neurophysiol* 109(3), 659–665, 2013.

Liew S-L, Rana M, Cornelsen S, Fortunato de Barros Filho M, Birbaumer N, Sitaram R, Cohen LG, Soekadar SR. Improving motor corticothalamic communication after stroke using real-time fMRI connectivity-based neurofeedback. *Neurorehabil Neural Repair* 30(7), 671–675, 2016.

Madsen KH, Karabanov AN, Krohne LG, Safeldt MG, Tomasevic L, Siebner HR. No trace of phase: Corticomotor excitability is not tuned by phase of pericentral mu-rhythm. *Brain Stimulat* 12(5), 1261–1270, 2019.

Mansour S, Ang KK, Nair KPS, Phua KS, Arvaneh M. Efficacy of brain-computer interface and the impact of its design characteristics on poststroke upper-limb rehabilitation: A systematic review and meta-analysis of randomized controlled trials. *Clin EEG Neurosci* 53(1), 79–90, 2022.

Marshall RS, Perera GM, Lazar RM, Krakauer JW, Constantine RC, DeLaPaz RL. Evolution of cortical activation during recovery from corticospinal tract infarction. *Stroke* 31(3), 656–661, 2000.

Mayaud L, Congedo M, Van Laghenhove A, Orlikowski D, Figère M, Azabou E, Cheliout-Heraut F. A comparison of recording modalities of P300 event-related potentials (ERP) for brain-computer interface (BCI) paradigm. *Neurophysiol Clin Neurophysiol* 43(4), 217–227, 2013.

McFarland DJ, McCane LM, David SV, Wolpaw JR. Spatial filter selection for EEG-based communication. *Electroencephalogr Clin Neurophysiol* 103(3), 386–394, 1997.

Meyer B-U, Röricht S, von Einsiedel HG, Kruggel F, Weindl A. Inhibitory and excitatory interhemispheric transfers between motor cortical areas in normal humans and patients with abnormalities of the corpus callosum. *Brain* 118(2), 429–440, 1995.

Mizuguchi N, Maudrich T, Kenville R, Carius D, Maudrich D, Villringer A, Ragert P. Structural connectivity prior to whole-body sensorimotor skill learning associates with changes in resting state functional connectivity. *NeuroImage* 197(1), 191–199, 2019.

Moher D, Schulz KF, Altman D. The CONSORT Statement: Revised recommendations for omproving the quality of reports of parallel-group randomized trials. *JAMA* 285(15), 1987–1991, 2001.

Moon HS, Jiang H, Vo TT, Jung WB, Vazquez AL, Kim S-G. Contribution of excitatory and inhibitory neuronal activity to BOLD fMRI. *Cereb Cortex* 31(9), 4053–4067, 2021.

Morishita T, Uehara K, Funase K. Changes in interhemispheric inhibition from active to resting primary motor cortex during a fine-motor manipulation task. *J Neurophysiol* 107(11), 3086–3094, 2012.

Muellbacher W, Richards C, Ziemann U, Wittenberg G, Weltz D, Boroojerdi B, Cohen L, Hallett M. Improving hand function in chronic stroke. *Arch Neurol* 59(8), 1278–1282, 2002.

Murase N, Duque J, Mazzocchio R, Cohen LG. Influence of interhemispheric interactions on motor function in chronic stroke. *Ann Neurol* 55(3), 400–409, 2004.

Nakayashiki K, Saeki M, Takata Y, Hayashi Y, Kondo T. Modulation of event-related desynchronization during kinematic and kinetic hand movements. *J NeuroEngineering Rehabil* 11(90), 9, 2014.

Naros G, Lehnertz T, Leão MT, Ziemann U, Gharabaghi A. Brain state-dependent gain modulation of corticospinal output in the active motor system. *Cereb Cortex* 30(1), 371–381, 2020.

Naros G, Naros I, Grimm F, Ziemann U, Gharabaghi A. Reinforcement learning of self-regulated sensorimotor β-oscillations improves motor performance. *NeuroImage* 134(1), 142–152, 2016.

Nelson AJ, Hoque T, Gunraj C, Ni Z, Chen R. Bi-directional interhemispheric inhibition during unimanual sustained contractions. *BMC Neurosci* 10(31), 13, 2009.

Neuper C, Scherer R, Reiner M, Pfurtscheller G. Imagery of motor actions: Differential effects of kinesthetic and visual–motor mode of imagery in single-trial EEG. *Cogn Brain Res* 25(3), 668–677, 2005.

Neuper C, Wörtz M, Pfurtscheller G. ERD/ERS patterns reflecting sensorimotor activation and deactivation. *Prog Brain Res* 159(14), 211–222, 2006.

Ni Z, Gunraj C, Nelson AJ, Yeh I-J, Castillo G, Hoque T, Chen R. Two phases of interhemispheric inhibition between motor related cortical areas and the primary motor cortex in human. *Cereb Cortex* 19(7), 1654–1665, 2009.

Ni Z, Müller-Dahlhaus F, Chen R, Ziemann U. Triple-pulse TMS to study interactions between neural circuits in human cortex. *Brain Stimulat* 4(4), 281–293, 2011.

Nojima I, Sugata H, Takeuchi H, Mima T. Brain-computer interface training based on brain activity can induce motor recovery in patients with stroke: A meta-analysis. *Neurorehabil Neural Repair* 36(2), 83–96, 2022.

Nolte G, Bai O, Wheaton L, Mari Z, Vorbach S, Hallett M. Identifying true brain interaction from EEG data using the imaginary part of coherency. *Clin Neurophysiol* 115(10), 2292–2307, 2004.

Notturno F, Marzetti L, Pizzella V, Uncini A, Zappasodi F. Local and remote effects of transcranial direct current stimulation on the electrical activity of the motor cortical network. *Hum Brain Mapp* 35(5), 2220–2232, 2014.

Oldfield RC. The assessment and analysis of handedness: The Edinburgh inventory. *Neuropsychologia* 9(1), 97–113, 1971.

Ono T, Kimura A, Ushiba J. Daily training with realistic visual feedback improves reproducibility of event-related desynchronisation following hand motor imagery. *Clin Neurophysiol* 124(9), 1779–1786, 2013.

Ono T, Shindo K, Kawashima K, Ota N, Ito M, Ota T, Mukaino M, Fujiwara T, Kimura A, Liu M, Ushiba J. Brain-computer interface with somatosensory feedback improves functional recovery from severe hemiplegia due to chronic stroke. *Front Neuroengineering* 7, 00019 (8 pages), 2014.

Ono T, Tomita Y, Inose M, Ota T, Kimura A, Liu M, Ushiba J. Multimodal sensory feedback associated with motor attempts alters BOLD Responses to paralyzed hand movement in chronic stroke patients. *Brain Topogr* 28(2), 340–351, 2015.

O'Sullivan LW, Gallwey TJ. Upper-limb surface electro-myography at maximum supination and pronation torques: The effect of elbow and forearm angle. *J Electromyogr Kinesiol* 12(4), 275–285, 2002.

Palmer LM, Schulz JM, Murphy SC, Ledergerber D, Murayama M, Larkum ME. The cellular basis of GABA(B)-mediated interhemispheric inhibition. *Science* 335(6071), 989–993, 2012.

Peña-Gómez C, Sala-Lonch R, Junqué C, Clemente IC, Vidal D, Bargalló N, Falcón C, Valls-Solé J, Pascual-Leone Á, Bartrés-Faz D. Modulation of large-scale brain networks by transcranial direct current stimulation evidenced by resting-state functional MRI. *Brain Stimulat* 5(3), 252–263, 2012.

Pereira J, Direito B, Sayal A, Ferreira C, Castelo-Branco M. Self-modulation of premotor cortex interhemispheric connectivity in a real-time functional magnetic resonance imaging neurofeedback study using an adaptive approach. *Brain Connect* 9(9), 662–672, 2019.

Pfurtscheller G. Functional brain imaging based on ERD/ERS. *Vision Res* 41(10–11), 1257–1260, 2001.

Pfurtscheller G, Lopes da Silva FH. Event-related EEG/MEG synchronization and desynchronization: basic principles. *Clin Neurophysiol* 110(11), 1842–1857, 1999.

Pfurtscheller G, Neuper C. Motor imagery activates primary sensorimotor area in humans. *Neurosci Lett* 239(2–3), 65–68, 1997.

Picazio S, Veniero D, Ponzo V, Caltagirone C, Gross J, Thut G, Koch G. Prefrontal control over motor cortex cycles at beta frequency during movement inhibition. *Curr Biol* 24(24), 2940–2945, 2014.

Pichiorri F, Fallani FDV, Cincotti F, Babiloni F, Molinari M, Kleih SC, Neuper C, Kübler A, Mattia D. Sensorimotor rhythm-based brain–computer interface training: The impact on motor cortical responsiveness. *J Neural Eng* 8, 025020 (9 pages), 2011.

Pichiorri F, Morone G, Petti M, Toppi J, Pisotta I, Molinari M, Paolucci S, Inghilleri M, Astolfi L, Cincotti F, Mattia D. Brain-computer interface boosts motor imagery practice during stroke recovery. *Ann Neurol* 77(5), 851–865, 2015.

Posse S, Fitzgerald D, Gao K, Habel U, Rosenberg D, Moore GJ, Schneider F. Real-time fMRI of temporolimbic regions detects amygdala activation during single-trial self-induced sadness. *NeuroImage* 18(3), 760–768, 2003.

Prasad G, Herman P, Coyle D, McDonough S, Crosbie J. Applying a brain-computer interface to support motor imagery practice in people with stroke for upper limb recovery: A feasibility study. *J Neuroengineering Rehabil* 7, 60 (17 pages), 2010.

Ramos-Murguialday A, Broetz D, Rea M, Läer L, Yilmaz Ö, Brasil FL, Liberati G, Curado MR, Garcia-Cossio E, Vyziotis A, Cho W, Agostini M, Soares E, Soekadar S,

Caria A, Cohen LG, Birbaumer N. Brain-machine-interface in chronic stroke rehabilitation: A controlled study. *Ann Neurol* 74(1), 100–108, 2013.

Rehme AK, Eickhoff SB, Wang LE, Fink GR, Grefkes C. Dynamic causal modeling of cortical activity from the acute to the chronic stage after stroke. *NeuroImage* 55(3), 1147–1158, 2011.

Robertson MM, Furlong S, Voytek B, Donoghue T, Boettiger CA, Sheridan MA. EEG power spectral slope differs by ADHD status and stimulant medication exposure in early childhood. *J Neurophysiol* 122(6), 2427–2437, 2019.

Ros T, Enriquez-Geppert S, Zotev V, Young KD, Wood G, Whitfield-Gabrieli S, Wan F, Vuilleumier P, Vialatte F, Van De Ville D, Todder D, Surmeli T, Sulzer JS, Strehl U, Sterman MB, Steiner NJ, Sorger B, Soekadar SR, Sitaram R, Sherlin LH, Schönenberg M, Scharnowski F, Schabus M, Rubia K, Rosa A, Reiner M, Pineda JA, Paret C, Ossadtchi A, Nicholson AA, Nan W, Minguez J, Micoulaud-Franchi J-A, Mehler DMA, Lührs M, Lubar J, Lotte F, Linden DEJ, Lewis-Peacock JA, Lebedev MA, Lanius RA, Kübler A, Kranczioch C, Koush Y, Konicar L, Kohl SH, Kober SE, Klados MA, Jeunet C, Janssen TWP, Huster RJ, Hoedlmoser K, Hirshberg LM, Heunis S, Hendler T, Hampson M, Guggisberg AG, Guggenberger R, Gruzelier JH, Göbel RW, Gninenko N, Gharabaghi A, Frewen P, Fovet T, Fernández T, Escolano C, Ehlis A-C, Drechsler R, Christopher deCharms R, Debener S, De Ridder D, Davelaar EJ, Congedo M, Cavazza M, Breteler MHM, Brandeis D, Bodurka J, Birbaumer N, Bazanova OM, Barth B, Bamidis PD, Auer T, Arns M, Thibault RT. Consensus on the reporting and experimental design of clinical and cognitive-behavioural neurofeedback studies (CRED-nf checklist). *Brain* 143(6), 1674–1685, 2020.

Ros T, Munneke MAM, Ruge D, Gruzelier JH, Rothwell JC. Endogenous control of waking brain rhythms induces neuroplasticity in humans. *Eur J Neurosci* 31(4), 770–778, 2010.

Rossi S, Hallett M, Rossini PM, Pascual-Leone A. Safety, ethical considerations, and application guidelines for the use of transcranial magnetic stimulation in clinical practice and research. *Clin Neurophysiol* 120(12), 2008–2039, 2009.

Rossini PM, Barker AT, Berardelli A, Caramia MD, Caruso G, Cracco RQ, Dimitrijević MR, Hallett M, Katayama Y, Lücking CH, Maertens de Noordhout AL, Marsden CD, Murray NMF, Rothwell JC, Swash M, Tomberg C. Non-invasive electrical and

magnetic stimulation of the brain, spinal cord and roots: Basic principles and procedures for routine clinical application. Report of an IFCN committee. *Electroencephalogr Clin Neurophysiol* 91(2), 79–92, 1994.

Rossini PM, Burke D, Chen R, Cohen LG, Daskalakis Z, Di Iorio R, Di Lazzaro V, Ferreri F, Fitzgerald PB, George MS, Hallett M, Lefaucheur JP, Langguth B, Matsumoto H, Miniussi C, Nitsche MA, Pascual-Leone A, Paulus W, Rossi S, Rothwell JC, Siebner HR, Ugawa Y, Walsh V, Ziemann U. Non-invasive electrical and magnetic stimulation of the brain, spinal cord, roots and peripheral nerves: Basic principles and procedures for routine clinical and research application. An updated report from an I.F.C.N. Committee. *Clin Neurophysiol* 126(6), 1071–1107, 2015.

Ruddy K, Balsters J, Mantini D, Liu Q, Kassraian-Fard P, Enz N, Mihelj E, Chander BS, Soekadar SR, Wenderoth N. Neural activity related to volitional regulation of cortical excitabili. *eLife* 7, 40843 (21 pages), 2018.

Safeldt MG, Tomasevic L, Karabanov A, Siebner H, Madsen KH. Towards brain-state dependent transcranial magnetic stimulation: Targeting the phase of oscillatory neocortical activity with singe-pulse TMS. *Brain Stimulat* 10(2), 449–450, 2017.

Sauseng P, Klimesch W, Gerloff C, Hummel FC. Spontaneous locally restricted EEG alpha activity determines cortical excitability in the motor cortex. *Neuropsychologia* 47(1), 284–288, 2009.

Schulz H, Ubelacker T, Keil J, Müller N, Weisz N. Now I am ready-now i am not: The influence of pre-TMS oscillations and corticomuscular coherence on motor-evoked potentials. *Cereb Cortex* 24(7), 1708–1719, 2014.

Schwerin S, Dewald JPA, Haztl M, Jovanovich S, Nickeas M, MacKinnon C. Ipsilateral versus contralateral cortical motor projections to a shoulder adductor in chronic hemiparetic stroke: Implications for the expression of arm synergies. *Exp Brain Res* 185(3), 509–519, 2008.

Seghier ML. Laterality index in functional MRI: Methodological issues. *Magn Reson Imaging* 26(5), 594–601, 2008.

Shekhawat GS, Vanneste S. Optimization of transcranial direct current stimulation of dorsolateral prefrontal cortex for tinnitus: A non-linear dose-response effect. *Sci Rep* 8, 8311 (8 pages), 2018.

Shibata K, Watanabe T, Sasaki Y, Kawato M. Perceptual learning incepted by decoded fMRI neurofeedback without stimulus presentation. *Science* 334(6061), 1413–1415, 2011.

Shindo K, Kawashima K, Ushiba J, Ota N, Ito M, Ota T, Kimura A, Liu M. Effects of neurofeedback training with an electroencephalogram-based brain-computer interface for hand paralysis in patients with chronic stroke: A preliminary case series study. *J Rehabil Med* 43(10), 951–957, 2011.

Sitaram R, Ros T, Stoeckel L, Haller S, Scharnowski F, Lewis-Peacock J, Weiskopf N, Blefari ML, Rana M, Oblak E, Birbaumer N, Sulzer J. Closed-loop brain training: The science of neurofeedback. *Nat Rev Neurosci* 18(2), 86–100, 2017.

Smania N, Paolucci S, Tinazzi M, Borghero A, Manganotti P, Fiaschi A, Moretto G, Bovi P, Gambarin M. Active finger extension: A simple movement predicting recovery of arm function in patients with acute stroke. *Stroke* 38(3), 1088–1090, 2007.

Soekadar SR, Birbaumer N, Slutzky MW, Cohen LG. Brain–machine interfaces in neurorehabilitation of stroke. *Neurobiol Dis* 83(1), 172–179, 2015a.

Soekadar SR, Witkowski M, Birbaumer N, Cohen LG. Enhancing hebbian learning to control brain oscillatory activity. *Cereb Cortex* 25(9), 2409–2415, 2015b.

Sommer M, Gileles E, Knappmeyer K, Rothkegel H, Polania R, Paulus W. Carbamazepine reduces short-interval interhemispheric inhibition in healthy humans. *Clin Neurophysiol* 123(2), 351–357, 2012.

Stancák A, Pfurtscheller G. The effects of handedness and type of movement on the contralateral preponderance of mu-rhythm desynchronisation. *Electroencephalogr Clin Neurophysiol* 99(2), 174–182, 1996.

Stefanou M-I, Desideri D, Belardinelli P, Zrenner C, Ziemann U. Phase synchronicity of μ-rhythm determines efficacy of interhemispheric communication between human motor cortices. *J Neurosci* 38(49), 10525–10534, 2018.

Takemi M, Maeda T, Masakado Y, Siebner HR, Ushiba J. Muscle-selective disinhibition of corticomotor representations using a motor imagery-based brain-computer interface. *NeuroImage* 183(1), 597–605, 2018.

Takemi M, Masakado Y, Liu M, Ushiba J. Event-related desynchronization reflects downregulation of intracortical inhibition in human primary motor cortex. *J Neurophysiol* 110(5), 1158–1166, 2013.

Takemi M, Masakado Y, Liu M, Ushiba J. Sensorimotor event-related desynchronization represents the excitability of human spinal motoneurons. *Neuroscience* 297(1), 58–67, 2015.

Takeuchi N, Oouchida Y, Izumi S-I. Motor control and neural plasticity through interhemispheric interactions. *Neural Plast* 2012, 823285 (13 pages), 2012.

Thabane L, Ma J, Chu R, Cheng J, Ismaila A, Rios LP, Robson R, Thabane M, Giangregorio L, Goldsmith CH. A tutorial on pilot studies: the what, why and how. *BMC Med Res Methodol* 10, 1 (10 pages), 2010.

Thies M, Zrenner C, Ziemann U, Bergmann TO. Sensorimotor mu-alpha power is positively related to corticospinal excitability. *Brain Stimulat* 11(5), 1119–1122, 2018.

Thompson AK, Chen XY, Wolpaw JR. Acquisition of a simple motor skill: Task-dependent adaptation plus long-term change in the human soleus H-reflex. *J Neurosci* 29(18), 5784–5792, 2009.

Thrasher TA, Zivanovic V, McIlroy W, Popovic MR. Rehabilitation of reaching and grasping function in severe hemiplegic patients using functional electrical stimulation therapy. *Neurorehabil Neural Repair* 22(6), 706–714, 2008.

Toriyama H, Ushiba J, Ushiyama J. Subjective vividness of kinesthetic motor imagery is associated with the similarity in magnitude of sensorimotor event-related desynchronization between motor execution and motor imagery. *Front Hum Neurosci* 12, 00295 (10 pages), 2018.

Tsuchimoto S, Shibusawa S, Iwama S, Hayashi M, Okuyama K, Mizuguchi N, Kato K, Ushiba J. Use of common average reference and large-Laplacian spatial-filters enhances EEG signal-to-noise ratios in intrinsic sensorimotor activity. *J Neurosci Methods* 353, 109089 (9 pages), 2021.

Tsuchimoto S, Shibusawa S, Mizuguchi N, Kato K, Ebata H, Liu M, Hanakawa T, Ushiba J. Resting-state fluctuations of EEG sensorimotor rhythm reflect BOLD activities in the pericentral areas: A simultaneous EEG-fMRI study. *Front Hum Neurosci* 11, 00356 (10 pages), 2017.

Tsutsumi R, Shirota Y, Ohminami S, Terao Y, Ugawa Y, Hanajima R. Conditioning intensity-dependent interaction between short-latency interhemispheric inhibition and short-latency afferent inhibition. *J Neurophysiol* 108(4), 1130–1137, 2012.

Ushiba J, Soekadar SR. Brain–machine interfaces for rehabilitation of poststroke hemiplegia. *Prog Brain Res* 228(1), 163–183, 2016.

Varela F, Lachaux J-P, Rodriguez E, Martinerie J. The brainweb: Phase synchronization and large-scale integration. *Nat Rev Neurosci* 2(4), 229–239, 2001.

Várkuti B, Guan C, Pan Y, Phua KS, Ang KK, Kuah CWK, Chua K, Ang BT, Birbaumer N, Sitaram R. Resting state changes in functional connectivity correlate with movement recovery for BCI and robot-assisted upper-extremity training after stroke. *Neurorehabil Neural Repair* 27(1), 53–62, 2013.

Vincent JL, Patel GH, Fox MD, Snyder AZ, Baker JT, Van Essen DC, Zempel JM, Snyder LH, Corbetta M, Raichle ME. Intrinsic functional architecture in the anaesthetized monkey brain. *Nature* 447(7140), 83–86, 2007.

Vukelić M, Gharabaghi A. Oscillatory entrainment of the motor cortical network during motor imagery is modulated by the feedback modality. *NeuroImage* 111(1), 1–11, 2015.

Ward NS, Brown MM, Thompson AJ, Frackowiak RSJ. Neural correlates of motor recovery after stroke: A longitudinal fMRI study. *Brain* 126(11), 2476–2496, 2003a.

Ward NS, Brown MM, Thompson AJ, Frackowiak RSJ. Neural correlates of outcome after stroke: A cross-sectional fMRI study. *Brain J Neurol* 126(6), 1430–1448, 2003b.

Waters S, Wiestler T, Diedrichsen J. Cooperation not competition: Bihemispheric tDCS and fMRI show role for ipsilateral hemisphere in motor learning. *J Neurosci* 37(31), 7500–7512, 2017.

Weiskopf N, Mathiak K, Bock SW, Scharnowski F, Veit R, Grodd W, Goebel R, Birbaumer N. Principles of a brain-computer interface (BCI) based on real-time functional magnetic resonance imaging (fMRI). *IEEE Trans Biomed Eng* 51(6), 966–970, 2004.

Westlake KP, Nagarajan SS. Functional connectivity in relation to motor performance and recovery after stroke. *Front Syst Neurosci* 5, 00008 (12 pages), 2011.

Williams JA, Pascual-Leone A, Fregni F. Interhemispheric modulation induced by cortical stimulation and motor training. *Phys Ther* 90(3), 398–410, 2010.

Witelson SF. The brain connection: The corpus callosum is larger in left-handers. *Science* 229(4714), 665–668, 1985.

Xu J, Branscheidt M, Schambra H, Steiner L, Widmer M, Diedrichsen J, Goldsmith J, Lindquist M, Kitago T, Luft AR, Krakauer JW, Celnik PA. Rethinking interhemispheric imbalance as a target for stroke neurorehabilitation. *Ann Neurol* 85(4), 502–513, 2019.

Young BM, Nigogosyan Z, Remsik A, Walton LM, Song J, Nair VA, Grogan SW, Tyler ME, Edwards DF, Caldera K, Sattin JA, Williams JC, Prabhakaran V. Changes in functional connectivity correlate with behavioral gains in stroke patients after therapy using a brain-computer interface device. *Front Neuroengineering* 7, 00025 (12 pages), 2014.

Young BM, Stamm JM, Song J, Remsik AB, Nair VA, Tyler ME, Edwards DF, Caldera K, Sattin JA, Williams JC, Prabhakaran V. Brain-Computer interface training after stroke affects patterns of brain-behavior relationships in corticospinal motor fibers. *Front Hum Neurosci* 10, 00457 (13 pages), 2016.

Yuan H, Liu T, Szarkowski R, Rios C, Ashe J, He B. Negative covariation between task-related responses in alpha/beta-band activity and BOLD in human sensorimotor cortex: An EEG and fMRI study of motor imagery and movements. *NeuroImage* 49(3), 2596–2606, 2010.

Zarkowski P, Shin CJ, Dang T, Russo J, Avery D. EEG and the variance of motor evoked potential amplitude. *Clin EEG Neurosci* 37(3), 247–251, 2006.

Zhang J, Jadavji Z, Zewdie E, Kirton A. Evaluating if children can use simple brain computer interfaces. *Front Hum Neurosci* 13, 00024 (7 pages), 2019.

Zrenner C, Desideri D, Belardinelli P, Ziemann U. Real-time EEG-defined excitability states determine efficacy of TMS-induced plasticity in human motor cortex. *Brain Stimulat* 11(2), 374–389, 2018.